STABILITY ANALYSIS OF REACTION-DIFFUSION MODELS WITH DELAYED REACTION KINETICS

by

Nancy Khalil

Submitted in partial fulfillment of the requirements
for the degree of Doctor of Philosophy

at

Dalhousie University
Halifax, Nova Scotia
December 2019

To my loving parents Ayad and Salwa Azer, and my brother John.
To my amazing husband Tarek Khalil,
and my precious daughters Rebecca, Rachel and Raeya.

Table of Contents

List of Figures

Abstract

The linear stability of localized spike solutions to the one-dimensional Gierer-Meinhardt activator-inhibitor model with delayed nonlinear reaction kinetics is analyzed both analytically and numerically. In the limit of slow activator diffusivity, we show that delay destabilizes the equilibrium solution, and we find critical values at which a Hopf bifurcation is observed in both the spike position and amplitude. For specific cases of delayed reaction kinetics, we formulate the nonlocal eigenvalue problem and we study the stability of both the small and large eigenvalues. For the small eigenvalues, we show that in some cases the reduced system of ordinary differential equations, for the motion of the slow evolving spikes, undergoes a Hopf bifurcation. Instabilities in the spike profile are also considered, and we show that the equilibrium solution is unstable as delay is increased beyond a critical Hopf bifurcation value. For one-spike solutions, we find that instability in the profile is triggered before the positional instability, except in the case where the degradation of activator is delayed where stable positional oscillations are observed. The analytical results are validated using numerical simulations.

In addition, we study an example of quorum sensing behaviour modelled by a two-dimensional cell-bulk model coupled to delayed intracellular dynamics. In this model, the essential process of cell-to-cell communication is achieved by the diffusion of a signalling molecule in a well-mixed bulk medium between spatially segregated active cells. Assuming a very large diffusion limit, we investigate the onset of oscillatory instabilities due to coupling with delayed intracellular dynamics. The cell-bulk model, for the case of a single active cell containing one intracellular species, is reduced to a finite system of nonlinear delay ordinary differential equations and studied both analytically and numerically. Using Hill function-type intracellular kinetics with fixed delay, we show that delayed cell-bulk coupling triggers sustained oscillations as delay increases beyond the critical Hopf bifurcation threshold.

List of Abbreviations and Symbols Used

GM	Gierer-Meinhardt
QS	quorum sensing
RD	reaction-diffusion
DDE	delay (ordinary) differential equation
IVP	initial value problem
ODE	ordinary differential equation
PDE	partial differential equation
DDAE	delay differential-algebraic system of equations
NLEP	nonlocal eigenvalue problem
$O(\epsilon)$	Landau notation
$a(x_0)$	activator concentration for a single spike
$a(x_j)$	activator concentration for k spikes
D	inhibitor diffusivity
T	time delay
ϵ	activator diffusivity
λ	eigenvalue
μ	inhibitor decay rate

Acknowledgements

First I would like to express my deepest gratitude to my supervisor Dr. David Iron for his invaluable guidance, patience, and continuous support. It has been an honour to be his graduate student over the past several years. I would also like to thank Dr. Ward and Dr. Kolokolnikov for being on my supervisory committee and for their continuous support and expert guidance. Chapter 4 is based on joint work with Dr. Ward and Dr. Kolokolnikov. I am very appreciative to Dr. Kolokolnikov for all his help with MatLab and Maple programming. I am also very grateful for all the faculty and staff in the Mathematics and Statistics department at Dalhousie.

Finally, I would like to thank my precious family and close friends. I am especially thankful to my parents, Ayad Azer and Salwa Azer, my husband Tarek Khalil, and my precious daughters Rebecca, Rachel and Raeya for their love, continuous support, and encouragement throughout my years of study.

Chapter 1

Introduction

1.1 Background and Motivation

Developmental biology is the science of explaining the various processes involved in the progressive development of identical cells into whole multicellular organisms. There are many different mechanisms involved in the development of an organism, such as gene regulation, cell proliferation, and cell-to-cell communication (see [23]). In contemporary experimental biology, there has been renewed interest in exploring some of the key processes involved in the generation and development of various heterogeneous organism structures from seemingly homogeneous embryonic components, (see [48]), with an increased focus on the effect of genetic and chemical interactions during development.

Many biological processes are regulated by biochemical reactions involving proteins, known as enzymes, that act as activators or inhibitors. There have been many attempts made in an effort to understand these complex processes; in particular, those involved in pattern formation and morphogenesis, where a group of initially equivalent cells differentiate and develop into the various structures and organs. Furthermore, it has been shown that the concept of feedback control plays a fundamental role in many biological systems, where in a multi-step reaction, one of the products resulting from one the steps may have the nonlinear effect of activating or inhibiting the production of another reactant produced by other reaction steps, (see [55, 63, 69]). In addition, some reactions may exhibit a form of autocatalysis, which is the process by which a reactant is involved in its own production (see [55]).

In 1952, Alan Turing [68] proposed an activator-inhibitor type system, of two interacting and diffusing chemical species (morphogens), as a possible model for morphogenesis. He suggested that this type of reaction-diffusion (RD) system may have a steady state where one of the two diffusing morphogens has locally elevated concentration levels, causing neighbouring cells to develop differently from the surrounding

cells, thereby forming a distinct organ. In addition, under certain constraints, these localized spikes in the concentration of one of the reaction components could be responsible for the process of morphogenesis. In his landmark paper [68], Turing uses linear analysis to examine the stability of a general two-component RD system near a spatially homogeneous equilibrium solution. Turing shows that in the case of a large diffusion ratio, the equilibrium solution may become unstable, and that this instability results in the formation of stable spatially complex patterns. Thus, the interaction of two diffusing morphogens may result in a diffusion-driven bifurcation, which then leads to spontaneous pattern formation.

The Turing model of two chemical species in one-spatial dimension domain, as considered in [54], has the general form

$$u_t = D_u\ u_{xx} + F(u,v)\ , \qquad v_t = D_v\ v_{xx} + G(u,v)\ , \tag{1.1}$$

where u and v are used to denote the activator and inhibitor concentrations, respectively. D_u and D_v denote the diffusion coefficients of u and v, respectively, such that $D_u < D_v$. Motivated by the pioneering work of Turing, many subsequent RD models have been proposed and analyzed for diffusion-driven instability and its applications in developmental biology and pattern formation [28, 50].

Incorporating time delays in reaction kinetics when modelling reaction-diffusion patterns makes them more realistic and sophisticated. This is due to the fact that a finite amount of time is required for the reactions to carry out the processes involved. Many types of delay (ordinary) differential equation (DDE) systems have been proposed for modelling different fields of life sciences, such as population biology, molecular and cellular biology, engineering and control theory, as well as chemical and biological pattern formation (see [1, 10, 16, 19, 29, 30, 42, 55, 81]). Moreover, the mathematical theory of DDEs has been studied and documented in [13, 16, 40, 63]. The effect of time delay on the stability of steady state solutions plays a central role in the analysis of delay differential equations. In the modelling of reaction-diffusion systems, it has been shown that time delay often triggers oscillatory instabilities, which may result in a significant destabilizing effect on the steady state solutions of a given system (see for example [17, 20, 21, 42, 43]). To illustrate the effect of delay on the stability of an equilibrium solution, we consider a simple initial value problem (IVP) involving a first-order linear delay differential equation in contrast to

an ordinary differential equation (ODE) model. In the absence of delay, the initial value problem given by

$$\frac{dx}{dt} = kx(t) \ , \qquad x(0) = 1 \ , \tag{1.2}$$

has the exponential solution of the form

$$x(t) = e^{kt} \ . \tag{1.3}$$

With delay, the problem in (1.2) becomes a DDE of the form

$$\frac{dx}{dt} = kx(t-T) \ , \qquad x(t) = 1 \ , \text{ when } \ -T \leq t < 0 \ , \tag{1.4}$$

for some fixed time delay parameter, T. The right hand side of (1.4) depends on the history; that is the solution x at time $t - T$. Moreover, the initial condition in (1.2) becomes an initial function, $x(t)$, which requires the value of the solution at the initial point as well as the values of $x(t)$ looking back in time over the interval $[-T, 0)$. In contrast with the exponential solution (1.3), the DDE in (1.4) has an oscillatory particular solution of the form

$$x = \alpha \sin(\omega t) \ . \tag{1.5}$$

Substituting (1.5) into the DDE in (1.4) gives

$$\omega\alpha \cos(\omega t) = k\alpha \left[\sin(\omega t)\cos(\omega T) - \cos(\omega t)\sin(\omega T)\right] \ . \tag{1.6}$$

Comparing coefficients on both sides of equation (1.6) yields two necessary conditions for ω and T given by

$$\cos(\omega T) = 0 \ , \qquad \text{and} \qquad \omega = -k\sin(\omega T) \ . \tag{1.7}$$

The first condition gives that $\omega T = \pi/2$ or $3\pi/2$, and using the second condition we obtain that

$$\omega T = \frac{\pi}{2} \ , \ kT = -\frac{\pi}{2} \ , \qquad \text{or} \qquad \omega T = \frac{3\pi}{2} \ , \ kT = \frac{3\pi}{2} \ . \tag{1.8}$$

Using the method of steps for the case where $k = -1$ and $T = 1$, equation (1.4) yields the solution $x = 1 - t$ over the interval $[0, 1)$, and the solution $x = -(t - 1) + \frac{1}{2}(t-1)^2$ when solved over the interval $[1, 2)$ using the previous solution as

initial data at time $t = 1$, as shown in [16]. Continuing in the same manner, we can obtain solutions for subsequent intervals. An interesting observation is the presence of jump discontinuities at time $t = 0$ which propagates in time to solutions of higher derivatives of the IVP, thereby suggesting that the presence of delay may induce oscillations. This property of propagated discontinuities caused by time delay is unique to delay differential equations, and is not observed in ordinary differential equations [16, 63, 55].

In spite of the many advances in computational techniques and mathematical tools, the study of delay differential equations remains a very difficult and challenging task. Different types of DDEs have been studied, with fixed and time-dependent lag functions, also known as neutral delays [2]. Several numerical and graphical tools have been developed for analyzing DDEs [61, 62], in particular those with oscillatory solutions. In general, it has been shown that delay can have a profound effect on the stability of dynamical systems by inducing oscillatory behaviour. In recent research, there have been extensive studies on the effect of both delay and diffusion in pattern formation for population and chemical models [15, 21, 22, 60], as well as the theory of Hopf bifurcation, Turing instability, and Turing-Hopf bifurcation. In [27], the authors investigate the possible relation between Turing instabilities and Hopf bifurcations, and they show that increasing delay or varying the diffusion parameters can result in periodic oscillations.

Time delays in reaction kinetics are well-motivated biologically, due to time lags needed for gene expression. As a result, there have been numerous interesting studies done on the possible effect of fixed time delays in reaction kinetics for various RD models for pattern formation [20, 43, 44]. In particular, the effect of delayed gene expression on the dynamics of a one-dimensional reaction-diffusion pattern formation system is studied in [20], where it has been shown numerically that delay causes a dramatic increase in the time needed for the induction of patterning in the RD system, and in some cases delay resulted in a failure of the Turing instability mechanism.

The incorporation of time delays undoubtedly results in more realistic models. However the steady state stability analysis for a delay system is often quite difficult mainly due to the complexity of the resulting transcendental characteristic equation,

which often has infinitely many complex roots. In [4] and [5], the effect of time delay in reaction kinetics has been rigorously studied. The authors provide a detailed analysis of the equilibrium stability and the associated Hopf bifurcation problem, using a systematic approach to solve for the pure imaginary roots of the corresponding transcendental polynomial. In [9], Hopf bifurcation analysis is done for a model where the characteristic equation is dependant on time delay.

One example of a feedback control system is the activator-inhibitor type model proposed by Gierer and Meinhardt in [23]. In this two-species model, characterized by a short-range activation and a long-range inhibition, it is assumed that one of the reactants, referred to as the activator, diffuses much slower than the other reactant referred to as the inhibitor. Furthermore, the activator molecule is auto-catalyzed, while the production of the inhibitor is catalyzed by the activator and inhibits the production of the activator. Analysis of the Gierer-Meinhardt (GM) model shows that the limiting of the slow diffusing activator may result in pattern formation for localized spikes in the activator concentration. In [42], the effect of gene expression time delays on a GM model is numerically analyzed, with the assumption that signal transduction is induced by reversible ligand binding at the cell surface. The study shows that, with increasing values of delay, spatial-temporal oscillations are observed, and that a further increase in time delay causes an uncontrolled increase in the amplitude of these oscillations. These results suggest the incorporation of only relatively small values of delay in gene expression can have a substantial destabilizing effect on the stability of the spatial patterning mechanism, and a significant temporal influence on the system dynamics and pattern formation.

The GM equations are a system of nonlinear reaction-diffusion equations which have been used as a model of organogenesis [23]. The nonlinear terms are used to represent the complex process of protein production regulation. Since this process evolves on a much slower time-scale than diffusion and decay, it is natural to consider using DDEs when modelling the system. The nonlinear terms are a simplification of a complex series of reactions which may proceed at different rates. In this thesis we will consider the effects of delaying various terms in the equations. In each case, we find a reduced system of DDEs which approximate the behaviour of the full system of delay partial differential equations (PDE). In the absence of delay, the GM model,

in dimensionless form, can be written as

$$a_t = \epsilon^2 a_{xx} - a + \frac{a^2}{h} \ , \qquad 0 < x < L \ , \ t > 0 \ , \tag{1.9a}$$

$$\sigma h_t = D h_{xx} - \mu h + \frac{a^2}{\epsilon} \ , \qquad 0 < x < L \ , \ t > 0 \ , \tag{1.9b}$$

with boundary conditions $a_x(0,t) = a_x(L,t) = h_x(0,t) = h_x(L,t) = 0$. Here a and h represent the activator concentration and the inhibitor concentration, respectively. The parameter $0 < \epsilon \ll 1$ represents the diffusivity of the activator component a, while the diffusivity of the inhibitor component h is given by $D > 0$, and we assume $D = O(1)$. We assume $\epsilon \ll 1$ so that the activator diffuses more slowly than the inhibitor. The parameters $0 \leq \sigma << 1$ and $\mu > 0$ represent a time scaling and decay constant for the inhibitor reaction. We have used subscripts to denote partial derivatives. We will use the notation $a_T = a(x, t-T)$ to represent a delayed term. The exponents in the nonlinear terms correspond to the activator-inhibitor model in the original paper [23]. We have chosen this system to simplify some of the calculations. However the analysis may be applied to the more general system with trivial modifications. A key feature of this system is the formation of solutions with spatial structure (see [33, 34]). In particular, $a(x,t)$ will be exponentially small except in well defined regions where the value of $a(x,t) = O(1)$. These localized elevated levels of the activator are thought to cause the localized differentiation of cells in organogenesis.

In the absence of delay, the stability and dynamics of spike-type solutions to the GM model, in one and two dimensions, have been rigorously studied and analyzed both asymptotically and numerically. Results for the existence of a Hopf bifurcation have been derived for some critical threshold values of the parameter σ in (1.9), for the one-dimensional shadow problem in the limit $D \to \infty$ (see [7, 12, 32, 76]), the one-dimensional infinite-line problem (see [14, 77]), and the two-dimensional multi-spot problem (see [80]). In these studies, the models are linearized about a localized steady state solution and the spectrum of the derived nonlocal eigenvalue problem (NLEP) is analyzed. Results show that steady state solutions are destabilized through a Hopf bifurcation as σ increases past a certain threshold, σ_H, (see also [6, 34, 71, 78], and the references therein). In addition, a one-dimensional GM model with undelayed kinetics is analyzed in [56], where the exponents are such that $p = 2m - 3$

and $m > 2$. The authors show that the NLEP in this case can be reduced to a simple transcendental equation, and is explicitly solvable. The special case when $p = m = 3$ is studied in [38], where the stability of steady state hot-spot patterns for a reaction-diffusion model of urban crime is analyzed. For the case of a single spike solution, in the regime where diffusion is at least logarithmically large as $\epsilon \to 0$, a differential equation representing the dynamics for the center of the spike was derived and analyzed in [74].

In [17], the linear stability of spike solutions is analyzed for the GM model with delayed reaction kinetics. The authors show that incorporating delay in certain reaction kinetics leads to unconditional instability of the equilibrium solution, and a Hopf bifurcation occurs as delay increases beyond a critical threshold value [17]. Moreover, analysis of the NLEP for the singularly perturbed two-component GM system with fixed time delay is considered in [18], where delay in only the activator kinetics has been shown to have a stabilizing effect on the stability of localized spike solutions.

In [4] and [42], the authors consider how delay can enter different terms of the equation. The exact nature of how delay enters the equation can depend on which steps in a complex sequence of reactions are rate limiting steps. We will consider delaying the individual components of the nonlinear reaction terms alone and in combination. We will use similar methods to those considered in [34] to construct a system of delay differential equations approximating the behaviour of the localized spike solutions. As well we will consider the stability of the slowly evolving spikes. In particular we will consider instability due to Hopf bifurcations occurring as the delay is increased. There are two classes of eigenvalues to consider, referred to as the large and small eigenvalues. The large eigenvalues correspond to profile instabilities and the small eigenvalues correspond to translation instabilities. A Hopf bifurcation occurring in the former will result in spikes which oscillate up and down and in the former spikes which move back and forth. A discussion on the nature and origin of these eigenvalues can be found in [33] and [34].

The main goal of the first two chapters of this thesis is to provide detailed analytical and numerical stability analysis of spike-type solutions to the one-dimensional GM model with delayed reaction kinetics. In particular, we show that in some cases

delay destabilizes the equilibrium solution through a Hopf bifurcation, which is observed as delay increases past a certain threshold T_H.

The GM model offers an example of cell-to-cell communication through the diffusion of chemicals. Another sophisticated mechanism of cell interaction through diffusive signals is found in the study of quorum sensing (QS) behaviour used by many intricate species to control the essential process of cell-to-cell communication. Quorum sensing is defined as the regulation of gene expression in response to fluctuations in cell-population density. QS behaviour has been observed and studied for various organisms and populations (see for example [66, 67]). Recent studies of bacterial populations show evidence of QS behaviour, whereby collective synchronized behaviour driven by chemical signalling between cells is triggered only when the number of cells in the population exceeds a certain threshold. See for example the study of bacterial bioluminescence in [65] and the references therein.

A realistic modelling of quorum behaviour is provided by a class of coupled cell-bulk models, where spatially segregated active cells communicate through a diffusing signalling molecule in a bulk region that is well-mixed. Models for the coupling of local compartments to bulk diffusion are studied in [8, 24, 41]. Analysis of Turing patterns due to coupled bulk and surface diffusion is given in [45]. In [25] and [26], a new class of two-dimensional quorum-sensing models is formulated and analyzed. In these models, spatially localized signalling compartments consisting of dynamically active small cells are coupled to nonlinear intracellular kinetics through a passive bulk diffusion field. In the absence of delay, the analysis in [25] shows that when the diffusion coefficient is large, the bulk region is well-mixed and the cell-bulk model can be reduced to a finite-dimensional ODE system for the bulk concentration field coupled to the intracellular dynamics, which is shown to have oscillatory instabilities triggered by the cell-bulk coupling. Similar coupled cell-bulk models have been analyzed in $\mathbb{R}^3$, for the study of quorum-sensing behaviour for yeast cells and bacteria (see [11, 52, 53, 59]). In some of these studies, for the case where a single ODE is used to model the intracellular dynamics, no triggered oscillations due to Hopf bifurcations were observed.

In this thesis, we extend the analysis in [25] and [26] to explore the effect of delay in the intracellular dynamics on the stability of the steady state solutions. We show

that in the limit of large diffusion, delaying the intracellular dynamics can destabilize the equilibrium solutions through a Hopf bifurcation. In a related class of models with small signalling compartments, it has been shown recently that time delay can lead to stable temporal oscillations (see [46, 47]).

1.2 Numerical Analysis of Delay Partial Differential Equations

Simulations of delay partial differential equations is a relatively new field and there are no preexisting software packages. Converting the partial differential equation to a system of ODEs by replacing the Laplacian by a second order centered difference approximation and using `dde23` in Matlab did not provide useful results. The system proved too stiff. A first order IMEX scheme was used instead. The diffusive terms where treated implicitly and the nonlinear terms explicitly. Some of the MatLab and Maple [49] codes used are provided in Appendix A. For all simulations of ordinary delay systems we use the MatLab code `ddesd` with default settings.

1.3 Thesis Outline

The outline of this thesis is as follows: In Chapter 2, we construct a one-dimensional GM model with various cases of delayed reaction kinetics, and we analyze the effect of delay on the stability and dynamics of the slow evolving one-spike solution. In each case the delay partial differential equation system is reduced to a DDE for the position of the spike. We then examine the possibility of oscillatory motion of a spike, by finding Hopf bifurcations in the reduced equations for spike position. We also examine Hopf bifurcations in the spike profile, and we find that in every case where a Hopf bifurcation occurs in the reduced system, a Hopf bifurcation in the profile has already made the partial differential equation spike solution unstable. Furthermore, we show that oscillations in spike position are possible for this system if the delay is in the activator degradation.

In Chapter 3, we extend our stability and dynamics analysis to the more general case of a k-spike equilibrium solution. For various cases of delayed reaction kinetics, we derive the corresponding NLEP associated with localized eigenfunctions near the spike locations. The stability of the k-spike solution is analyzed using the resulting

large eigenvalues. The corresponding eigenvalue problem, governing localized spike profile instabilities, is studied as delay is introduced, using analytical techniques which are verified numerically for each case.

Motivated by the work done in [25], we analyze in Chapter 4 a cell-bulk model coupled to delayed intracellular dynamics through bulk diffusion, in a two-dimensional bounded domain. In this model, a dynamically active signalling cell consisting of multiple interacting species releases a signalling molecule into an exterior bulk region. This release is regulated by both the outer concentration of the molecule as well as its intracellular density. We extend the analysis in [25] to allow for delayed intracellular dynamics. In the limit of very fast diffusivity, where the bulk region is well-mixed, we show that the model can be reduced to a nonlinear system of DDEs with finite dimension, and we analyze the destabilizing effect of delay in the intracellular dynamics on the steady state solutions. Numerical simulations are used to confirm our results and the corresponding Hopf bifurcation thresholds are calculated.

In Chapter 5, we summarize and discuss the results of this thesis, as well as suggest some future work and possible extensions to our studies.

Chapter 2

Stability and Dynamics of a One-Spike Solution to the One-Dimensional Gierer-Meinhardt Model with Delayed Reaction Kinetics

In this chapter, we analyze the linear stability and dynamics of the one-spike steady state solution to the GM Model in (1.9), with $\sigma = 0$, in the limit $\epsilon \to 0$, and when the nonlinear reaction terms have a time delay T. The goal of this chapter is to show that for some cases of delayed reaction kinetics, time delay has a destabilizing effect on the stability of the spike solution. Moreover, we show that, for certain cases of delayed reaction kinetics, a Hopf bifurcation occurs in both the spike position and amplitude as delay is increased past a critical threshold value T_H. Furthermore, we show numerically that these sustained oscillations due to a Hopf bifurcation are observed first in the spike amplitude.

In §2.1, we derive the equation of motion for a single spike for various cases of delayed nonlinear reaction terms. This is done by first introducing a slow time-scale variable to the model and then using it to reduce the system of partial differential equations to a system of ODEs. We then compare the reduced system to the full PDE system using numerical methods. In §2.2, we find critical delay values for position instabilities due to a Hopf bifurcation in the reduced spike location equation. We then formulate and analyze, in §2.3, the NLEP for the various cases of delayed kinetics, and we find conditions under which the corresponding large eigenvalues may undergo a Hopf bifurcation. Finally, in §2.4, we show that delay in the degradation of the activator is the only case in which sustained positional oscillation are observed.

2.1 Derivation of Differential Equation for Spike Position

We begin by considering the GM Model in (1.9) with fixed delay in some of the nonlinear reaction terms. In each case, we will show that the PDE system can

be reduced to a system of ODEs representing the motion for the corresponding spike solution. Throughout this section we use the method of matched asymptotic expansions and the Van Dyke matching condition in [72] to match the outer and inner asymptotic approximations.

2.1.1 Delay in the Catalyzed Production of Inhibitor

In this section, we will consider the addition of delay to the nonlinear term in (1.9b). The model equations are:

$$a_t = \epsilon^2 a_{xx} - a + \frac{a^2}{h} \ , \qquad 0 < x < L \ , \ t > 0 \ , \tag{2.1a}$$

$$0 = D h_{xx} - \mu h + \frac{a_T^2}{\epsilon} \ , \qquad 0 < x < L \ , \ t > 0 \ , \tag{2.1b}$$

$$a_x(0,t) = a_x(L,t) = h_x(0,t) = h_x(L,t) = 0 \ , \tag{2.1c}$$

where $a_T(x,t) = a(x,t-T)$. We assume $0 < \epsilon \ll 1$, and $D = O(1)$. We note that when $\sigma \neq 0$ and $T = 0$, the eigenvalue problem associated with linearizing the model in (1.9) around the equilibrium solution becomes a NLEP and a Hopf bifurcation can occur. To simplify the analysis and isolate the effect of time delay T, we have assumed $\sigma = 0$. The Neumann boundary conditions (2.1c) and assumptions for (2.1) will be used throughout this thesis.

In this case the limiting reaction rate step would be in the enhanced production of h by a, and therefore we have that the catalyzed production of h is slow. This is the simplest case we will consider. The methods used in [34] carry over with few changes and the system of differential equations in [34] becomes a system of delay differential equations here.

We consider a single spike equilibrium solution localized about $x = x_0$. We expect the motion of the spike to be on an $O(\epsilon^2)$ time-scale, and therefore we consider the scaling $\tau = \epsilon^2 t$. Moreover, we define

$$y = \frac{x - x_0(\tau)}{\epsilon} \ , \qquad \tau = \epsilon^2 t \ , \tag{2.2}$$

as an inner coordinate. With y as the dependant variable, we use the method of matched asymptotic expansions to construct the equilibrium solution. In the inner region, defined near x_0, the value of h is constant to leading order, and the activator

concentration is localized. This will allow us to solve for the leading order behaviour of a in the inner region. In the outer region, away from the spike location x_0, the activator concentration is exponentially small, and therefore a will act like a multiple of a Dirac delta function, $\delta(x)$. By matching the inner and outer regions, we will construct the leading order solution to h in the outer region. The second order equations will then result in a solvability condition which results in an equation governing the motion of the spike.

In the inner region, we introduce the new variables

$$A(y) = a(x_0 + \epsilon y) \ , \qquad H(y) = h(x_0 + \epsilon y) \ . \tag{2.3}$$

Thus the model in (2.1) becomes

$$-\epsilon A' \ \dot{x}_0 = A'' - A + \frac{A^2}{H} \ , \qquad -\infty < y < \infty \ , \tag{2.4a}$$

$$0 = \frac{D}{\epsilon^2} H'' - \mu H + \frac{A_T^2}{\epsilon} \ , \qquad -\infty < y < \infty \ , \tag{2.4b}$$

where $A_T = A(y, \tau - T)$, and $\dot{x}_0 = dx_0/d\tau$. Here the primes indicate differentiation with respect to y. Using the expansion

$$A(y) = A_0(y) + \epsilon A_1(y) + \cdots \ , \qquad H(y) = H_0(y) + \epsilon H_1(y) + \cdots \ , \tag{2.5}$$

we get, to leading order in ϵ,

$$0 = A_0'' - A_0 + \frac{A_0^2}{H_0} \ , \qquad -\infty < y < \infty \ , \tag{2.6a}$$

$$0 = D H_0'' \ , \qquad -\infty < y < \infty \ . \tag{2.6b}$$

Matching to the outer solution requires that H_0 be bounded and that $A_0 \to 0$ as $|y| \to \infty$. It follows from (2.6b) that $H_0(y) \approx \widetilde{H}_0$, for some constant $\widetilde{H}_0$ to be determined by matching to the outer solution. Thus, in the limit $\epsilon \to 0$, the solution to (2.6a) is given by

$$A_0 = \widetilde{H}_0 \ w(y) \ , \tag{2.7}$$

where $w(y)$ is the unique positive homoclinic curve solution to the system

$$\begin{gathered} w'' - w + w^2 = 0 \ , \qquad -\infty < y < \infty \ , \\ w(y) \to 0 \ \ \text{as} \ \ |y| \to \infty \ , \quad w'(0) = 0 \ , \quad w(0) > 0 \ , \end{gathered} \tag{2.8a}$$

given by

$$w(y) = \frac{3}{2}\,\mathrm{sech}^2\left(\frac{y}{2}\right) \ . \tag{2.8b}$$

Substituting the inner expansion in (2.5) into (2.4) gives the $O(\epsilon)$ equations

$$A_1'' - A_1 + 2\frac{A_0}{H_0}A_1 = -\dot{x}_0 A_0' + \frac{A_0^2}{H_0^2}H_1 \ , \tag{2.9a}$$

$$DH_1'' = -A_{0T}^2 \ . \tag{2.9b}$$

Substituting (2.7) into (2.9) yields

$$A_1'' - A_1 + 2wA_1 = -\dot{x}_0\widetilde{H}_0 w' + w^2 H_1 \ , \tag{2.10a}$$

$$DH_1'' = -\widetilde{H}_{0T}^2\ w^2 \ . \tag{2.10b}$$

Since $w(y) \to 0$ as $|y| \to \infty$, the right hand side of (2.10a) must be orthogonal to the solution $w'(y)$. Using this solvability condition, it follows that

$$\dot{x}_0 \int_{-\infty}^{\infty} (w')^2 \ dy = \frac{1}{\widetilde{H}_0}\int_{-\infty}^{\infty} w^2 w' H_1 \ dy \ . \tag{2.11}$$

Integrating (2.11) by parts twice gives

$$\dot{x}_0 \int_{-\infty}^{\infty} (w')^2 \ dy = -\frac{1}{6\widetilde{H}_0}\left(\int_{-\infty}^{\infty} w^3 \ dy\right)\left[H_1'(\infty) + H_1'(-\infty)\right] \ , \tag{2.12}$$

where we use that H_1'' and $w(y)$ are even functions. Integrating (2.10b) from $y = -\infty$ to $y = \infty$ gives

$$H_1'(\infty) - H_1'(-\infty) = -\frac{\widetilde{H}_{0T}^2}{D}\int_{-\infty}^{\infty} w^2 \ dy \ , \tag{2.13}$$

which results in a jump condition for the outer solution.

In the outer region, defined away from an $O(\epsilon)$ neighbourhood of $x = x_0$, we have that $a \to 0$ for $|x - x_0| \gg \epsilon$, since a is exponentially localized to an $O(\epsilon)$ region about x_0. Thus, in the outer region, the term $\epsilon^{-1}a_T^2$ in (2.1) behaves like a multiple of the Dirac delta function, $\delta(x)$. Also, for $\epsilon \ll 1$, we get that h satisfies $Dh_{xx} - \mu h = 0$ on the interval $[0, L]$, subject to a jump condition at $x = x_0$. Matching to the inner variables, and using the expansion $h = h_0 + O(\epsilon)$, as $\epsilon \to 0$, gives that h_0 satisfies

$$\begin{aligned} Dh_{0xx} - \mu h_0 &= -\beta\ \delta(x - x_0(\tau - T)) \ , \quad 0 < x < L \ , \\ h_{0x}(0) &= h_{0x}(L) = 0 \ , \end{aligned} \tag{2.14a}$$

where

$$\beta = \int_{-\infty}^{\infty} A_0^2(y)\ dy\ . \tag{2.14b}$$

The solution to (2.14) is given by

$$h_0 = \beta G(x; x_{0T})\ , \tag{2.15}$$

where $G(x; x_0)$ is the Green's function satisfying

$$\begin{aligned} DG_{xx} - \mu G &= -\delta(x - x_{0T})\ , \qquad 0 < x < L\ , \\ G_x(0; x_0) &= G_x(L; x_0) = 0\ . \end{aligned} \tag{2.16a}$$

To simplify the notation, we assume $\mu = 1$ and $D = 1$ and we vary the length of the domain L. This yields the solution

$$G(x; x_{0T}) = \frac{1}{\sinh(L)} \begin{cases} \cosh(x)\cosh(x_{0T} - L)\ , & 0 < x < x_{0T}\ , \\ \cosh(x_{0T})\cosh(x - L)\ , & x_{0T} < x < L\ , \end{cases} \tag{2.16b}$$

where $G(x; x_{0T}) = G(x; x_0(\tau - T))$.

Moreover, since $A_0 = \widetilde{H}_0\ w(y)$ where $\widetilde{H}_0$ is the value of h_0 in the inner region, therefore $\widetilde{H}_0$ can be determined by matching the inner and outer regions. This gives that

$$\widetilde{H}_0 = h_0(x_0) = \beta G(x_0; x_{0T}) = \widetilde{H}_0^2 \left(\int_{-\infty}^{\infty} w^2(y)\ dy \right) G(x_0; x_{0T})\ . \tag{2.17}$$

Solving for $\widetilde{H}_0$ in (2.17) gives

$$\widetilde{H}_0 = \frac{1}{6\ G(x_0; x_{0T})}\ , \tag{2.18}$$

where we use that $\displaystyle\int_{-\infty}^{\infty} w^2(y)\ dy = 6$. Substituting (2.18) into (2.12) and solving for $\dot{x}_0$ yields the DDE

$$\dot{x}_0 = -\frac{G_x^- + G_x^+}{G(x_0; x_{0T})}\ . \tag{2.19}$$

From (2.16b), we get that

$$\begin{aligned} G_x^- &= G_x(x_0^-; x_{0T}) = \frac{\sinh(x_0)\cosh(x_{0T} - L)}{\sinh(L)}\ , \\ G_x^+ &= G_x(x_0^+; x_{0T}) = \frac{\cosh(x_{0T})\sinh(x_0 - L)}{\sinh(L)}\ . \end{aligned} \tag{2.20}$$

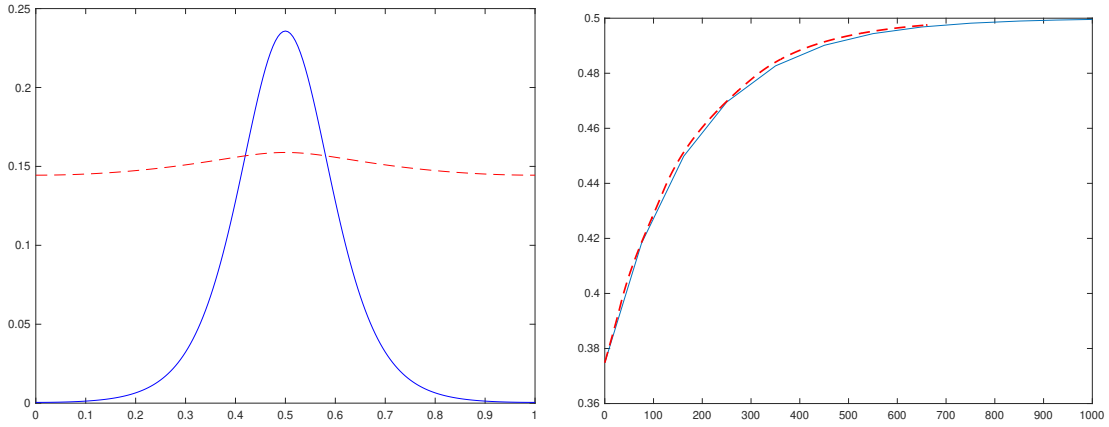

(a) (b)

Figure 2.1: Left: Plot of a one-spike equilibrium solution to (2.1), with delay in the nonlinear term of the inhibitor equation. The solid curve is the activator concentration and the dotted curve is the inhibitor concentration. Right: Plot of the trajectory $x_0(t)$ versus time t. The dotted curve shows the full numerical simulation of (2.1), and the solid curve is the asymptotic result computed from (2.21). Parameter values are $T = 0.1$, $\epsilon = 0.06$, $L = 1$, $\mu = 1$, and $D = 1$.

Reverting back to the initial time-scale and substituting (2.16b) and (2.20) into (2.19) yields the DDE for the motion of the spike described by

$$\frac{dx_0}{dt} = -\epsilon^2 \left(\frac{\sinh(x_0)\cosh(x_{0T} - L) + \cosh(x_{0T})\sinh(x_0 - L)}{\cosh(x_{0T})\cosh(x_0 - L)} \right) . \tag{2.21}$$

We remark that for $T = 0$ the equilibrium equation in (2.21) has similar terms to the one derived in [34] for the model without delay. In Figure 2.1, we plot an equilibrium solution to (2.1), and we compare the asymptotic result obtained from (2.21), for $x_0 = 0.5$ and $L = 1$, with full numerical results computed from (2.1). We find a close agreement between the two results. In §2.2, we analyze the stability of the quasi-equilibrium solution, as T increases, and we find that it is not possible to get a Hopf bifurcation in this case. In fact, using increasing values of the delay T, we show that the trajectories of the quasi-equilibrium solution obtained from (2.21) slowly converge to the stable equilibrium $x_0 = L/2$, and therefore the spike slowly moves on an $O(\epsilon^2)$ time-scale towards this stable position.

We remark that numerical simulations for the case when $T = 0$ yields almost an identical plot to Figure 2.1(b).

2.1.2 Delay in the Regulation of Activator Production

In this section we analyze the model in (1.9) with delay in the nonlinear term of the activator equation, and the rate limiting step is in the negative feedback process. In §2.1.4 we consider delaying the entire term, but this analysis is more involved. The PDEs for the model are

$$a_t = \epsilon^2 a_{xx} - a + \frac{a^2}{h_T} \ , \qquad 0 < x < L \ , \ t > 0 \tag{2.22a}$$

$$0 = Dh_{xx} - \mu h + \frac{a^2}{\epsilon} \ , \qquad 0 < x < L \ , \ t > 0 \ , \tag{2.22b}$$

with the same assumptions and boundary conditions as in §2.1.1. The analysis here is similar to the one in §2.1.1. However we note that in this case even a small delay will result in significant changes in the behaviour of the system. Using the dependant variable y, as defined in (2.2), we use the method of matched asymptotic expansions to construct the equilibrium solution. As before, the value of h is constant to leading order in the inner region, and we solve for the leading order behaviour of a. In the outer region, we again treat a as a multiple of a Dirac delta function, $\delta(x)$, and we construct the leading order solution to h in the outer region, and use it to find an equation governing the motion of the spike.

In the inner region, the model in (2.22) written in terms of the inner variables becomes

$$-\epsilon A' \dot{x}_0 = A'' - A + \frac{A^2}{H_T} \ , \qquad -\infty < y < \infty \ , \tag{2.23a}$$

$$0 = \frac{D}{\epsilon^2} H'' - \mu H + \frac{A^2}{\epsilon} \ , \qquad -\infty < y < \infty \ , \tag{2.23b}$$

where $H_T = H(y, \tau - T)$, $x_0 = x_0(\tau)$, and $\tau = \epsilon^2 t$. Using the inner expansion in (2.5) for $A(y)$ and $H(y)$, we get to leading order in ϵ

$$0 = A_0'' - A_0 + \frac{A_0^2}{H_{0T}} \ , \qquad -\infty < y < \infty \ , \tag{2.24a}$$

$$0 = DH_0'' \ , \qquad -\infty < y < \infty \ . \tag{2.24b}$$

As before, it follows from (2.24b) that $H_0(y) \approx \widetilde{H}_0$, for some constant $\widetilde{H}_0$ to be determined by matching to the outer solution. Thus, in the limit $\epsilon \to 0$, the solution

to (2.24a) is given by

$$A_0 = \widetilde{H}_{0T}\ w(y)\ , \tag{2.25}$$

where $w(y)$ satisfies (2.8). The $O(\epsilon)$ equations obtained from substituting (2.5) and (2.25) into (2.23) are given by

$$A_1'' - A_1 + 2wA_1 = -\dot{x}_0\widetilde{H}_{0T}\ w' + w^2 H_{1T}\ , \tag{2.26a}$$

$$DH_1'' = -\widetilde{H}_{0T}^2\ w^2\ . \tag{2.26b}$$

The solvability condition for (2.26a) gives that

$$\dot{x}_0 \int_{-\infty}^{\infty} (w')^2\ dy = \frac{1}{\widetilde{H}_{0T}} \int_{-\infty}^{\infty} w^2 w' H_{1T}\ dy\ . \tag{2.27}$$

Integrating (2.27) by parts twice gives

$$\dot{x}_0 \int_{-\infty}^{\infty} (w')^2\ dy = -\frac{1}{6\widetilde{H}_{0T}} \left(\int_{-\infty}^{\infty} w^3\ dy \right) \left[H_{1T}'(\infty) + H_{1T}'(-\infty) \right]\ . \tag{2.28}$$

In the outer region, a decays exponentially and h satisfies $Dh_{xx} - \mu h = 0$ on the interval $[0, L]$, subject to a jump condition at $x = x_0$. Using the expansion $h = h_0 + O(\epsilon)$, as $\epsilon \to 0$, while treating a as a multiple of the Dirac delta function, and matching to the inner solution gives

$$\begin{aligned} Dh_{0xx} - \mu h_0 &= -\beta\delta(x - x_0(\tau))\ , \quad 0 < x < L\ , \\ h_{0x}(0) &= h_{0x}(L) = 0\ , \end{aligned} \tag{2.29}$$

where β is as defined in (2.14b). In terms of the Green's function given in (2.16b), with $\mu = 1$ and $D = 1$, the solution h_0 for the system in (2.29) is given by

$$h_0 = \beta G(x; x_0)\ , \tag{2.30}$$

which yields the solution

$$\widetilde{H}_{0T} = h_{0T} = \beta G(x_{0T}; x_{0T})\ . \tag{2.31}$$

Substituting (2.31) into (2.28) and simplifying gives

$$\dot{x}_0 = -\frac{G_{x_T}^- + G_{x_T}^+}{G(x_{0T}; x_{0T})}\ , \tag{2.32a}$$

where

$$G^{-}_{x_T} = G_x(x^{-}_{0T}; x_{0T}) = \frac{\cosh(x_{0T} - L)\sinh(x_{0T})}{\sinh(L)} ,$$
$$G^{+}_{x_T} = G_x(x^{+}_{0T}; x_{0T}) = \frac{\cosh(x_{0T})\sinh(x_{0T} - L)}{\sinh(L)} . \tag{2.32b}$$

Thus, in terms of the initial time-scale we get

$$\frac{dx_0}{dt} = -\epsilon^2 \left(\frac{\sinh(2x_{0T} - L)}{\cosh(x_{0T})\cosh(x_{0T} - L)} \right) . \tag{2.33}$$

We observe that delay appears in every term of (2.33), which results in considerably different dynamics than the one derived in §2.1.1. Numerical simulations of this system are illustrated in Figure 2.2. In §2.2, we find that even a small delay will have a significant effect on the dynamics, and we also show that a Hopf bifurcation occurs at some critical values of the delay T.

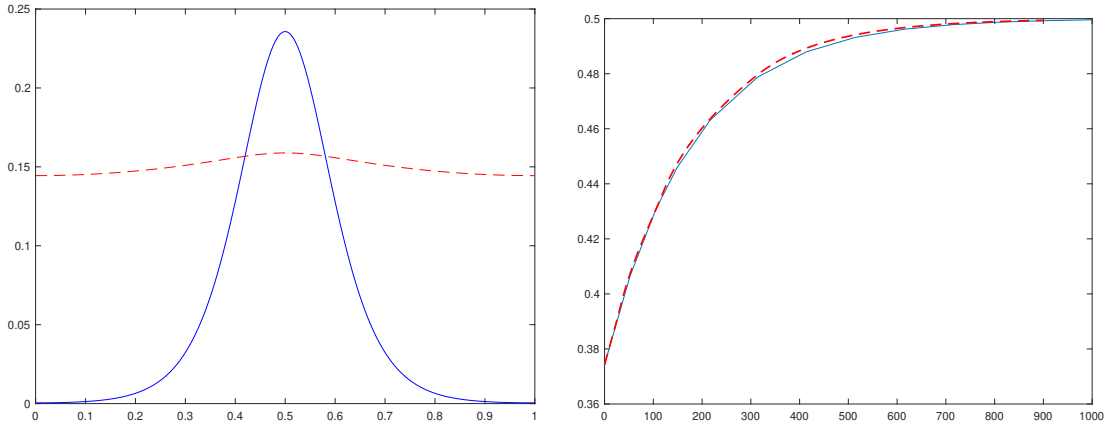

(a) (b)

Figure 2.2: Left: Plot of a one-spike equilibrium solution to (2.22), with delay in the h term of the activator equation. The solid curve is the activator concentration and the dotted curve is the inhibitor concentration. Right: Plot of the trajectory $x_0(t)$ versus time t. The dotted curve shows the full numerical simulation of (2.22), and the solid curve is the asymptotic result as obtained from (2.33). Parameter values are as in the caption of Figure 2.1.

2.1.3 Delay in Activator Regulation and Inhibitor Production

Next, we consider the following model with delay in the nonlinear terms of both equations:

$$a_t = \epsilon^2 a_{xx} - a + \frac{a^2}{h_T} \ , \qquad 0 < x < L \ , \ t > 0 \ , \tag{2.34a}$$

$$0 = D h_{xx} - \mu h + \frac{a_T^2}{\epsilon} \ , \qquad 0 < x < L \ , \ t > 0 \ , \tag{2.34b}$$

with the same boundary conditions and assumptions as before.

In the inner region, substituting the new variables in (2.2) and (2.3) into (2.34) gives

$$-\epsilon A' \dot{x}_0 = A'' - A + \frac{A^2}{H_T} \ , \qquad -\infty < y < \infty \ , \tag{2.35a}$$

$$0 = \frac{D}{\epsilon^2} H'' - \mu H + \frac{A_T^2}{\epsilon} \ , \qquad -\infty < y < \infty \ . \tag{2.35b}$$

Using the inner expansion for $A(y)$ and $H(y)$ given in (2.5), yields the solution $A_0 = \widetilde{H}_{0T}\, w(y)$, for $w(y)$ as defined in (2.8), as well as the motion equation in (2.28).

In the outer region, since $w \to 0$ as $y \to \pm\infty$, in terms of the Green's function in (2.16b) together with the solution h_0 in (2.15), and the expression (2.18) for $\widetilde{H}_0$, we get that

$$\widetilde{H}_{0T} = h_0(x_{0T}) = \beta G(x_{0T_1}; x_{0T_2}) \ , \tag{2.36}$$

where $x_{0T_1} = x_0(\tau - T)$, and $x_{0T_2} = x_0(\tau - 2T)$. Substituting (2.36) into (2.28) gives

$$\dot{x}_0 = -\frac{G_x^-(x_{0T_1}; x_{0T_2}) + G_x^+(x_{0T_1}; x_{0T_2})}{G(x_{0T_1}; x_{0T_2})} \ . \tag{2.37}$$

Therefore, for $0 < x < L$, using the initial time-scale gives the following asymptotic DDE for the motion of the spike:

$$\frac{dx_0}{dt} = -\epsilon^2 \left(\frac{\sinh\left(x_{0T_1} + x_{0T_2} - L\right)}{\cosh\left(x_{0T_1} - L\right) \cosh\left(x_{0T_2}\right)} \right) \ . \tag{2.38}$$

Similar to the previous result given in (2.33), we have delay appearing in every term of the quasi-equilibrium equation (2.38), but with two different values. In Figure 2.3 we compare this asymptotic result with the full numerical simulation of the system in (2.34). In §2.2, we numerically analyze the stability of the equilibrium solution

for the spike position obtained from (2.38) and we compare these results to the full numerical simulation of the corresponding PDE system in (2.34). We find that a Hopf bifurcation occurs for some values of the delay T and we illustrate in the section Figures the effect of increasing delay, beyond the critical Hopf value, on the stability of the equilibrium solution.

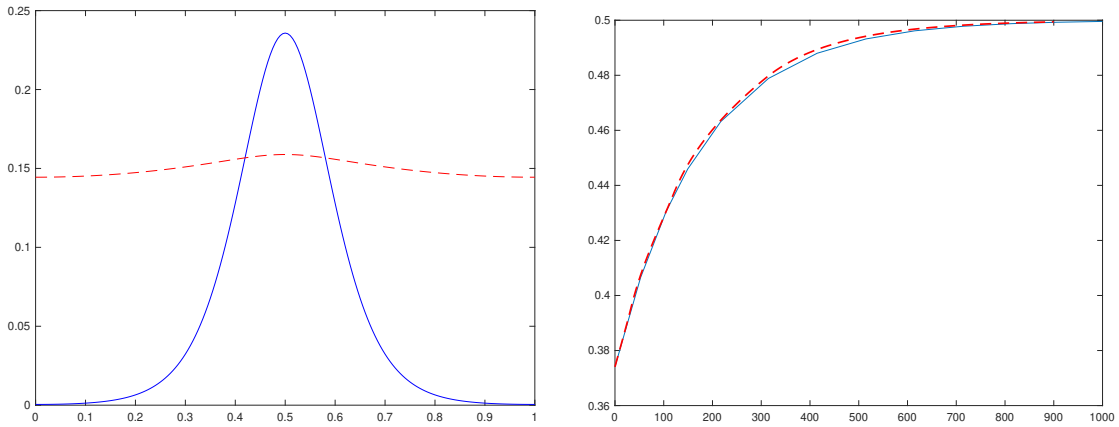

(a) (b)

Figure 2.3: Left: Plot of a one-spike equilibrium solution to (2.34), with delay in both the activator regulation and inhibitor production. The solid curve is the activator concentration and the dotted curve is the inhibitor concentration. Right: Plot of the trajectory $x_0(t)$ versus time t. The dotted curve shows the full numerical simulation of (2.34), and the solid curve is the asymptotic result computed from (2.38). Parameter values are as in the caption of Figure 2.1.

2.1.4 Delay in the Activator Regulation and Catalyzation

In this subsection, we analyze the more difficult problem where the nonlinear term of the activator equation is delayed. The PDEs for this model are given by

$$a_t = \epsilon^2 a_{xx} - a + \frac{a_T^2}{h_T} , \qquad 0 < x < L , \ t > 0 , \tag{2.39a}$$

$$0 = D h_{xx} - \mu h + \frac{a^2}{\epsilon} , \qquad 0 < x < L , \ t > 0 , \tag{2.39b}$$

with the same boundary conditions and assumptions used for the model in (2.1).

Placing the delay in the nonlinear term of the activator equation changes the dynamics of the system and makes it quite difficult to analyze. To simplify the analysis, we assume localized activator concentrations.

In the inner region, we let $x_0(\tau)$ be the center of the spike, where $\tau = \epsilon^2 t$. In terms of the inner coordinate y and the inner variables $A(y)$ and $H(y)$, as defined in (2.2) and (2.3), respectively, we can rewrite (2.39) as

$$-\epsilon A' \dot{x}_0 = A'' - A + \frac{A_T^2}{H_T} \ , \qquad -\infty < y < \infty \ , \tag{2.40a}$$

$$0 = \frac{D}{\epsilon^2} H'' - \mu H + \frac{A^2}{\epsilon} \ , \qquad -\infty < y < \infty \ . \tag{2.40b}$$

By definition, we have that

$$A_T = A\left(\frac{x - x_0(\tau - T)}{\epsilon}\right) = A\left(\frac{x - x_0(\epsilon^2 t - \epsilon^2 T)}{\epsilon}\right) \ . \tag{2.41}$$

Using the expansion

$$x_0(\epsilon^2 t - \epsilon^2 T) \approx x_0(\epsilon^2 t) - \epsilon^2 T \dot{x}_0 + \ldots = x_0(\tau) - \epsilon^2 T \dot{x}_0 + \ldots \ , \tag{2.42}$$

we rewrite (2.41) as

$$A_T \approx A\left(\frac{x - x_0(\tau) + \epsilon^2 T \dot{x}_0}{\epsilon}\right) = A\left(y + \epsilon T \dot{x}_0\right) \ . \tag{2.43}$$

Expanding the right hand side of (2.43) gives

$$A_T \approx A(y) + \epsilon \ T \dot{x}_0 A' \ . \tag{2.44}$$

Using the inner variable expansion in (2.5), and the approximation

$$A_{0T} \approx A_0 + \epsilon \ T \dot{x}_0 A_0' \ , \qquad A_{1T} \approx A_1 + \epsilon \ T \dot{x}_0 A_1' \ , \tag{2.45}$$

equation (2.40a), to leading order, becomes

$$\begin{aligned} -\epsilon A_0' \dot{x}_0 =& A_0'' - A_0 + \frac{A_0^2}{H_{0T}} \\ &+ \epsilon \left[A_1'' - A_1 + 2\frac{A_0}{H_{0T}} A_1 - \frac{A_0^2}{H_{0T}^2} H_{1T} + 2T \frac{A_0}{H_{0T}} A_0' \dot{x}_0 \right] + O(\epsilon^2) \ . \end{aligned} \tag{2.46}$$

It follows that

$$0 = A_0'' - A_0 + \frac{A_0^2}{H_{0T}} \ , \tag{2.47a}$$

$$A_1'' - A_1 + 2\frac{A_0}{H_{0T}} A_1 = -A_0' \dot{x}_0 \left[1 + 2T \frac{A_0}{H_{0T}}\right] + \left(\frac{A_0}{H_{0T}}\right)^2 H_{1T} \ . \tag{2.47b}$$

The $O(1)$ equations for the model in (2.39) are

$$0 = A_0'' - A_0 + \frac{A_0^2}{H_{0T}} \ , \qquad -\infty < y < \infty \ , \tag{2.48a}$$

$$0 = DH_0'' \ , \qquad -\infty < y < \infty \ , \tag{2.48b}$$

and thus we get that $H_0(y) \approx \widetilde{H}_0$, for some constant $\widetilde{H}_0$ to be determined. The solution A_0 to (2.48a) is given by $A_0 = \widetilde{H}_{0T}\ w(y)$, where $w(y)$ satisfies (2.8). For the next order expansion given in (2.47b), we introduce the operator $L(A_1)$ such that

$$L(A_1) \equiv A_1'' - A_1 + 2\frac{A_0}{H_{0T}}A_1 = -A_0'\dot{x}_0\left[1 + 2T\frac{A_0}{H_{0T}}\right] + \left(\frac{A_0}{H_{0T}}\right)^2 H_{1T} \ . \tag{2.49}$$

Since $A_0 = \widetilde{H}_{0T}\ w(y)$, we can rewrite equation (2.49) as

$$L(A_1) \equiv A_1'' - A_1 + 2wA_1 = -\dot{x}_0\left[A_0' + 2\ T\ A_0'w\right] + \left(\frac{A_0}{\widetilde{H}_{0T}}\right)^2 H_{1T} \ . \tag{2.50}$$

As before, we have that the right hand side of (2.50) must be orthogonal to w'. Using this solvability condition and integrating by parts twice gives

$$\begin{aligned} \dot{x}_0\left[\int_{-\infty}^{\infty}(w')^2\ dy + 2T\int_{-\infty}^{\infty} w\,(w')^2\ dy\right] \\ = -\frac{1}{6\widetilde{H}_{0T}}\left(\int_{-\infty}^{\infty} w^3\ dy\right)\left[H_{1T}'(\infty) + H_{1T}'(-\infty)\right] \ , \end{aligned} \tag{2.51}$$

where we again use the even property of H_1'' and $w(y)$.

In the outer region, in terms of the Green's function (2.16b), we have that $\widetilde{H}_{0T}$ satisfies (2.31). Substituting this solution into (2.51) and simplifying gives

$$\dot{x}_0 = -\left(\frac{7}{7+12T}\right)\frac{G^-_{x_T} + G^+_{x_T}}{G(x_{0T}; x_{0T})} \ , \tag{2.52}$$

where $G^-_{x_T}$ and $G^+_{x_T}$ are as defined in (2.32b). In terms of the initial time-scale, we get the following asymptotic DDE for the motion of the spike:

$$\frac{dx_0}{dt} = -\epsilon^2\left(\frac{7}{7+12T}\right)\left(\frac{\sinh\left(2x_{0T} - L\right)}{\cosh\left(x_{0T} - L\right)\cosh\left(x_{0T}\right)}\right) \ . \tag{2.53}$$

In Figure 2.4, we compare this asymptotic result with the one obtained numerically for the full system in (2.39). We also give numerical examples in §2.2 to show that the equilibrium solution is stable for all values of the delay T, and therefore no Hopf bifurcation is observed in the position of the spike.

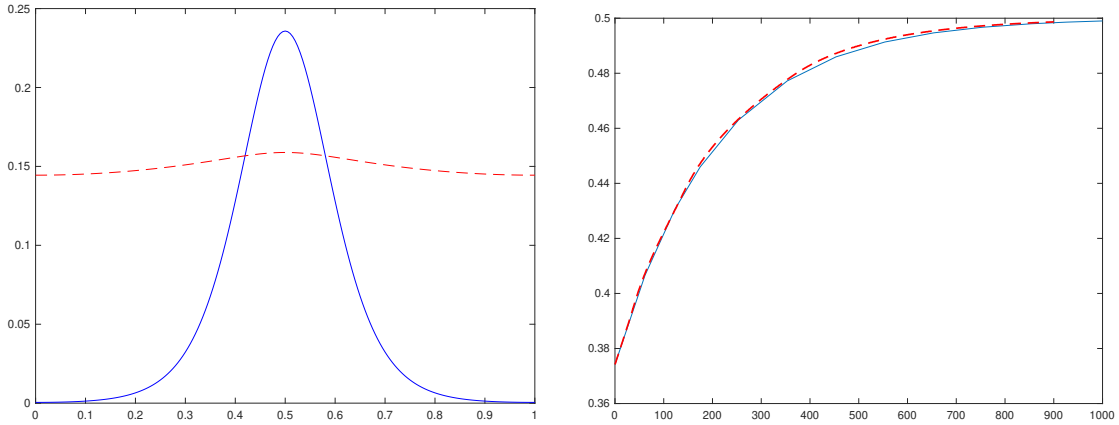

(a) (b)

Figure 2.4: Left: Plot of a one-spike equilibrium solution to (2.39), with delay in the activator regulation and catalyzation. The solid curve is the activator concentration and the dotted curve is the inhibitor concentration. Right: Plot of the trajectory $x_0(t)$ versus time t. The dotted curve shows the full numerical simulation of (2.39), and the solid curve is the asymptotic result computed from (2.53). Parameter values are as in the caption of Figure 2.1.

2.1.5 Delay in All Nonlinear Terms in Both Equations

We now use the analysis and results in §2.1.3 and §2.1.4 to derive the DDE corresponding to the following model where the nonlinear terms of both equations are delayed:

$$a_t = \epsilon^2 a_{xx} - a + \frac{a_T^2}{h_T} , \qquad 0 < x < L , \ t > 0 , \tag{2.54a}$$

$$0 = D h_{xx} - \mu h + \frac{a_T^2}{\epsilon} , \qquad 0 < x < L , \ t > 0 , \tag{2.54b}$$

$$a_x(0,t) = a_x(L,t) = h_x(0,t) = h_x(L,t) = 0 . \tag{2.54c}$$

In the original time-scale, the DDE for the motion of the spike corresponding to the system in (2.54) is given by

$$\frac{dx_0}{dt} = -\epsilon^2 \left(\frac{7}{7 + 12 T_1} \right) \left(\frac{\sinh\left(x_{0T_1} + x_{0T_2} - L\right)}{\cosh\left(x_{0T_1} - L\right) \cosh\left(x_{0T_2}\right)} \right) , \text{ where } T_2 = 2\, T_1 . \tag{2.55}$$

Numerical analysis for this model is provided in §2.2. We again find a close agreement between the asymptotic and the full numerical results obtained from (2.55) and (2.54), respectively, as shown in Figure 2.5. Numerical verification again supports the stability of the equilibrium solution for all values of the delay T, and no

Hopf bifurcation is observed in the position of the spike.

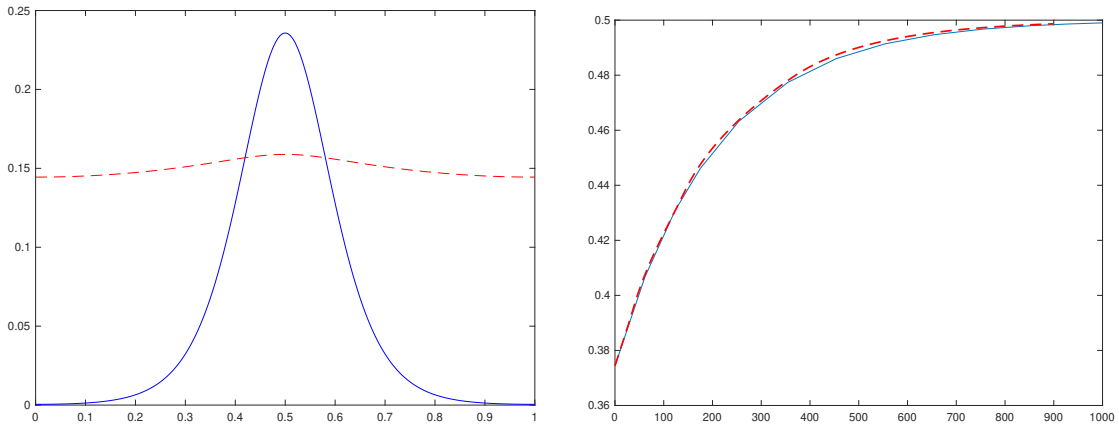

(a) (b)

Figure 2.5: Left: Plot of a one-spike equilibrium solution to (2.54), with delay in all the nonlinear terms of both equations. The solid curve is the activator concentration and the dotted curve is the inhibitor concentration. Right: Plot of the trajectory $x_0(t)$ versus time t. The dotted curve shows the full numerical simulation of (2.54), and the solid curve is the asymptotic result as obtained from (2.55). Parameter values are as in the caption of Figure 2.1.

We remark that the one-spike plots in Figures 2.1-2.5 are almost the same for all the cases considered.

2.2 Hopf Bifurcation in the Reduced Equation for Spike Position

In this section, we consider how increasing the delay can bring about oscillations in the spike position for the reduced system. It is also possible for the large eigenvalues to undergo a Hopf bifurcation resulting in oscillation of the spike amplitudes. This will be considered in §2.3. For the delay models in §2.1, the spikes evolve on a slow $O(\epsilon^2)$ time-scale. We consider here the slowly moving spike as a quasi-equilibrium solution and analyze its stability by determining critical delay values at which a Hopf bifurcation occurs. The scaling of the critical delay for this Hopf bifurcation will thus be $O(\epsilon^{-2})$. The critical delay for Hopf bifurcation considered in §2.3 will be scaled as $O(1)$ in ϵ, so in general a Hopf bifurcation of the large eigenvalues will occur for smaller critical delay then that of the small eigenvalue.

In §2.1, we derived asymptotic DDEs of the form

$$\frac{dx_0}{dt} = f(x_0, x_{0T}) \ , \qquad 0 < x < L \ . \tag{2.56}$$

We introduce a small perturbation to the equilibrium position

$$x_0(t) = x_0 + e^{\lambda t}\eta \ , \qquad \text{where } |\eta| << |x_0| \ , \tag{2.57}$$

and we substitute (2.57) into (2.56) to get the following nonlinear transcendental eigenvalue equation for λ:

$$\frac{dx_0}{dt} + \lambda e^{\lambda t}\eta = f(x_0, x_{0T}) + f_{x_0}(x_0, x_{0T})e^{\lambda t}\eta + f_{x_{0T}}(x_0, x_{0T})e^{\lambda(t-T)}\eta \ . \tag{2.58}$$

Since x_0 is a solution to (2.56), therefore (2.58) simplifies to

$$\lambda = f_{x_0}(x_0, x_{0T}) + f_{x_{0T}}(x_0, x_{0T})e^{-\lambda T} \ . \tag{2.59}$$

Our goal is to solve (2.59) for critical values of the delay T which give rise to pure imaginary eigenvalues. Setting $\lambda = i\omega$, for some positive $\omega \in \mathbb{R}$, in (2.59) and rearranging gives

$$\cos(\omega T) - i\sin(\omega T) = -\frac{f_{x_0}}{f_{x_{0T}}} + i\frac{\omega}{f_{x_{0T}}} \ . \tag{2.60}$$

Comparing the real and imaginary parts on both sides of equation (2.60), gives that ω and the time delay T parameters must satisfy the following system of equations:

$$f_{x_0} + f_{x_{0T}}\cos(\omega T) = 0 \ , \qquad f_{x_{0T}}\sin(\omega T) = -\omega \ . \tag{2.61}$$

Without loss of generality, we now look for a positive solution (ω_H, T_H) satisfying the equations in (2.61).

First, we consider the right hand side of (2.21). In terms of the initial time-scale, we have that

$$f(x_0, x_{0T}) = -\epsilon^2\left(\frac{\sinh(x_0)\cosh(x_{0T} - L) + \cosh(x_{0T})\sinh(x_0 - L)}{\cosh(x_{0T})\cosh(x_0 - L)}\right) \ , \tag{2.62}$$

with partial derivatives

$$f_{x_{0T}} = -\epsilon^2\left(\frac{\sinh(x_0)\sinh(L)}{\cosh^2(x_{0T})\cosh^2(x_0 - L)}\right) \ , \tag{2.63}$$

$$f_{x_0} = -2\epsilon^2\left(\frac{3\cosh(x_{0T}) + \cosh(x_{0T} - 2L)}{\cosh(2x_0 - x_{0T} - 2L) + \cosh(2x_0 + x_{0T} - 2L) + 2\cosh(x_{0T})}\right) \ .$$

At the equilibrium position $x_0 = x_{0T} = L/2$, substituting (2.63) into (2.61) yields

$$\cos(\omega T) = -\frac{f_{x_0}}{f_{x_{0T}}} = -\frac{\cosh(L)+1}{\cosh(L)-1} = \coth^2(L/2) > 1 \ . \tag{2.64}$$

This is a contradiction to the property of the cosine function which requires that $|\cos(\omega T)| \leq 1$. It follows that no positive real solution (ω_H, T_H) exists, and no Hopf bifurcation is observed in this case. This result is verified by numerical simulations of the full PDE model in (2.1) and the asymptotic result obtained from (2.21) for the position of the spike. In Figure 2.1(a), we plot the equilibrium solution to (2.1). Spike position $x_0 = L/2$ is stable, and the slow moving spike tends towards this stable equilibrium for any choice of T, as shown in Figure 2.6.

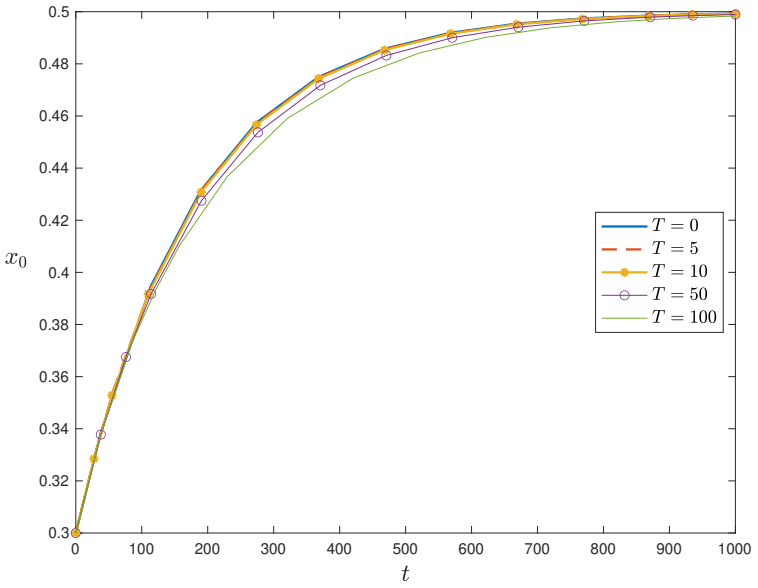

Figure 2.6: Plot of trajectories $x_0(t)$ computed from the asymptotic DDE (2.21) for the motion of the spike versus time t, for various values of delay in the nonlinear term of the inhibitor equation. Initial condition as indicated. No oscillations are observed in this case, and all trajectories approach the stable equilibrium position $x_0 = 0.5$. Parameter values are $\epsilon = 0.06$, $L = 1$, $\mu = 1$, and $D = 1$.

For the result in (2.33), where delay appears in every term of the DDE, the asymptotic result is validated when compared to the full numerical simulation of (2.22). Moreover, we have that

$$f(x_0, x_{0T}) = -\epsilon^2 \left(\frac{\sinh(2x_{0T} - L)}{\cosh(x_{0T})\cosh(x_{0T} - L)} \right) \ , \tag{2.65}$$

$$f_{x_{0T}} = -\epsilon^2 \left(\frac{2\cosh(2x_{0T} - L)\cosh(x_{0T} - L)\cosh(x_{0T}) - \sinh^2(2x_{0T} - L)}{\cosh^2(x_{0T})\cosh^2(x_{0T} - L)} \right) \ .$$

From (2.59), we get that

$$\lambda = f_{x_{0T}}(x_0, x_{0T})e^{-\lambda T} \ . \tag{2.66}$$

Substituting $\lambda = i\omega$ into (2.66), and comparing the real and imaginary parts on both sides of the equation gives

$$i\omega = \frac{\partial f}{\partial x_{0T}} e^{-i\omega T} \qquad \Longleftrightarrow \qquad \begin{cases} f_{x_{0T}} \cos(\omega T) = 0 \ , \\ f_{x_{0T}} \sin(\omega T) = -\omega \ . \end{cases} \tag{2.67}$$

A solution to (2.67) can be calculated explicitly. At equilibrium position $x_{0T} = L/2$, (2.67) becomes

$$2\epsilon^2 \operatorname{sech}^2(L/2) \cos(\omega T) = 0 \ , \qquad 2\epsilon^2 \operatorname{sech}^2(L/2) \sin(\omega T) = \omega \ . \tag{2.68}$$

The first equation yields

$$\cos(\omega T) = 0 \ , \qquad \text{which is satisfied when} \quad \omega T = \pi/2 \ . \tag{2.69}$$

Substituting $\omega T = \pi/2$ into the second equation gives the solution

$$\omega_H = 2\epsilon^2 \operatorname{sech}^2(L/2) \ , \qquad T_H = \frac{\pi}{4} \ \epsilon^{-2} \cosh^2(L/2) \ . \tag{2.70}$$

The results are given in Figure 2.7, where we plot the solutions T_H and ω_H for various values of L. For $L = 2$, using $\epsilon = 1$ to account for the slow time-scale of the spike motion, we compute $T_H = 1.870$ and $\omega_H = 0.8399$.

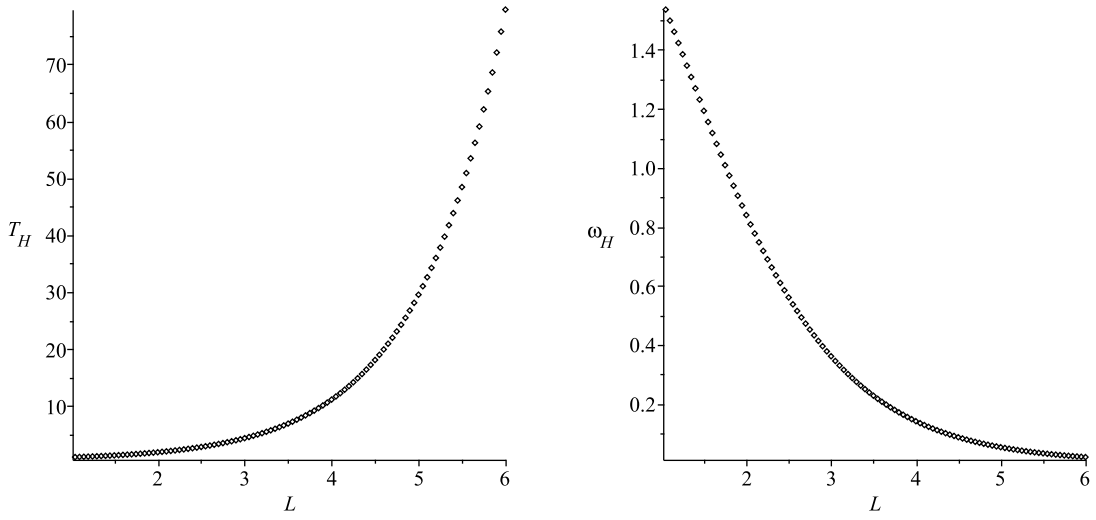

(a) T_H versus L (b) ω_H versus L

Figure 2.7: Solutions to (2.67) for various values of L, using $\epsilon = 1$ to account for the slow time-scale of the spike motion.

These results are verified numerically, as illustrated in Figure 2.8. We find that for delay $T < T_H$ the real part of λ is negative which gives rise to decaying oscillations that approach the stable equilibrium $x_0 = L/2$. However, for $T > T_H$, the equilibrium solution is destabilized as the eigenvalue crosses the imaginary axis and the real part of λ becomes positive giving rise to sustained oscillations.

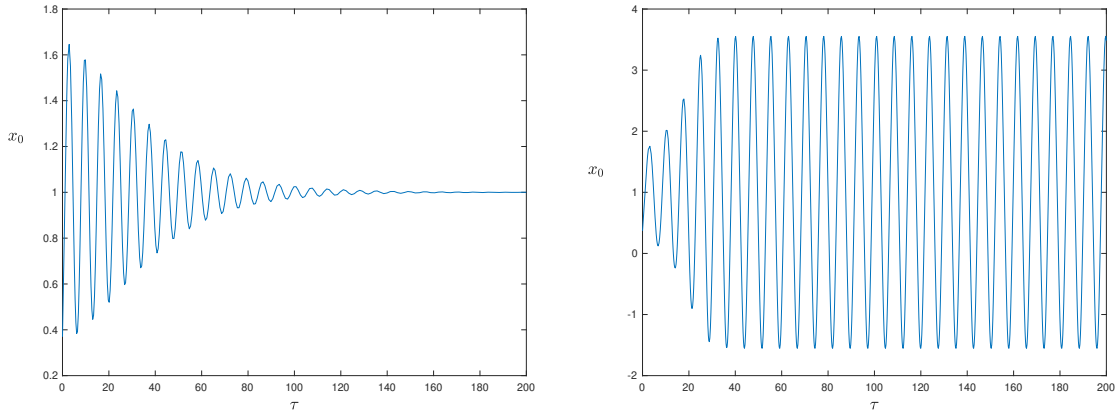

(a) $T = 1.7 < T_H$ (b) $T = 1.9 > T_H$

Figure 2.8: Plot of trajectories $x_0(\tau)$ versus τ, as computed from the asymptotic DDE (2.33) for the motion of the spike, with delay in the h term of the activator equation. Numerical simulations show decaying oscillations when $T = 1.7 < T_H$ (left figure) and sustained oscillations when $T = 1.9 > T_H$ (right figure). Parameters used are $\epsilon = 1$ (slow time-scale of motion), $L = 2$, $\mu = 1$, and $D = 1$.

Next, we consider the asymptotic result in (2.38), where

$$\frac{dx_0}{dt} = f(x_{0T_1}, x_{0T_2}) = -\epsilon^2 \left(\frac{\sinh\left(x_{0T_1} + x_{0T_2} - L\right)}{\cosh\left(x_{0T_1} - L\right)\cosh\left(x_{0T_2}\right)} \right) \ , \tag{2.71}$$

where $T_2 = 2\ T_1$.

$$f_{x_{0T_1}} = -\epsilon^2 \operatorname{sech}^2\left(x_{0T_1} - L\right) \ , \qquad f_{x_{0T_2}} = -\epsilon^2 \operatorname{sech}^2\left(x_{0T_2}\right) \ . \tag{2.72}$$

Substituting the small perturbation (2.57) into (2.71) gives the transcendental eigenvalue equation

$$\lambda = f_{x_{0T_1}} e^{-\lambda T_1} + f_{x_{0T_2}} e^{-\lambda T_2} \ , \qquad \text{where} \ \ T_2 = 2\ T_1 \ . \tag{2.73}$$

Setting $\lambda = i\omega$ in (2.73), and comparing the real and imaginary parts on both sides of the equation, gives that ω and delays T_1 and T_2 must satisfy the following system

of equations:

$$\begin{aligned} f_{x_{0T_1}} \cos(\omega T_1) + f_{x_{0T_2}} \cos(\omega T_2) &= 0 \ , \\ f_{x_{0T_1}} \sin(\omega T_1) + f_{x_{0T_2}} \sin(\omega T_2) &= -\omega \ . \end{aligned} \tag{2.74}$$

Using $T_2 = 2T_1 = 2T$ and $x_{0T} = L/2$, the system in (2.74) becomes

$$\epsilon^2 \ \frac{\cos(\omega T) + \cos(2\omega T)}{\cosh^2(L/2)} = 0 \ , \qquad \epsilon^2 \ \frac{\sin(\omega T) + \sin(2\omega T)}{\cosh^2(L/2)} = \omega \ . \tag{2.75}$$

The first equation is satisfied when

$$\omega T = \frac{\pi}{3} \qquad \text{or} \qquad \omega T = \pi \ . \tag{2.76}$$

Since $\omega > 0$ by assumption, the equations in (2.75) hold simultaneously only when $\omega T = \pi/3$. This yields the solution

$$\omega_H = \sqrt{3} \ \epsilon^2 \operatorname{sech}^2(L/2) \ , \qquad T_H = \frac{\pi}{3\sqrt{3}} \ \epsilon^{-2} \cosh^2(L/2) \tag{2.77}$$

In Figure 2.9, we plot critical values of T and ω for various values of L. For $L = 2$, using $\epsilon = 1$ (slow time-scale of motion), we find $T_H \sim 1.44$ and $\omega_H \sim 0.727$.

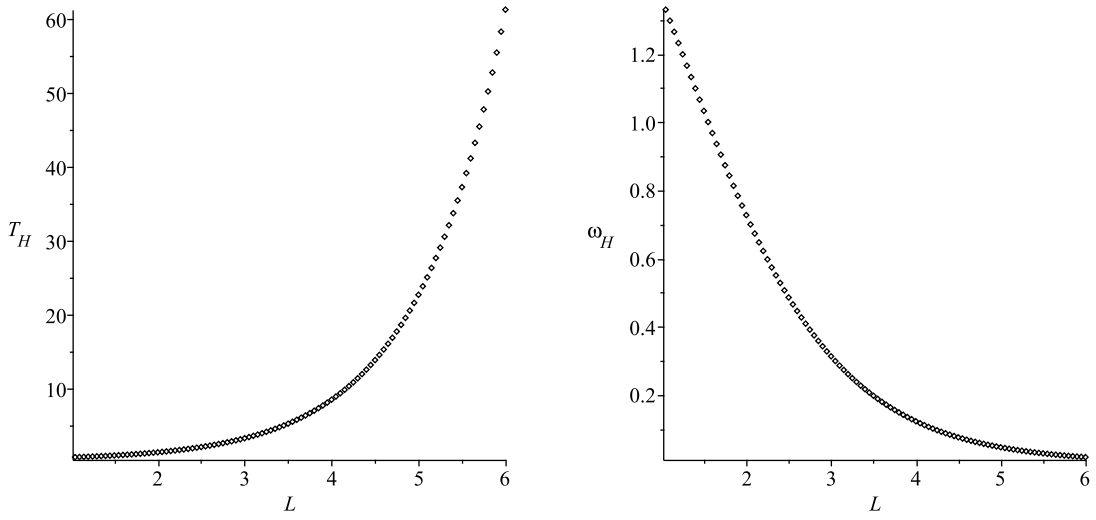

(a) T_H versus L (b) ω_H versus L

Figure 2.9: Solutions to (2.74) for a range of L, using $\epsilon = 1$ (slow time-scale of motion).

The asymptotic DDE for this case is validated when compared to the full numerical simulation, as shown in Figure 2.3. Moreover, as illustrated in Figure 2.10, for

delay less than the critical value we have that the real part of the eigenvalue is negative and the decaying oscillations approach the stable equilibrium position $x_0 = L/2$. However, as we increase the delay beyond the Hopf value, the equilibrium solution is destabilized as the eigenvalue crosses the imaginary axis resulting in sustained oscillations.

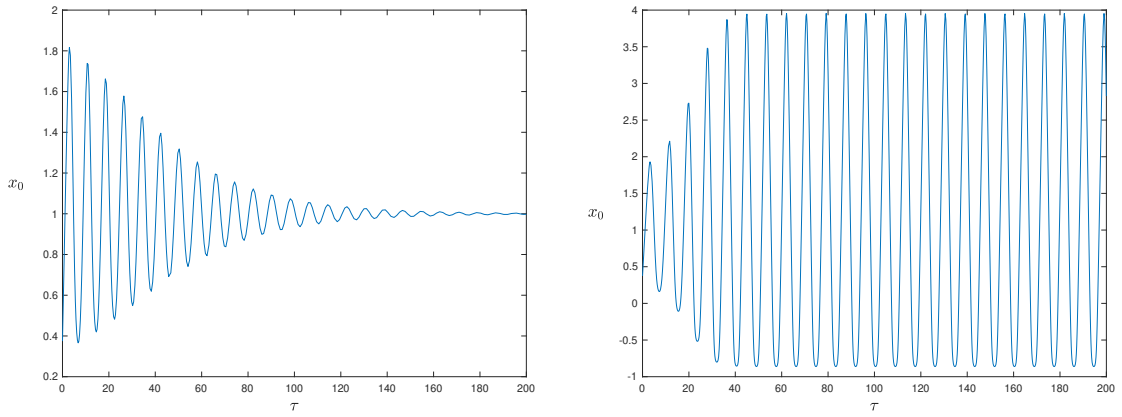

(a) $T = 1.3 < T_H$ (b) $T = 1.45 > T_H$

Figure 2.10: Plot of trajectories $x_0(\tau)$ versus τ, as computed from the asymptotic DDE (2.38) for the motion of the spike, with delay in both the activator regulation and inhibitor production. Numerical simulations show decaying oscillations when $T = 1.3 < T_H$ (left figure) and sustained oscillations when $T = 1.45 > T_H$ (right figure). Parameters values are as in the caption of Figure 2.8.

Similarly, for the result in (2.53) we have that

$$f(x_{0T}, x_0) = -\epsilon^2 \left(\frac{7}{7+12T}\right)\left(\frac{\sinh(2x_{0T}-L)}{\cosh(x_{0T}-L)\cosh(x_{0T})}\right) , \tag{2.78}$$

$$f_{x_{0T}} = -\epsilon^2 \left(\frac{7}{7+12T}\right)\left(\frac{2\cosh(2x_{0T}-L)\cosh(x_{0T}-L)\cosh(x_{0T}) - \sinh^2(2x_{0T}-L)}{\cosh^2(x_{0T}-L)\cosh^2(x_{0T})}\right) ,$$

with the same eigenvalue problem as in (2.67). With $x_{0T} = L/2$, we get that the derivative $f_{x_{0T}} = -\epsilon^2 \left(\frac{14}{7+12T}\right) \operatorname{sech}^2(L/2)$, and thus ω and T must satisfy the two equations

$$\epsilon^2 \left(\frac{14\operatorname{sech}^2(L/2)}{7+12T}\right)\cos(\omega T) = 0 , \quad \epsilon^2 \left(\frac{14\operatorname{sech}^2(L/2)}{7+12T}\right)\sin(\omega T) = \omega . \tag{2.79}$$

From the first equation, we get that $\omega T = \pi/2$. Thus, the second equation is satisfied only when

$$\omega = 2\epsilon^2 \operatorname{sech}^2(L/2) - \frac{6}{7}\pi . \tag{2.80}$$

However, since $\operatorname{sech}(L/2) < 1$ and ϵ is very small by assumption, (2.80) implies that $\omega < 0$, which is a contradiction to our assumption that $\omega > 0$. It follows that no positive solution (ω_H, T_H) exists in this case, and the spike solution is stable for all values of delay T. In Figure 2.4, we compare the asymptotic DDE with the full numerical simulation, and in Figure 2.11 the results above are validated with numerical simulations, where we plot various trajectories of the asymptotic solution $x_0(t)$ for increasing values of delay as they approach the stable equilibrium position $x_0 = L/2$.

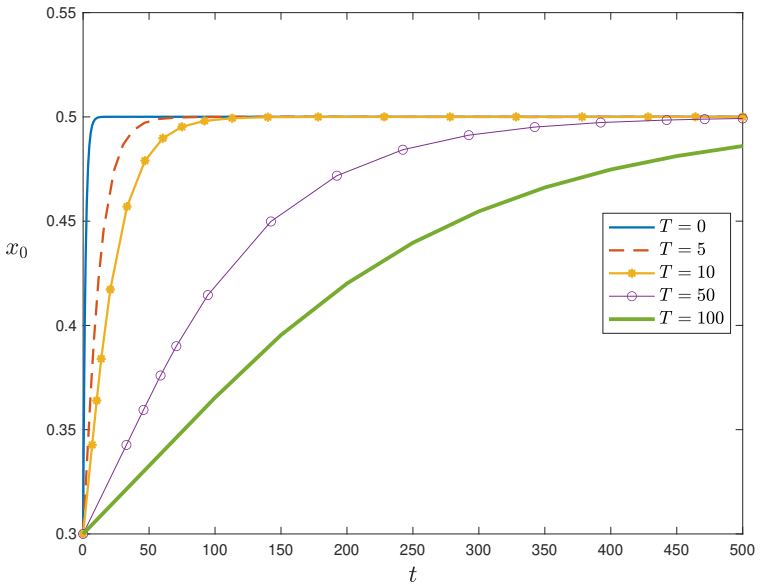

Figure 2.11: Plot of trajectories $x_0(t)$ computed from the asymptotic DDE (2.53) for the motion of the spike versus time t, for various values of delay in the nonlinear term of the activator equation. Initial condition as indicated. No oscillations are observed in this case, and all trajectories approach the stable equilibrium position $x_0 = 0.5$. Parameter values are $\epsilon = 0.6$, $L = 1$, $\mu = 1$, and $D = 1$.

A similar outcome to the one illustrated in Figure 2.11 is obtained when the full PDE model (2.54) and the asymptotic DDE (2.55) are numerically analyzed. As in the previous case, for $\epsilon < 1$, there is no positive solution (ω, T) such that (2.67) is satisfied, and all trajectories $x_0(t)$ approach the stable equilibrium $x_0 = L/2$ for all values of the time delay parameter T.

2.3 Stability Analysis for the Spike Profile: Formulation of Nonlocal Eigenvalue Problem

In this section, we consider various cases of the GM model with fixed time delay, analyzed in §2.1, and we study oscillatory-type instabilities in the height of the one-spike solution for each model. This analysis is an extension of the work done in [77] with no delay. We begin by formulating the NLEP in each case, and we find conditions for the onset of a Hopf bifurcation. The results are then compared with the full numerical simulation of the system.

For the model in (2.1), with delay in the inhibitor equation, we assume $0 < \sigma \ll 1$ and $D = O(1)$. By symmetry, the spike location is $x_0 = L/2$. Using the notation in [77], as $\epsilon \to 0$, the one-spike equilibrium solution to (2.1) is given by

$$a_e(x) \sim \widetilde{H}_0 \; w\left(\frac{x - x_0}{\epsilon}\right) \;, \quad h_e(x) \sim \frac{\widetilde{H}_0}{a_g} \; G(x; x_0) \;, \qquad 0 < x < L \;, \tag{2.81}$$

where $w(y)$ is the unique positive solution given in (2.8), $G(x; x_0)$ is the Green's function in (2.16), and

$$\widetilde{H}_0 = \frac{1}{b_w \; a_g} \;, \qquad b_w = \int_{-\infty}^{\infty} w^2 \; dy = 6 \;, \qquad a_g = G(x_0; x_0) \;. \tag{2.82}$$

To analyze the stability of the equilibrium solution (2.81), we introduce the small perturbations

$$a = a_e + e^{\lambda t}\phi \;, \quad h = h_e + e^{\lambda t}\eta \;, \qquad \text{where} \quad \phi \ll a_e \;, \eta \ll h_e \;. \tag{2.83}$$

Substituting (2.83) into the original PDE model (2.1) gives the following eigenvalue problem:

$$\lambda\phi = \epsilon^2\phi_{xx} - \phi + 2 \; \frac{a_e}{h_e} \; \phi - \frac{a_e^2}{h_e^2} \; \eta \;, \qquad 0 < x < L \;, \tag{2.84a}$$

$$D\eta_{xx} - \mu\eta = -2 \; \frac{a_e}{\epsilon} \; e^{-\lambda T}\phi \;, \qquad 0 < x < L \;, \tag{2.84b}$$

with the Neumann boundary conditions

$$\phi_x(0) = \phi_x(L) = \eta_x(0) = \eta_x(L) = 0 \;. \tag{2.84c}$$

We introduce the new variables

$$\phi = \widetilde{H}_0 \; \bar{\phi} \;, \qquad h_e = \widetilde{H}_0 \; v \;, \qquad \eta = \widetilde{H}_0 \; \bar{\eta} \;. \tag{2.85}$$

Substituting (2.81) and (2.85) into (2.84), and dropping the bar notation, yields the eigenvalue problem

$$\lambda\phi = \epsilon^2\phi_{xx} - \phi + 2\,\frac{w}{v}\phi - \frac{w^2}{v^2}\eta\ , \qquad 0 < x < L\ , \tag{2.86a}$$

$$D\eta_{xx} - \mu\eta = -\frac{2\ e^{-\lambda T}\ w}{\epsilon\ b_w\ a_g}\ \phi\ , \qquad 0 < x < L\ , \tag{2.86b}$$

with boundary conditions (2.84c). The constants b_w and a_g are as defined in (2.82).

As shown in [34] and [77], using the symmetry of the equilibrium solution and the localization of the coefficients in (2.86), we seek a localized eigenfunction $\phi(x)$ of the form

$$\phi(x) \sim C_0\ \Phi\left(\frac{x - x_0}{\epsilon}\right)\ , \qquad \text{where} \quad \Phi(y) \to 0 \text{ as } |y| \to \infty\ , \tag{2.87}$$

for some C_0. Since the eigenfunction $\phi(x)$ is localized near x_0, therefore we can treat the right-hand side of (2.86b) as a multiple of the Dirac delta function as $\epsilon \to 0$. Thus, for $\epsilon \ll 1$, we get that η satisfies

$$\begin{aligned} D\eta_{xx} - \mu\eta &= -\frac{2e^{-\lambda T}}{b_w a_g}\left(\int_{-\infty}^{\infty} w\Phi(y)dy\right) C_0\ \delta(x - x_0)\ , \quad 0 < x < L\ , \\ \eta_x(0) &= \eta_x(L) = 0\ . \end{aligned} \tag{2.88}$$

Using the results and conditions in [75], [77] and [78], while accounting for the effect of delay, we get that the NLEP for $\Phi(y)$ is of the form

$$\begin{aligned} L_0\Phi - \chi\ e^{-\lambda T}\ w^2\left(\frac{\int_{-\infty}^{\infty} w\Phi(y)\ dy}{\int_{-\infty}^{\infty} w^2\ dy}\right) &= \lambda\Phi, \qquad -\infty < y < \infty\ , \\ \Phi(y) \to 0 \quad \text{as} \quad |y| &\to \infty\ , \end{aligned} \tag{2.89a}$$

where the local operator L_0 and χ are defined by

$$L_0\Phi \equiv \Phi'' - \Phi + 2w\Phi\ , \qquad \chi = \frac{2}{a_g\sqrt{D}}\ . \tag{2.89b}$$

Let $\lambda_0 \neq 0$ be the eigenvalue of (2.89) with the largest real part, then $\mathrm{Re}(\lambda_0) < 0$ if $\chi > 1$ (see [75] and [78]).

As shown in [17] and [77], any unstable eigenvalue of (2.89) must be a root of $g(\lambda) = 0$, where

$$g(\lambda) = C(\lambda) - f(\lambda)\ , \quad C(\lambda) = \frac{1}{e^{-\lambda T}\chi}\ , \quad f(\lambda) = \frac{\int_{-\infty}^{\infty} w\ [L_0 - \lambda]^{-1} w^2\ dy}{\int_{-\infty}^{\infty} w^2\ dy}\ . \tag{2.90}$$

To determine the smallest positive delay value at which a Hopf bifurcation occurs, we seek pure imaginary eigenvalues along the positive imaginary axis, that satisfy (2.90). Setting $\lambda = i\lambda_I$ in (2.90) and separating the real and imaginary components give the coupled system

$$g_R(\lambda_I) = g_I(\lambda_I) = 0 \ , \tag{2.91}$$

where,

$$\begin{aligned} g_R(\lambda_I) &= C_R(\lambda_I) - f_R(\lambda_I) \ , & g_I(\lambda_I) &= C_I(\lambda_I) - f_I(\lambda_I) \ , \\ C_R(\lambda_I) &= \mathrm{Re}\left[C(i\lambda_I)\right] \ , & C_I(\lambda_I) &= \mathrm{Im}\left[C(i\lambda_I)\right] \ , \\ f_R(\lambda_I) &= \frac{\int_{-\infty}^{\infty} wL_0[L_0^2 + \lambda_I^2]^{-1} w^2 dy}{\int_{-\infty}^{\infty} w^2 dy} \ , & f_I(\lambda_I) &= \frac{\lambda_I \int_{-\infty}^{\infty} w[L_0^2 + \lambda_I^2]^{-1} w^2 dy}{\int_{-\infty}^{\infty} w^2 dy}. \end{aligned} \tag{2.92a}$$

To simplify the notation, we let $D = 1$ and $\mu = 1$. Thus, for $x_0 = L/2$ we get $a_g = \cosh^2(L/2)/\sinh(L)$, which gives

$$C_R(\lambda_I) = \frac{\cosh^2(L/2)}{2\sinh(L)} \cos(\lambda_I T) \ , \qquad C_I(\lambda_I) = \frac{\cosh^2(L/2)}{2\sinh(L)} \sin(\lambda_I T) \ . \tag{2.92b}$$

We use an iterative method to approximate the solution to (2.91), and we plot the critical values of the delay T and λ_I for various interval length values, L, in Figure 2.12.

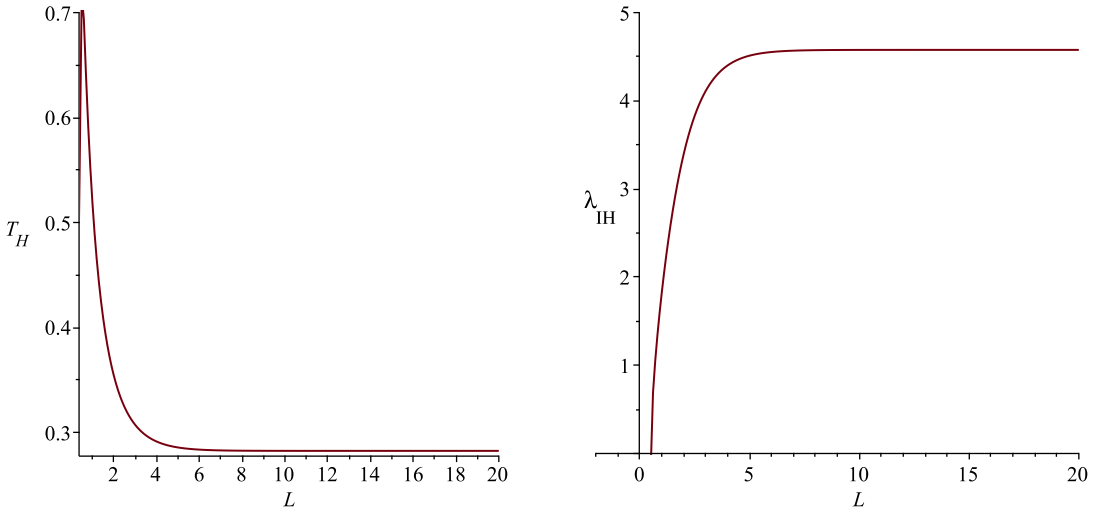

(a) T_H versus L

(b) λ_{IH} versus L

Figure 2.12: Solution to (2.91) for various values of L

For $L = 1$, we find that a Hopf bifurcation occurs at the critical parameter values

$$(\lambda_{IH}, T_H) \approx (1.829, 0.49) \ . \tag{2.93}$$

To confirm our results, we compute full numerical solutions to the system in (2.1) for delay values above and below the critical value T_H. For $L = 1$, we show that delay values higher than T_H trigger an oscillatory instability in the spike amplitude. This is shown in Figure 2.13, where we plot the amplitude of the spike $a(x_0)$ as a function of time, for T above and below T_H. The amplitude $a(x_0)$ is defined as the value of the activator concentration at the center of the spike.

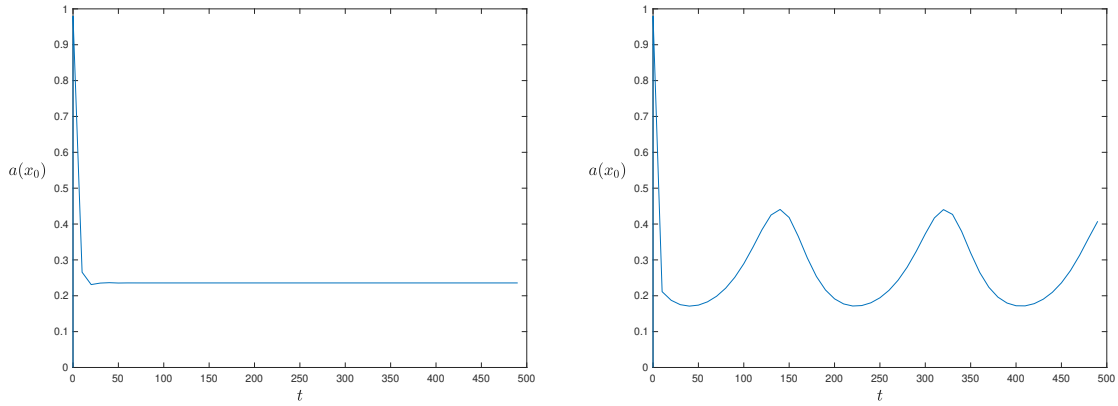

(a) $T = 0.45 < T_H$ (b) $T = 0.5 > T_H$

Figure 2.13: Plot of the spike amplitude $a(x_0)$ versus time, for (2.1). Numerical simulations show decaying(left figure) and sustained (right figure) oscillations for delay values below and above the bifurcation threshold value $T_H \approx 0.49$, respectively. Here $\epsilon = 0.06$, $L = 1$, $\mu = 1$, and $D = 1$.

The model in (2.22), with delay in the h term of the activator equation, yields the NLEP in (2.89), where χ is defined by (2.89b). Thus, the results for this case are identical to the one delay case considered above.

Next we consider the model in (2.34), where delay is in the nonlinear reaction terms of both equations. The eigenvalue problem for this case is given by

$$\lambda\phi = \epsilon^2\phi_{xx} - \phi + 2\,\frac{a_e}{h_e}\,\phi - \frac{a_e^2}{h_e^2}\,e^{-\lambda T}\,\eta \ , \quad 0 < x < L \ , \tag{2.94a}$$

$$D\eta_{xx} - \mu\eta = -2\,\frac{a_e}{\epsilon}\,e^{-\lambda T}\phi \ , \qquad 0 < x < L \ , \tag{2.94b}$$

$$\phi_x(0) = \phi_x(L) = \eta_x(0) = \eta_x(L) = 0 \ . \tag{2.94c}$$

The corresponding NLEP is given by

$$L_0\Phi - \chi\, e^{-2\lambda T}\, w^2 \left(\frac{\int_{-\infty}^{\infty} w\Phi(y)\, dy}{\int_{-\infty}^{\infty} w^2\, dy} \right) = \lambda\Phi\ , \qquad -\infty < y < \infty\ , \tag{2.95}$$
$$\Phi(y) \to 0 \quad \text{as} \quad |y| \to \infty\ ,$$

where χ is given in (2.89b). The only difference here is that the delay is multiplied by a factor of 2. Thus the critical value of delay should be half of that in the cases previously considered. In Figure 2.14, we simulate system (2.34) above and below the critical delay values.

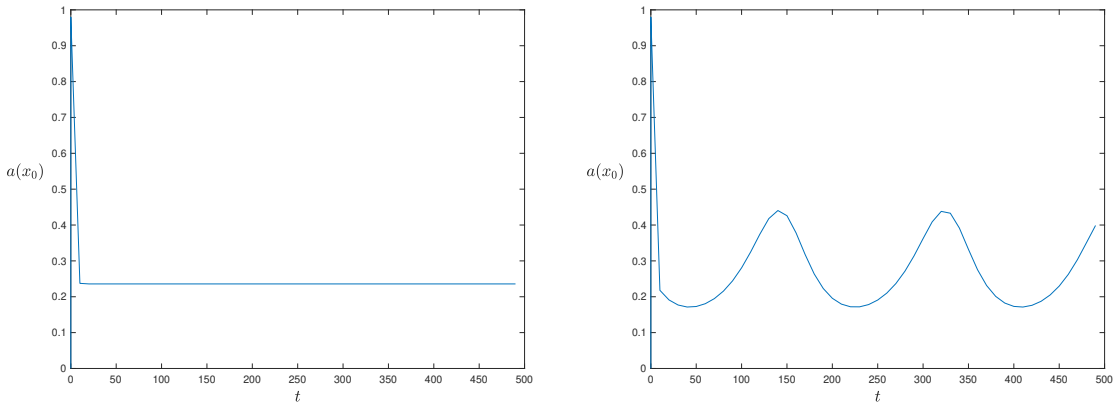

(a) $T = 0.2 < T_H$ (b) $T = 0.25 > T_H$

Figure 2.14: Plot of the spike amplitude $a(x_0)$ versus time, for (2.34). Numerical simulations show decaying(left figure) and sustained (right figure) oscillations for delay values below and above the bifurcation threshold value $T_H \approx 0.245$, respectively. Here $\epsilon = 0.06$, $L = 1$, $\mu = 1$, and $D = 1$.

We now consider the more difficult case in (2.39), where the nonlinear reaction term of the activator equation is delayed. The corresponding NLEP for $\Phi(y)$ is given by

$$\Phi'' - \Phi + 2we^{-\lambda T}\Phi - \chi e^{-\lambda T} w^2 \left(\frac{\int_{-\infty}^{\infty} w\Phi(y)\, dy}{\int_{-\infty}^{\infty} w^2\, dy} \right) = \lambda\Phi\ , \quad -\infty < y < \infty\ , \tag{2.96}$$
$$\Phi(y) \to 0 \quad \text{as} \quad |y| \to \infty\ ,$$

where χ is defined in (2.89b). Due to the presence of the right hand side term $2we^{-\lambda T}\Phi$, we are not able to utilize the methods used earlier. Instead, a numerical method is used to approximate and analyze the corresponding large eigenvalues.

Assuming $\epsilon \ll 1$, we split the right hand side of (2.96) into two parts,

$$\mathcal{A}(\Phi) \equiv \Phi'' - \Phi + 2we^{-\lambda T}\Phi \ , \quad \text{and} \quad \mathcal{B}(\Phi) \equiv \chi e^{-\lambda T} w^2 \left(\frac{\int_{-\infty}^{\infty} w\Phi(y)\ dy}{\int_{-\infty}^{\infty} w^2\ dy} \right) \ , \quad (2.97)$$

and we introduce a new operator $L_\delta\Phi$ defined by

$$L_\delta\Phi \equiv \mathcal{A}(\Phi) - \delta\mathcal{B}(\Phi) \ , \qquad -\infty < y < \infty \ . \quad (2.98)$$

We note that for $\delta = 0$ we get a Sturm-Liouville equation similar to the ones analyzed above.

Next, we discretize the finite domain problem for $\epsilon \ll 1$. The operator L_δ can be approximated using a discrete linear operator, denoted by $\mathcal{M}$, using the centered difference approximation of the second derivative for the operator $\mathcal{A}(\Phi)$, and the Trapezoidal rule approximation for $\mathcal{B}(\Phi)$. Thus the corresponding eigenvalues can be approximated by the eigenvalues of the matrix $\mathcal{M}$, denoted by $\lambda_i(\delta)$.

In the absence of delay, we set $T = 0$ and we use a continuation method where we start with an initial guess for $\delta = 0$, and we continue to track the principal eigenvalue of the matrix as δ increases. As expected, we find that $\lambda_0 \to 5/4$ as $\delta \to 0$, which is the eigenvalue corresponding to the eigenfunction $\Phi_0 = \text{sech}^2(y/2)$. Furthermore, as the value of δ is increased, we find that $\lambda_0 \approx 0$ for $\delta = 1/2$. Shortly after this point, the eigenvalues collide and eventually become complex with the real part of λ_0 remaining negative as $\delta \to 1$.

Next, we introduce delay, and we use the method of successive substitution to track the eigenvalues. We continue with this iterative method until the difference between successive iterates is less than 10^{-11}. This is repeated as the delay value T increases from 0.005 to 2.2. The results are illustrated in Figure 2.15, which shows that the real part of λ_0 remains negative as T increases. Thus, in this case the solution is stable and no oscillations are observed. We repeated the process for different values of L and similar results are found in each case. In [18] it is found that this form of delay can actually aid in the stabilization of spike solutions. Simulations of (2.39) with delay values of up to 50 resulted in stable solutions with no oscillations.

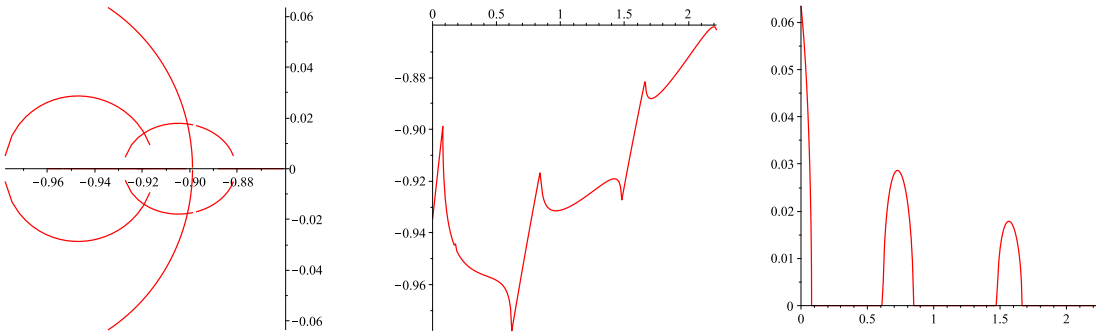

(a) $Re(\lambda_0)$ vs $Im(\lambda_0)$ (b) $Re(\lambda_0)$ vs T (c) $Im(\lambda_0)$ vs T

Figure 2.15: Plot of $Re(\lambda_0)$ and $Im(\lambda_0)$, for the eigenvalue of matrix $\mathcal{M}$, as T increases.

Finally, for the case in (2.54), where all nonlinear reaction terms are delayed, the corresponding NLEP is

$$\begin{aligned} &\Phi'' - \Phi + 2we^{-\lambda T}\Phi - \chi e^{-2\lambda T} w^2 \left(\frac{\int_{-\infty}^{\infty} w\Phi(y)\, dy}{\int_{-\infty}^{\infty} w^2\, dy} \right) = \lambda\Phi \ , \quad -\infty < y < \infty \ , \\ &\Phi(y) \to 0 \ \text{ as } \ |y| \to \infty \ , \end{aligned} \tag{2.99}$$

where χ is defined in (2.89b). The resulting system is very similar to the previous case. Again we find that no Hopf bifurcations occur as the delay is increased and simulations of the system with delay values up to fifty show no signs of oscillation.

2.4 Oscillations in Spike Position with Delayed Activator Degradation

The critical value of delay causing oscillations in the spike position scales as $O(\epsilon^{-2})$ as compared to $O(1)$ in ϵ for amplitude oscillations. For all the cases we have considered, amplitude oscillations are triggered well before the onset of oscillations in spike position. In this section, we will consider what can happen if we have delay in the degradation of the activator. The model equations are given by

$$a_t = \epsilon^2 a_{xx} - a_T + \frac{a^2}{h} \ , \qquad 0 < x < L \ , \ t > 0 \ , \tag{2.100a}$$

$$\sigma h_t = D h_{xx} - \mu h + \frac{a^2}{\epsilon} \ , \qquad 0 < x < L \ , \ t > 0 \ . \tag{2.100b}$$

We cannot justify this case biologically. However this is the only case we have found in which spike positional oscillations for the GM system can occur and the behaviour

is worthy of study. It is fairly simple to see how oscillations arise in this case. If we derive the eigenvalue problem in the usual way, we find

$$\lambda\phi = \epsilon^2\phi_{xx} - e^{-\lambda T}\phi + 2\,\frac{a_e}{h_e}\,\phi - \frac{a_e^2}{h_e^2}\,\eta\,, \qquad 0 < x < L\,, \tag{2.101a}$$

$$D\eta_{xx} - (1+\sigma\lambda)\eta = -2\,\frac{a_e}{\epsilon}\phi\,, \qquad 0 < x < L\,, \tag{2.101b}$$

with the Neumann boundary conditions

$$\phi_x(0) = \phi_x(L) = \eta_x(0) = \eta_x(L) = 0\,. \tag{2.101c}$$

Since the eigenvalues associated with the translation eigenfunctions are small, we set $\lambda = \epsilon^2\lambda_0 + \cdots$, plug into our system and expand in a Taylor Series. The first equation in (2.101) then becomes

$$(\epsilon^2\lambda_0 + \cdots)\phi = \epsilon^2\phi_{xx} - (1 - \epsilon^2\lambda_0 T + \dots)\phi + 2\,\frac{a_e}{h_e}\,\phi - \frac{a_e^2}{h_e^2}\,\eta\,, \tag{2.102}$$

which can be written as

$$(\epsilon^2\lambda_0(1-T) + \cdots)\phi = \epsilon^2\phi_{xx} - (1 + \dots)\phi + 2\,\frac{a_e}{h_e}\,\phi - \frac{a_e^2}{h_e^2}\,\eta\,. \tag{2.103}$$

The leading order term or the small eigenvalue is simply multiplied by $(1-T)$. So, as T crosses 1, the small eigenvalue changes sign. In the numerical simulations below, we find clear evidence of a Hopf bifurcation in the spike location as T increases past 1.

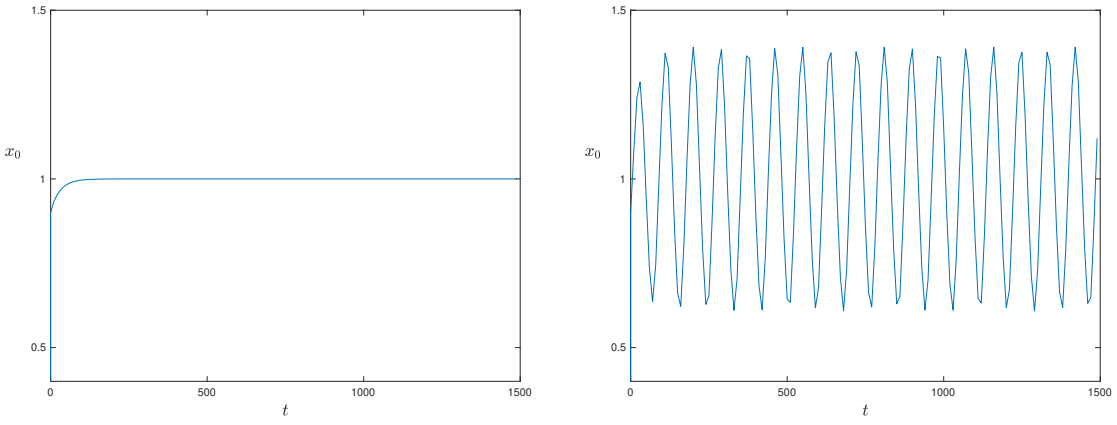

(a) $T = 0.9$ (b) $T = 1.04$

Figure 2.16: Numerical simulation of (2.100) with $\epsilon = 0.06$, $L = 2$, $\mu = 1$, and $D = 1$, for delay $T = 0.9$ (left figure) and $T = 1.04$ (right figure).

To be complete, we would need to show that at $T = 1$, the eigenvalue associated with the spike amplitude is negative. However such a calculation would require converting to a discrete operator and approximating the eigenvalue numerically. However a numerical simulation of the partial differential equations such as that illustrated in Figure 2.16(b) suggests such an eigenvalue is negative, at least in that particular case.

Chapter 3

Stability and Dynamics of k-Spike Solution to the One-Dimensional Gierer-Meinhardt Model with Delayed Reaction Kinetics

In this chapter, we construct a k-spike equilibrium solution to the GM system in (1.9), and we analyze the effect of various cases of delayed reaction kinetics on the dynamics and stability of the k-spike solution, similar to what has been done in Chapter 2. To simplify the analysis, we let $\mu = 1$, $D = 1$, and $\sigma = 0$. For the limit $\epsilon \to 0$, a k-spike equilibrium solution to (1.9), denoted by $(a_{e,k}, h_{e,k})$, satisfies the following model equations:

$$a_t = \epsilon^2 a_{xx} - a + \frac{a^2}{h} \ , \qquad 0 < x < L \ , \ t > 0 \ , \tag{3.1a}$$

$$0 = h_{xx} - h + \frac{a^2}{\epsilon} \ , \qquad 0 < x < L \ , \ t > 0 \ , \tag{3.1b}$$

$$a_x(0,t) = a_x(L,t) = h_x(0,t) = h_x(L,t) = 0 \ , \tag{3.1c}$$

where $a_{e,k} \sim 0$ except in $O(\epsilon)$ regions about each spike location.

Many recent studies have considered and analyzed the k-spike equilibrium problem for various forms of the GM model. Construction and stability dynamics of both symmetric and asymmetric k-spike equilibrium solutions to the GM system with no delay have been thoroughly studied and analyzed, (see [33, 34, 38, 75, 77, 79] and the references therein). The existence of a k-spike equilibrium solution to the one-dimensional GM system in (3.1) has been proved in [64], and a formal stability analysis is given in [79]. In [34] and [77], the authors construct asymptotically a symmetric k-spike equilibrium solution to (3.1), in the limit $\epsilon \to 0$, using the method of matched asymptotic expansions. The authors also provide a formal asymptotic analysis for studying the stability and dynamics of the solution. In our analysis, we will follow a similar approach to the one used in [34] and [77] for the construction and analysis of the equilibrium solution and the corresponding eigenvalue problem. In

addition, we will use a Floquet-based approach, as used in [37, 58, 71], to study the stability of the k-spike equilibrium solution and the associated eigenvalue problem subject to Floquet-type boundary conditions over the length of the domain.

In §3.1, we construct a k-spike equilibrium solution to (3.1) using the method of matched asymptotic expansion [34]. For a k-spike solution, the eigenvalue problem admits two types of eigenvalues: k eigenvalues of $O(\epsilon^2)$ that approach zero as $\epsilon \to 0$, referred to as small eigenvalues, and k eigenvalues of $O(1)$ that are bounded away from zero as $\epsilon \to 0$, and these are referred to as large eigenvalues. In §3.2, we analyze the stability of the small eigenvalues, through studying the derived delay differential-algebraic system of equations (DDAE) describing the dynamics of the k-spike locations for various cases of delayed kinetics. In §3.3, we find critical parameter values for position instabilities due to Hopf bifurcations. In §3.4, we study the stability of the equilibrium solution constructed in §3.1 with respect to the large eigenvalues of order $\lambda = O(1)$ for the GM model with delayed reaction kinetics. In §3.4.1, we describe the formulation of the NLEP for the case with no delay. Two cases of delayed reaction kinetics are analyzed in §3.4.2 and §3.4.3. For these cases, we show numerically that delay destabilizes the system via a Hopf bifurcation, so that oscillations in the spike amplitudes are observed as delay exceeds some threshold value.

3.1 Asymptotic Construction of k-Spike Solution

In this section, we use the method of matched asymptotic expansion, used in [34] and [77], to construct a k-spike equilibrium solution to (3.1), in the limit $\epsilon \to 0$, with equal amplitudes. In a one dimensional domain, true equilibrium solutions have equally spaced spikes. Thus, for a k-spike steady state solution, with $k \geq 1$ evenly spaced interior spikes, over the interval $[0, L]$, the spike locations satisfies

$$x_j = \frac{L}{2k} + j\ \frac{L}{k}\ , \qquad \text{for} \quad j = 0, 1, \ldots, k-1\ . \tag{3.2}$$

In Chapter 2, for a single spike solution, the activator concentration is localized in the inner region near the center of the spike, and is exponentially small in the outer region away from the spike location. This is also true for the k-spike equilibrium solution to (3.1) (see [34]).

In the inner region near the j^{th} spike, we define the variables

$$y = \frac{x - x_j}{\epsilon} \ , \quad A_j(y) = a(x_j + \epsilon y) \ , \quad H_j(y) = h(x_j + \epsilon y) \ . \tag{3.3}$$

Using (3.3), the equilibrium problem for (3.1) becomes

$$0 = A_j'' - A_j + \frac{A_j^2}{H_j} \ , \qquad -\infty < y < \infty \ , \tag{3.4a}$$

$$0 = H_j'' + \epsilon A_j^2 + O(\epsilon^2) \ , \qquad -\infty < y < \infty \ , \tag{3.4b}$$

where the primes indicate differentiation with respect to y. Substituting the inner variable expansion

$$A_j(y) = A_{j0}(y) + \epsilon A_{j1}(y) + \dots \ , \quad H_j(y) = H_{j0}(y) + \epsilon H_{j1}(y) + \dots \ , \tag{3.5}$$

into (3.4) gives, to leading order in ϵ,

$$0 = A_{j0}'' - A_{j0} + \frac{A_{j0}^2}{H_{j0}} \ , \qquad -\infty < y < \infty \ , \tag{3.6a}$$

$$0 = H_{j0}'' \ , \qquad -\infty < y < \infty \ . \tag{3.6b}$$

Matching to the outer solution requires that H_{j0} be bounded and $A_{j0} \to 0$ as $y \to \pm\infty$. Thus, it follows from (3.6b) that $H_{j0} = H$, where H is a constant, independent of y, to be determined by matching to the outer solution. In the limit $\epsilon \to 0$, the solution to (3.6a) is

$$A_{j0}(y) = H_{j0} \ w(y) \ , \qquad j = 0, \dots, k-1 \ , \tag{3.7}$$

where $w(y)$ satisfies

$$\begin{gathered} w'' - w + w^2 = 0 \ , \qquad -\infty < y < \infty \ , \\ w(y) \to 0 \ \text{ as } \ |y| \to \infty \ , \quad w'(0) = 0 \ , \quad w(0) > 0 \ , \end{gathered} \tag{3.8a}$$

whose solution is the unique positive homoclinic curve given by

$$w(y) = \frac{3}{2} \operatorname{sech}^2\left(\frac{y}{2}\right) \ . \tag{3.8b}$$

Substituting the inner expansion in (3.5) into (3.4) gives the $O(\epsilon)$ equations

$$A_{j1}'' - A_{j1} + 2\frac{A_{j0}}{H_{j0}} A_{j1} = \frac{A_{j0}^2}{H_{j0}^2} H_{j1} \ , \tag{3.9a}$$

$$H_{j1}'' = -A_{j0}^2 \ . \tag{3.9b}$$

From (3.9b), we have that H''_{j1} is an even function. Integrating (3.9b) from $y = -\infty$ to $y = \infty$, gives

$$\lim_{y\to\infty} H'_{j1} - \lim_{y\to-\infty} H'_{j1} = -\int_{-\infty}^{\infty} A_{j0}^2 \, dy \ , \tag{3.10}$$

which results in a jump condition for the outer solution.

In the outer region, we have that $a \to 0$ for $|x - x_j| \gg O(\epsilon)$, thereby reducing the model equations in (3.1) to

$$a \equiv 0 \ , \qquad \text{and} \qquad \begin{cases} h_{xx} - h = -\dfrac{a^2}{\epsilon} \ , & 0 < x < L \ , \\ h_x(0) = h_x(L) = 0 \ , \end{cases} \tag{3.11}$$

where h_x is discontinuous at each $x = x_j$. Thus, in the outer region, the term $\epsilon^{-1}a^2$ in (3.1) behaves like a linear combination of Dirac delta functions, $\delta(x)$, centered at x_j, for $j = 0, 1, \ldots, k-1$. Substituting the expansion $h = h_0 + O(\epsilon)$, as $\epsilon \to 0$, into (3.11) gives that h_0 satisfies

$$\begin{aligned} h_{0xx} - h_0 &= -\beta \sum_{i=0}^{k-1} \delta(x - x_i) \ , \quad 0 < x < L \ , \\ h_{0x}(0) &= h_{0x}(L) = 0 \ , \end{aligned} \tag{3.12a}$$

where

$$\beta = \int_{-\infty}^{\infty} A_{j0}^2(y) \, dy \ , \qquad j = 0, \ldots, k-1 \ . \tag{3.12b}$$

The solution h_0 to (3.12) is

$$h_0(x) = \beta \sum_{i=0}^{k-1} G(x; x_i) \ , \tag{3.13}$$

where the Green's function, $G(x; x_i)$, satisfies

$$\begin{aligned} G_{xx} - G &= -\delta(x - x_i) \ , \qquad 0 < x < L \ , \\ G_x(0; x_i) &= G_x(L; x_i) = 0 \ , \end{aligned} \tag{3.14a}$$

whose solution is given by

$$G(x; x_i) = \frac{1}{\sinh(L)} \begin{cases} \cosh(x) \cosh(x_i - L) \ , & 0 < x < x_i \ , \\ \cosh(x_i) \cosh(x - L) \ , & x_i < x < L \ . \end{cases} \tag{3.14b}$$

Next, we determine the constant H by matching the inner and outer solutions near each x_j, using that $\sum_{i=0}^{k-1} G(x_j;x_i)$ is independent of j at the spike locations in (3.2) (see [34]). This requires that

$$H = h_0(x_j) = \beta \sum_{i=0}^{k-1} G(x_j;x_i) \ , \qquad \text{for} \quad j = 0,1,\ldots,k-1 \ , \tag{3.15a}$$

where β is defined in (3.12b). Using (3.7), the equation in (3.15a) yields

$$H = \left(6 \ \sum_{i=0}^{k-1} G(x_j;x_i) \right)^{-1} , \qquad j = 0,1,\ldots,k-1 \ , \tag{3.15b}$$

where we have used that $\int_{-\infty}^{\infty} w^2(y)\ dy = 6$.

A k-spike equilibrium solution to the GM model in (3.1) is constructed in [34], in the limit $\epsilon \to 0$, using the method of matched asymptotic expansions. The result is summarized in the following Proposition.

Proposition 3.1. *(From [34]): Using the method of matched asymptotic expansion, in the limit $\epsilon \to 0$, a k-spike equilibrium solution to* (3.1)*, denoted by $(a_{e,k}(x), h_{e,k}(x))$, is given asymptotically by*

$$a_{e,k}(x) \sim H \sum_{i=0}^{k-1} w\left(\frac{x-x_i}{\epsilon} \right) \ , \quad h_{e,k}(x) \sim H \ \frac{\sum_{i=0}^{k-1} G(x;x_i)}{\sum_{i=0}^{k-1} G(x_j;x_i)} \ , \tag{3.16}$$

where H is given in (3.15)*. Here x_i satisfies* (3.2)*, $w(y)$ is the positive solution in* (3.8b)*, and G is the Green's function in* (3.14b)*.*

A two-spike equilibrium solution, obtained from (3.16), is plotted in Figure 3.1.

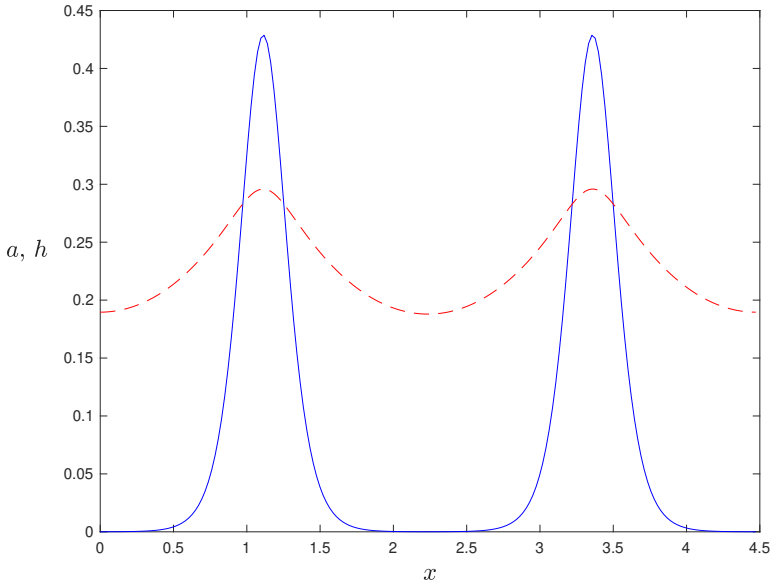

Figure 3.1: Plot of a two-spike equilibrium solution to (3.1) with equal amplitudes, for the case with no delay. The solid curve is the activator concentration and the dotted curve is the inhibitor concentration. Parameter values are $\epsilon = 0.1$, $L = 2/\sqrt{0.2}$, $\mu = 1$, and $D = 1$.

3.2 Dynamics of k-Spike Solution

In this section, we consider the dynamics of the spike locations for multi-spike type solution to the one-dimensional GM model with delayed reaction kinetics. In Chapter 2, we use asymptotic analysis and we derive a system of ODEs describing the location of the one-spike equilibrium solution. In this section, we show that the PDE system can be reduced to a delay differential-algebraic system of equations. To simplify the analysis, we assume $0 < \epsilon \ll 1$, and we let $D = 1$, $\mu = 1$, and $\sigma = 0$. As before, we expect that the spikes evolve on a slow time-scale $t = O(\epsilon^{-2})$, and therefore we have that $x_j = x_j(\tau)$, where $\tau = \epsilon^2 t$. In all the examples considered, we find that the numerical solutions of the DDAE systems agree well with the full numerical solutions of the PDE models.

3.2.1 Delay in the Catalyzed Production of Inhibitor

We now analyze the dynamics of the k-spike equilibrium solution to the GM model with delay in the nonlinear term of the inhibitor equation. The model PDEs are

given by

$$a_t = \epsilon^2 a_{xx} - a + \frac{a^2}{h} \ , \qquad 0 < x < L \ , \ t > 0 \ , \tag{3.17a}$$

$$0 = h_{xx} - h + \frac{a_T^2}{\epsilon} \ , \qquad 0 < x < L \ , \ t > 0 \ , \tag{3.17b}$$

subject to the Neumann boundary conditions in (3.1c).

In the inner region, near each x_j in (3.2), we rewrite the system in (3.17) in terms of the inner variables defined in (3.3), where $x_j = x_j(\epsilon^2\, t) = x_j(\tau)$, for $j = 0, \ldots, k-1$. This yields the equations

$$-\epsilon \ A_j' \ \dot{x}_j = A_j'' - A_j + \frac{A_j^2}{H_j} \ , \qquad -\infty < y < \infty \ , \tag{3.18a}$$

$$0 = H_j'' + \epsilon A_{jT}^2 + O(\epsilon^2) \ , \qquad -\infty < y < \infty \ , \tag{3.18b}$$

where primes are used to indicate derivatives with respect to the inner variable y. Moreover, substituting the inner variable expansion in (3.5) into the system in (3.18) yields the $O(1)$ equations in (3.6), as well as the leading order inner solution given in (3.7) and (3.8).

Since matching to the outer solution requires that H_{j0} be bounded and $A_{j0} \to 0$ as $|y| \to \infty$, therefore it follows that $H_{j0}(y) = H_{j0}(\tau)$, where H_{j0} is to be determined by matching to the outer solution. In addition, substituting the inner variable expansion (3.5) into (3.18) yields the $O(\epsilon)$ equations

$$A_{j1}'' - A_{j1} + 2\frac{A_{j0}}{H_{j0}} A_{j1} = -\dot{x}_j A_{j0}' + \left(\frac{A_{j0}}{H_{j0}}\right)^2 H_{j1} \ , \tag{3.19a}$$

$$H_{j1}'' = -A_{j0T}^2 \ , \tag{3.19b}$$

where $\dot{x}_j = dx_j/d\tau$, for $j = 0, \ldots, k-1$. Integrating (3.19b) from $y = -\infty$ to $y = \infty$ gives

$$H_{j1}'(\infty) - H_{j1}'(-\infty) = -\int_{-\infty}^{\infty} A_{j0T}^2 \ dy \ , \tag{3.20}$$

which results in a jump condition for the outer solution. The right hand side of (3.19a) must satisfy the solvability condition that it be orthogonal to $A_{j0}' = \dfrac{d}{d\tau}\left(H_{j0} w(y)\right)$. Integrating by parts twice, and using the even property of H_{j1}'' and

$w(y)$, yields

$$-\dot{x}_j = \frac{\int_{-\infty}^{\infty} w^3 \, dy}{6 \, H_{j0} \int_{-\infty}^{\infty} (w')^2 \, dy} \left(H'_{j1}(\infty) + H'_{j1}(-\infty) \right) \ , \tag{3.21}$$

where we have used

$$\begin{aligned} \frac{d}{d\tau} \left(H_{j0} w(y) \right) &= H_{j0} \frac{d}{d\tau} \left(w(y) \right) + w(y) \frac{d}{d\tau} \left(H_{j0} \right) \\ &\approx H_{j0} \frac{d}{d\tau} \left(w(y) \right) \ . \end{aligned} \tag{3.22}$$

We note that the second term of the sum in (3.22) above need not be retained since the spikes are moving on a slow time-scale by assumption, and therefore the change in their corresponding heights are also assumed to occur at a very slow rate. Using $\dfrac{\int_{-\infty}^{\infty} w^3 \, dy}{3 \int_{-\infty}^{\infty} (w')^2 \, dy} = 2$, the equation in (3.21) simplifies to

$$\dot{x}_j = -\frac{1}{H_{j0}} \left(\lim_{y \to \infty} H'_{j1} + \lim_{y \to -\infty} H'_{j1} \right) \ , \qquad j = 0, \ldots, k-1 \ . \tag{3.23}$$

In the outer region, defined away from an $O(\epsilon)$ neighbourhood of each x_j, we have that $a \to 0$ for $|x - x_j| \gg \epsilon$, for $j = 0, \ldots, k-1$, since a is exponentially localized to an $O(\epsilon)$ region about each x_j. Thus, in the outer region, the term $\epsilon^{-1} a_T^2$ in (3.17) behaves as a linear combination of the Dirac delta function centered at each x_j. Also, for $\epsilon \ll 1$, we get that h satisfies $h_{xx} - h = 0$ on the interval $[0, L]$, subject to a jump condition at $x = x_j$. Matching to the inner variables, and using the expansion $h = h_0 + O(\epsilon)$, as $\epsilon \to 0$, gives that h_0 satisfies

$$\begin{aligned} h_{0xx} - h_0 &= -\beta \sum_{i=0}^{k-1} \delta(x - x_{iT}) \ , \quad 0 < x < L \ , \\ h_{0x}(0) &= h_{0x}(L) = 0 \ . \end{aligned} \tag{3.24}$$

Here $x_{iT} = x_i(\tau - T)$ and β is as defined in (3.12b). The solution to (3.24) is

$$h_0(x) = \beta \sum_{i=0}^{k-1} G(x; x_{iT}) \ , \tag{3.25}$$

where $G(x; x_{iT}) = G(x; x_i(\tau - T))$ is the Green's function satisfying

$$\begin{aligned} G_{xx} - G &= -\delta(x - x_{iT}) \ , \qquad 0 < x < L \ , \\ G_x(0; x_i) &= G_x(L; x_i) = 0 \ , \end{aligned} \tag{3.26a}$$

whose solution is given by

$$G(x;x_{iT}) = \frac{1}{\sinh(L)} \begin{cases} \cosh(x)\cosh(x_{iT}-L) \ , & 0 < x < x_{iT} \ , \\ \cosh(x_{iT})\cosh(x-L) \ , & x_{iT} < x < L \ . \end{cases} \tag{3.26b}$$

Since the spikes in this case are not in equilibrium positions, therefore the spike heights are not equal, and thus the value of H_{j0} will be different for each spike.

Matching of the inner and outer solutions near each x_j, and using (3.7), gives the following nonlinear algebraic system of equations for the heights of the spikes, H_{j0}:

$$H_{j0} = h_0(x_j) = 6 \sum_{i=0}^{k-1} H_{i0}^2 \ G(x_j;x_{iT}) \ , \qquad j = 0,\ldots,k-1 \ , \tag{3.27}$$

where we have used that $\displaystyle\int_{-\infty}^{\infty} w^2 \ dy = 6$. Using (3.27), the limit in (3.23) evaluates to

$$\begin{aligned} \lim_{y\to\infty} H_{j1}' + \lim_{y\to-\infty} H_{j1}' &= \lim_{x\to x_j^+} h_{0x} + \lim_{x\to x_j^-} h_{0x} \qquad (3.28a) \\ &= 12\left[H_{j0}^2 \left(\frac{G_x(x_j^+;x_{jT}) + G_x(x_j^-;x_{jT})}{2} \right) + \sum_{\substack{i=0 \\ i\neq j}}^{k-1} H_{i0}^2 G_x(x_j;x_{iT}) \right] \ , \end{aligned}$$

where

$$\begin{aligned} G_x(x_j^-;x_{iT}) &= \frac{\sinh(x_j)\cosh(x_{iT}-L)}{\sinh(L)} \ , \\ G_x(x_j^+;x_{iT}) &= \frac{\cosh(x_{iT})\sinh(x_j-L)}{\sinh(L)} \ , \end{aligned} \tag{3.28b}$$

for $j = 0,\ldots,k-1$. Substituting (3.27) and (3.28) into (3.23), yields the coupled delay differential-algebraic system for x_j and H_j given by

$$\dot{x}_j = -\frac{12}{H_j} \left(H_j^2 \ \langle G_x(x_j;x_{jT})\rangle + \sum_{\substack{i=0 \\ i\neq j}}^{k-1} H_i^2 G_x(x_j;x_{iT}) \right) \ , \tag{3.29a}$$

$$H_j = 6 \sum_{i=0}^{k-1} H_i^2 \ G(x_j;x_{iT}) \ . \tag{3.29b}$$

Here $H_j = H_j(\tau)$, $\langle G_x(x_j;x_{jT})\rangle = \dfrac{G_x(x_j^+;x_{jT}) + G_x(x_j^-;x_{jT})}{2}$, and $x_{jT} = x_j(\tau - T)$, for $j = 0,\ldots,k-1$.

Using matrices, the system in (3.29) becomes

$$\dot{\mathbf{x}} = -12\ \mathcal{H}^{-1}\ \mathcal{P}\ \boldsymbol{H}^2\ , \qquad \boldsymbol{H} = 6\ \mathcal{G}\ \boldsymbol{H}^2\ , \tag{3.30a}$$

where

$$\dot{\mathbf{x}} \equiv \begin{bmatrix} \dot{x}_0(\tau) \\ \dot{x}_1(\tau) \\ \vdots \\ \dot{x}_j(\tau) \end{bmatrix}\ , \quad \boldsymbol{H} \equiv \begin{bmatrix} H_0 \\ H_1 \\ \vdots \\ H_j \end{bmatrix}\ , \quad \boldsymbol{H}^2 \equiv \begin{bmatrix} H_0^2 \\ H_1^2 \\ \vdots \\ H_j^2 \end{bmatrix}\ , \quad \mathcal{H} \equiv \begin{bmatrix} H_0 & 0 & \cdots & 0 \\ 0 & \ddots & \cdots & 0 \\ \vdots & \vdots & \ddots & \vdots \\ 0 & 0 & \cdots & H_j \end{bmatrix}\ ,$$

$$\mathcal{P} \equiv \begin{bmatrix} \langle G_x(x_0; x_{0T})\rangle & \cdots & G_x(x_0; x_{jT}) \\ \vdots & \ddots & \vdots \\ G_x(x_j; x_{0T}) & \cdots & \langle G_x(x_j; x_{jT})\rangle \end{bmatrix},\ \mathcal{G} \equiv \begin{bmatrix} G(x_0; x_{0T}) & \cdots & G(x_0; x_{jT}) \\ \vdots & \ddots & \vdots \\ G(x_j; x_{0T}) & \cdots & G(x_j; x_{jT}) \end{bmatrix}. \tag{3.30b}$$

Here we have that

$$\begin{aligned} G(x_j; x_{iT}) &= \frac{\cosh(x_{iT})\cosh(x_j - L)}{\sinh(L)}\ , \\ G_x(x_j; x_{iT}) &= \frac{\cosh(x_{iT})\sinh(x_j - L)}{\sinh(L)}\ , \\ \langle G_x(x_j; x_{iT})\rangle &= \frac{\cosh(x_{iT})\sinh(x_j - L) + \sinh(x_j)\cosh(x_{iT} - L)}{2\sinh(L)}\ . \end{aligned} \tag{3.30c}$$

In Figure 3.2, we compare the trajectories x_j, for $j = 0, 1$, computed numerically from the DDAE system (3.29) with the full numerical results for (3.17), for the case of two spikes. The agreement is found to be close.

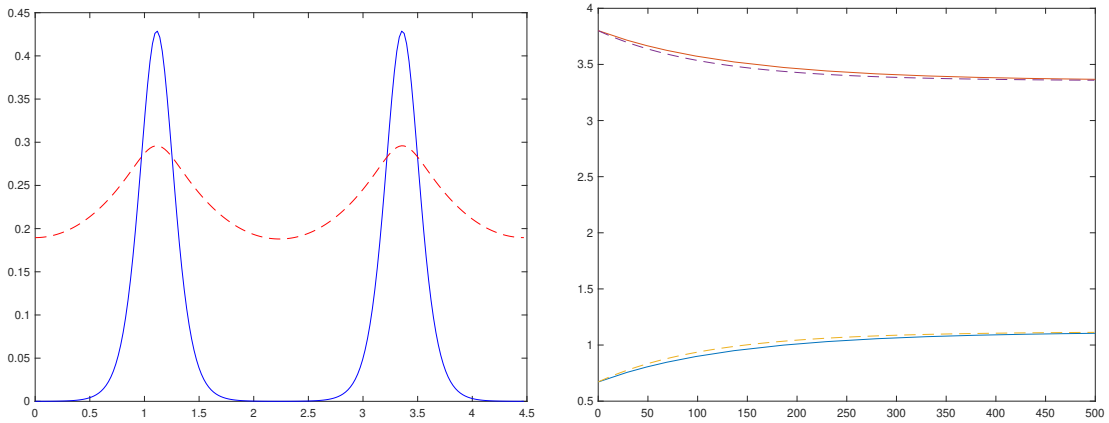

(a) (b)

Figure 3.2: Left: Plot of a two-spike equilibrium solution to (3.17) with delay in the nonlinear term of the inhibitor equation. The solid curve is the activator concentration and the dotted curve is the inhibitor concentration. Right: Plot of the trajectories $x_j(t)$ (solid curves) versus time t, for $j = 0, 1$, as computed from (3.29) in the original time-scale. The dotted curves correspond to the full numerical simulation of (3.17). Parameter values are $T = 0.1$, $\epsilon = 0.1$, $L = 2/\sqrt{0.2}$, $\mu = 1$, and $D = 1$.

3.2.2 Delay in the Regulation of Activator Production

We now analyze the dynamics of the k-spike equilibrium to the one-dimensional GM model, where delay is in the nonlinear term of the activator equation. The model PDEs are given by

$$a_t = \epsilon^2 a_{xx} - a + \frac{a^2}{h_T} , \qquad 0 < x < L , \ t > 0 , \tag{3.31a}$$

$$0 = h_{xx} - h + \frac{a^2}{\epsilon} , \qquad 0 < x < L , \ t > 0 , \tag{3.31b}$$

subject to the Neumann boundary conditions (3.1c).

In the inner region near each x_j, rewriting the system in (3.31) in terms of the new variables defined in (3.3) yields the equations

$$-\epsilon \, A_j' \, \dot{x}_j = A_j'' - A_j + \frac{A_j^2}{H_{jT}} , \tag{3.32a}$$

$$0 = H_j'' + \epsilon A_j^2 + O(\epsilon^2) , \tag{3.32b}$$

where primes are used to indicate derivatives with respect to the inner variable y. Moreover, substituting the inner variable expansion in (3.5) into the system in (3.32)

yields the $O(1)$ equations

$$0 = A''_{j0} - A_{j0} + \frac{A_{j0}^2}{H_{j0T}} \ , \qquad -\infty < y < \infty \ , \tag{3.33a}$$

$$0 = H''_{j0} \ , \qquad -\infty < y < \infty \ . \tag{3.33b}$$

This yields the solution

$$A_{j0}(y) = H_{j0T}\ w(y) \ , \qquad j = 0, \ldots, k-1 \ , \tag{3.34}$$

where $w(y)$ satisfies (3.8). Substituting the inner variable expansion (3.5) into (3.32) yields the $O(\epsilon)$ equations

$$A''_{j1} - A_{j1} + 2\frac{A_{j0}}{H_{j0T}}A_{j1} = -\dot{x}_j A'_{j0} + \left(\frac{A_{j0}}{H_{j0T}}\right)^2 H_{j1T} \ , \tag{3.35a}$$

$$H''_{j1} = -A_{j0}^2 \ , \tag{3.35b}$$

where $\dot{x}_j = dx_j/d\tau$, for $j = 0, \ldots, k-1$. Using the same solvability condition as before, we get

$$\dot{x}_j \int_{-\infty}^{\infty} (w')^2\, dy = \frac{1}{H_{j0T}} \int_{-\infty}^{\infty} w^2 w' H_{j1T}\ dy \ , \qquad j = 0, \ldots, k-1 \ , \tag{3.36}$$

where we use the solution (3.34) and the result in (3.22). Integrating by parts twice and using the even property of H''_{j1} and $w(y)$ gives

$$\dot{x}_j = -\frac{1}{6\ H_{j0T}} \left(\frac{\int_{-\infty}^{\infty} w^3\ dy}{\int_{-\infty}^{\infty} (w')^2\, dy} \right) \left(H'_{j1T}(\infty) + H'_{j1T}(-\infty) \right) \ . \tag{3.37}$$

Using $\dfrac{\int_{-\infty}^{\infty} w^3\ dy}{3\int_{-\infty}^{\infty} (w')^2\, dy} = 2$, the equation in (3.37) simplifies to

$$\dot{x}_j = -\frac{1}{H_{j0T}} \left(\lim_{y\to\infty} H'_{j1T} + \lim_{y\to-\infty} H'_{j1T} \right) \ , \qquad j = 0, \ldots, k-1 \ . \tag{3.38}$$

In the outer region, we again treat a as a multiple of the Dirac delta function centered at x_j, in the limit $\epsilon \to 0$. This gives the system in (3.12) and the solution (3.13). Upon matching of the inner and outer solutions near each x_j, and using (3.34), we obtain the following nonlinear algebraic system of equations for the heights of the spikes H_{j0}:

$$H_{j0} = h_0(x_j) = 6 \sum_{i=0}^{k-1} H_{i0}^2\ G(x_j; x_i) \ , \quad j = 0, \ldots, k-1 \ , \tag{3.39}$$

where we have used that $\displaystyle\int_{-\infty}^{\infty} w^2 \, dy = 6$. Using (3.39), the limit in (3.38) evaluates to

$$\lim_{y\to\infty} H'_{j1T} + \lim_{y\to-\infty} H'_{j1T} = \lim_{x\to x_j^+} h_{0xT} + \lim_{x\to x_j^-} h_{0xT} \tag{3.40a}$$

$$= 12\left[H_{j0T}^2\left(\frac{G_x(x_{jT}^+;x_{jT}) + G_x(x_{jT}^-;x_{jT})}{2}\right) + \sum_{\substack{i=0\\ i\neq j}}^{k-1} H_{i0T}^2 G_x(x_{jT};x_{iT})\right] ,$$

where

$$\begin{aligned} G_x(x_{jT}^-;x_{iT}) &= \frac{\sinh(x_{jT})\cosh(x_{iT}-L)}{\sinh(L)} , \\ G_x(x_{jT}^+;x_{iT}) &= \frac{\cosh(x_{iT})\sinh(x_{jT}-L)}{\sinh(L)} . \end{aligned} \tag{3.40b}$$

Substituting (3.39) and (3.40) into (3.38), and relabelling H_{j0T} by H_{jT}, yields the coupled delay differential-algebraic system for $x_j(\tau)$ and H_{jT} given by

$$\dot{x}_j = -\frac{12}{H_{jT}}\left(H_{jT}^2 \;\langle G_x(x_{jT};x_{jT})\rangle + \sum_{\substack{i=0\\ i\neq j}}^{k-1} H_{iT}^2 G_x(x_{jT};x_{iT})\right) , \tag{3.41a}$$

$$H_{jT} = 6\sum_{i=0}^{k-1} H_{iT}^2 \, G(x_{jT};x_{iT}) . \tag{3.41b}$$

Here $H_{jT} = H_j(\tau - T)$, $\langle G_x(x_{jT};x_{jT})\rangle = \dfrac{G_x(x_{jT}^+;x_{jT}) + G_x(x_{jT}^-;x_{jT})}{2}$, and $x_{jT} = x_j(\tau - T)$, for $j = 0,\ldots,k-1$.

Using matrices, the system in (3.41) becomes

$$\dot{\mathbf{x}} = -12\;{\mathcal{H}_{\mathcal{T}}}^{-1}\;\mathcal{P}_{\mathcal{T}}\;\boldsymbol{H}_T^2 , \qquad \boldsymbol{H}_T = 6\;\mathcal{G}_{\mathcal{T}}\;\boldsymbol{H}_T^2 , \tag{3.42a}$$

where

$$\dot{\mathbf{x}} \equiv \begin{bmatrix} \dot{x}_0(\tau) \\ \dot{x}_1(\tau) \\ \vdots \\ \dot{x}_j(\tau) \end{bmatrix} , \quad \boldsymbol{H}_T \equiv \begin{bmatrix} H_{0T} \\ H_{1T} \\ \vdots \\ H_{jT} \end{bmatrix} , \quad \boldsymbol{H}_T^2 \equiv \begin{bmatrix} H_{0T}^2 \\ H_{1T}^2 \\ \vdots \\ H_{jT}^2 \end{bmatrix} , \quad \mathcal{H}_{\mathcal{T}} \equiv \begin{bmatrix} H_{0T} & 0 & \cdots & 0 \\ 0 & \ddots & \cdots & 0 \\ \vdots & \vdots & \ddots & \vdots \\ 0 & 0 & \cdots & H_{jT} \end{bmatrix} ,$$

$$\mathcal{P}_{\mathcal{T}} \equiv \begin{bmatrix} \langle G_x(x_{0T}; x_{0T}) \rangle & \cdots & G_x(x_{0T}; x_{jT}) \\ \vdots & \ddots & \vdots \\ G_x(x_{jT}; x_{0T}) & \cdots & \langle G_x(x_{jT}; x_{jT}) \rangle \end{bmatrix} , \; \mathcal{G}_{\mathcal{T}} \equiv \begin{bmatrix} G(x_{0T}; x_{0T}) & \cdots & G(x_{0T}; x_{jT}) \\ \vdots & \ddots & \vdots \\ G(x_{jT}; x_{0T}) & \cdots & G(x_{jT}; x_{jT}) \end{bmatrix} . \tag{3.42b}$$

Here we have that

$$\begin{aligned} G(x_{jT}; x_{iT}) &= \frac{\cosh(x_{iT}) \cosh(x_{jT} - L)}{\sinh(L)} , \\ G_x(x_{jT}; x_{iT}) &= \frac{\cosh(x_{iT}) \sinh(x_{jT} - L)}{\sinh(L)} , \quad \text{and} \\ \langle G_x(x_{jT}; x_{iT}) \rangle &= \frac{\cosh(x_{iT}) \sinh(x_{jT} - L) + \sinh(x_{jT}) \cosh(x_{iT} - L)}{2 \sinh(L)} . \end{aligned} \tag{3.42c}$$

In Figure 3.3, we compare the trajectories $x_j(t)$, for $j = 0, 1$, computed numerically from the DDAE system (3.41), with the full numerical results for (3.31), for the case of two spikes. The agreement is found to be close.

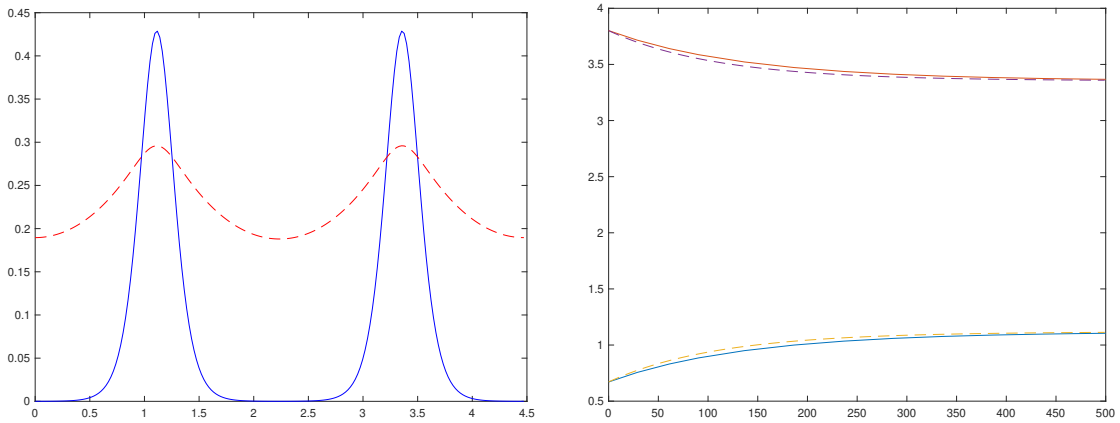

(a) (b)

Figure 3.3: Left: Plot of a two-spike equilibrium solution to (3.31), with delay in the h term of the activator equation. The solid curve is the activator concentration and the dotted curve is the inhibitor concentration. Right: Plot of the trajectories $x_j(t)$ (solid curves) versus time t, for $j = 0, 1$, as computed from (3.41) in the original time-scale. The dotted curves correspond to the full numerical simulation of (3.31). Parameter values are as in the caption of Figure 3.2.

3.2.3 Delay in Activator Regulation and Inhibitor Production

Next, we consider the following GM model, where the nonlinear terms in both equations are delayed:

$$a_t = \epsilon^2 a_{xx} - a + \frac{a^2}{h_T} , \qquad 0 < x < L , \ t > 0 , \tag{3.43a}$$

$$0 = h_{xx} - h + \frac{a_T^2}{\epsilon} , \qquad 0 < x < L , \ t > 0 , \tag{3.43b}$$

subject to the same Neumann boundary conditions and assumptions as before. We again use the slow time-scaling $\tau = \epsilon^2 t$.

In the inner region near each x_j, in terms of the inner variables defined in (3.3), the system in (3.43) becomes

$$-\epsilon \, A_j' \, \dot{x}_j = A_j'' - A_j + \frac{A_j^2}{H_{jT}} , \tag{3.44a}$$

$$0 = H_j'' + \epsilon A_{jT}^2 + O(\epsilon^2) , \tag{3.44b}$$

where $\dot{x}_j = dx_j/d\tau$, for $j = 0, \ldots, k-1$, and primes indicate derivatives with respect to the inner variable y. Substituting the inner variable expansion (3.5) into (3.44)

yields the $O(1)$ equations in (3.33), and the inner solution (3.34). The $O(\epsilon)$ equations corresponding to (3.44) are given by

$$A''_{j1} - A_{j1} + 2\frac{A_{j0}}{H_{j0T}}A_{j1} = -\dot{x}_j A'_{j0} + \left(\frac{A_{j0}}{H_{j0T}}\right)^2 H_{j1T} \ , \tag{3.45a}$$

$$H''_{j1} = -A^2_{j0T} \ , \tag{3.45b}$$

which yields the equation in (3.36). Thus, we get

$$\dot{x}_j = -\frac{1}{H_{j0T}}\left(\lim_{y\to\infty} H'_{j1T} + \lim_{y\to-\infty} H'_{j1T}\right) \ , \qquad j = 0, \ldots, k-1 \ . \tag{3.46}$$

In the outer region, as $\epsilon \to 0$, we treat a as a weighted sum of Dirac delta functions centred at x_j, which yields the system in (3.24) and the solution in (3.25). Matching to the inner solution near each x_j yields the nonlinear algebraic system of equations for H_{j0T} given by

$$H_{j0T} = h_0(x_{jT}) = 6 \sum_{i=0}^{k-1} H^2_{i0T} \ G(x_{jT_1}; x_{iT_2}) \ , \tag{3.47}$$

where $x_{jT_1} = x_j(\tau - T)$ and $x_{jT_2} = x_j(\tau - 2T)$, for $j = 0, \ldots, k-1$. Using (3.47), the right hand side of (3.46) evaluates to

$$12\left[H^2_{j0T}\left(\frac{G_x(x^+_{jT_1}; x_{jT_2}) + G_x(x^-_{jT_1}; x_{jT_2})}{2}\right) + \sum_{\substack{i=0\\ i\neq j}}^{k-1} H^2_{i0T} G_x(x_{jT_1}; x_{iT_2})\right], \tag{3.48a}$$

where

$$\begin{aligned} G_x(x^-_{jT_1}; x_{iT_2}) &= \frac{\sinh(x_{jT_1})\cosh(x_{iT_2} - L)}{\sinh(L)} \ , \\ G_x(x^+_{jT_1}; x_{iT_2}) &= \frac{\cosh(x_{iT_2})\sinh(x_{jT_1} - L)}{\sinh(L)} \ , \end{aligned} \tag{3.48b}$$

for $j = 0, \ldots, k-1$. Substituting (3.47) and (3.48) into (3.46) yields the coupled delay differential-algebraic system of equations for x_j and H_j given by

$$\dot{x}_j = -\frac{12}{H_{jT}}\left(H^2_{jT}\left\langle G_x(x_{jT_1}; x_{jT_2})\right\rangle + \sum_{\substack{i=0\\ i\neq j}}^{k-1} H^2_{iT} G_x(x_{jT_1}; x_{iT_2})\right) \ , \tag{3.49a}$$

$$H_{jT} = 6 \sum_{i=0}^{k-1} H^2_{iT} \ G(x_{jT_1}; x_{iT_2}) \ , \qquad j = 0, \ldots, k-1 \ . \tag{3.49b}$$

Here $H_{jT} = H_j(\tau - T)$, and $\langle G_x(x_{jT_1}; x_{jT_2})\rangle = \dfrac{G_x(x^+_{jT_1}; x_{jT_2}) + G_x(x^-_{jT_1}; x_{jT_2})}{2}$.

Using matrix notation, the system in (3.49) can be written as

$$\dot{\mathbf{x}} = -12\ \mathcal{H}_T^{-1}\ \mathcal{P}_T\ \boldsymbol{H}_T^2\ , \qquad \boldsymbol{H}_T = 6\ \mathcal{G}_T\ \boldsymbol{H}_T^2\ , \tag{3.50a}$$

where

$$\dot{\mathbf{x}} \equiv \begin{bmatrix} \dot{x}_0(\tau) \\ \dot{x}_1(\tau) \\ \vdots \\ \dot{x}_j(\tau) \end{bmatrix}\ , \quad \boldsymbol{H}_T \equiv \begin{bmatrix} H_{0T} \\ H_{1T} \\ \vdots \\ H_{jT} \end{bmatrix}\ , \quad \boldsymbol{H}_T^2 \equiv \begin{bmatrix} H_{0T}^2 \\ H_{1T}^2 \\ \vdots \\ H_{jT}^2 \end{bmatrix}\ , \quad \mathcal{H}_T \equiv \begin{bmatrix} H_{0T} & 0 & \cdots & 0 \\ 0 & \ddots & \cdots & 0 \\ \vdots & \vdots & \ddots & \vdots \\ 0 & 0 & \cdots & H_{jT} \end{bmatrix}\ ,$$

$$\mathcal{P}_T \equiv \begin{bmatrix} \langle G_x(x_{0T_1}; x_{0T_2})\rangle & \cdots & G_x(x_{0T_1}; x_{jT_2}) \\ \vdots & \ddots & \vdots \\ G_x(x_{jT_1}; x_{0T_2}) & \cdots & \langle G_x(x_{jT_1}; x_{jT_2})\rangle \end{bmatrix},\ \mathcal{G}_T \equiv \begin{bmatrix} G(x_{0T_1}; x_{0T_2}) & \cdots & G(x_{0T_1}; x_{jT_2}) \\ \vdots & \ddots & \vdots \\ G(x_{jT_1}; x_{0T_2}) & \cdots & G(x_{jT_1}; x_{jT_2}) \end{bmatrix}. \tag{3.50b}$$

Here we have that

$$\begin{aligned} G(x_{jT_1}; x_{iT_2}) &= \frac{\cosh(x_{iT_2})\cosh(x_{jT_1} - L)}{\sinh(L)}\ , \\ G_x(x_{jT_1}; x_{iT_2}) &= \frac{\cosh(x_{iT_2})\sinh(x_{jT_1} - L)}{\sinh(L)}\ , \\ \langle G_x(x_{jT_1}; x_{iT_2})\rangle &= \frac{\cosh(x_{iT_2})\sinh(x_{jT_1} - L) + \sinh(x_{jT_1})\cosh(x_{iT_2} - L)}{2\sinh(L)}\ . \end{aligned} \tag{3.50c}$$

In Figure 3.4, we compare the trajectories x_j, for $j = 0, 1$, computed numerically from the DDAE system (3.49), with the full numerical results for (3.43), for the case of two spikes. The agreement is found to be close.

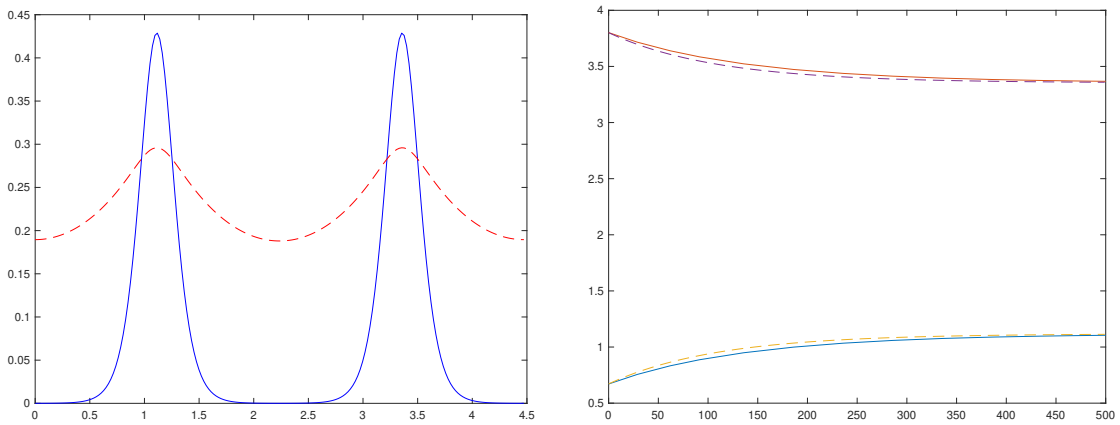

(a) (b)

Figure 3.4: Left: Plot of a two-spike equilibrium solution to (3.43), with delay in both the activator regulation and inhibitor production. The solid curve is the activator concentration and the dotted curve is the inhibitor concentration. Right: Plot of the trajectories $x_j(t)$ (solid curves) versus time t, for $j = 0, 1$, as computed from (3.49) in the original time-scale. The dotted curves correspond to the full numerical simulation of (3.43). Parameter values are as in the caption of Figure 3.2.

3.3 Hopf Bifurcation in the Reduced System of Delay Differential-Algebraic Equations for the Spike Locations

In §2.2, we studied the dynamics and stability of one-spike solution to the GM model, and we showed that for some cases of delayed reaction kinetics, increasing time delay results in sustained oscillations, due to a Hopf bifurcation, in the positions of the spikes for the corresponding reduced delay differential-algebraic system. In this section, we extend our analysis to the more general case of k-spike solution, and we analyze its stability by computing critical values of delay at which a Hopf bifurcation occurs. As before, for the models considered in §3.2, the spikes evolve on a slow time-scale $t = O(\epsilon^{-2})$. The stability of the large eigenvalues is studied in §3.4.2, where we show that the Hopf bifurcation is observed in the spikes amplitude for some cases of the GM model with delayed kinetics.

In §3.2.1, we derived the DDAEs in (3.29) corresponding to the GM model in (3.17). For $k = 2$, the system in (3.30) becomes

$$\dot{\mathbf{x}} = -12\, \mathcal{H}^{-1}\, \mathcal{P}\, \boldsymbol{H}^2\,, \qquad \boldsymbol{H} = 6\, \mathcal{G}\, \boldsymbol{H}^2\,, \tag{3.51a}$$

where we have defined

$$\dot{\mathbf{x}} \equiv \begin{bmatrix} \dot{x}_0(\tau) \\ \dot{x}_1(\tau) \end{bmatrix} \ , \quad \boldsymbol{H} \equiv \begin{bmatrix} H_0 \\ H_1 \end{bmatrix} \ , \quad \boldsymbol{H}^2 \equiv \begin{bmatrix} H_0^2 \\ H_1^2 \end{bmatrix} \ , \quad \mathcal{H} \equiv \begin{bmatrix} H_0 & 0 \\ 0 & H_1 \end{bmatrix} \ ,$$
$$\mathcal{P} \equiv \begin{bmatrix} \langle G_x(x_0; x_{0T}) \rangle & G_x(x_0; x_{1T}) \\ G_x(x_1; x_{0T}) & \langle G_x(x_1; x_{1T}) \rangle \end{bmatrix} \ , \quad \mathcal{G} \equiv \begin{bmatrix} G(x_0; x_{0T}) & G(x_0; x_{1T}) \\ G(x_1; x_{0T}) & G(x_1; x_{1T}) \end{bmatrix} \ . \tag{3.51b}$$

Thus, using the original time-scale, we get that

$$\begin{bmatrix} \dfrac{dx_0}{dt} \\ \dfrac{dx_1}{dt} \end{bmatrix} = -\epsilon^2 \frac{12}{H_0 H_1} \begin{bmatrix} H_0^2 \ H_1 \langle G_x(x_0; x_{0T}) \rangle + H_1^3 \ G_x(x_0; x_{1T}) \\ H_0^3 \ G_x(x_1; x_{0T}) + H_0 H_1^2 \langle G_x(x_1; x_{1T}) \rangle \end{bmatrix} \ ,$$
$$\begin{bmatrix} H_0 \\ H_1 \end{bmatrix} = 6 \begin{bmatrix} H_0^2 \ G(x_0; x_{0T}) + H_1^2 \ G(x_0; x_{1T}) \\ H_0^2 \ G(x_1; x_{0T}) + H_1^2 \ G(x_1; x_{1T}) \end{bmatrix} \ . \tag{3.52}$$

Substituting the expressions given in (3.30c) into (3.52) gives

$$\frac{dx_0}{dt} = -\epsilon^2 \frac{6H_0}{\sinh(L)} \Bigg[\cosh(x_{0T}) \sinh(x_0 - L) + \sinh(x_0) \cosh(x_{0T} - L) + 2 \left(\frac{H_1}{H_0} \right)^2 \cosh(x_{1T}) \sinh(x_0 - L) \Bigg] \ ,$$
$$\frac{dx_1}{dt} = -\epsilon^2 \frac{6H_1}{\sinh(L)} \Bigg[\cosh(x_{1T}) \sinh(x_1 - L) + \sinh(x_1) \cosh(x_{1T} - L) + 2 \left(\frac{H_0}{H_1} \right)^2 \cosh(x_{0T}) \sinh(x_1 - L) \Bigg] \ , \tag{3.53a}$$

coupled to the algebraic system of equations

$$H_0 = \frac{6}{\sinh(L)} \Big[H_0^2 \cosh(x_{0T}) \cosh(x_0 - L) + H_1^2 \cosh(x_{1T}) \cosh(x_0 - L) \Big] ;$$
$$H_1 = \frac{6}{\sinh(L)} \Big[H_0^2 \cosh(x_{0T}) \cosh(x_1 - L) + H_1^2 \cosh(x_{1T}) \cosh(x_1 - L) \Big] . \tag{3.53b}$$

Next, we rewrite the equations in (3.53a) as

$$\frac{dx_0}{dt} = F(x_0, x_{0T}, x_1, x_{1T}) \ , \quad \text{and} \quad \frac{dx_1}{dt} = M(x_0, x_{0T}, x_1, x_{1T}) \ , \tag{3.54}$$

and we introduce the following small perturbations to the equilibrium position of the j^{th} spike:

$$x_j(t) = x_j + e^{\lambda t} \eta_j \ , \qquad \text{where} \quad |\eta_j| << |x_j| \ , \ \text{for } j = 0, 1 \ . \tag{3.55}$$

Substituting (3.55) into (3.54) gives

$$\begin{aligned}
\frac{dx_0}{dt} + \lambda e^{\lambda t}\eta_0 &= F + F_{x_{0T}} e^{\lambda(t-T)}\eta_0 + F_{x_0} e^{\lambda t}\eta_0 + F_{x_{1T}} e^{\lambda(t-T)}\eta_0 + F_{x_1} e^{\lambda t}\eta_0 \ , \\
\frac{dx_1}{dt} + \lambda e^{\lambda t}\eta_1 &= M + M_{x_{0T}} e^{\lambda(t-T)}\eta_1 + M_{x_0} e^{\lambda t}\eta_1 + M_{x_{1T}} e^{\lambda(t-T)}\eta_1 + M_{x_1} e^{\lambda t}\eta_1,
\end{aligned} \tag{3.56}$$

where the partial derivatives of F (and similarly for M) are calculated using the chain rule:

$$F_{x_i} = \sum_{j=0}^{1} \frac{\partial F}{\partial H_j}\frac{\partial H_j}{\partial x_i} \ , \quad F_{x_{iT}} = \sum_{j=0}^{1} \frac{\partial F}{\partial H_j}\frac{\partial H_j}{\partial x_{iT}} \ , \qquad \text{for} \quad i = 0, 1 \ . \tag{3.57}$$

Since x_0 and x_1 are solutions to (3.54), the equations in (3.56) can be reduced to

$$\begin{aligned}
\lambda &= F_{x_0} + F_{x_1} + \left(F_{x_{0T}} + F_{x_{1T}}\right) e^{-\lambda T} \ , \\
\lambda &= M_{x_0} + M_{x_1} + \left(M_{x_{0T}} + M_{x_{1T}}\right) e^{-\lambda T} \ .
\end{aligned} \tag{3.58}$$

We now seek critical Hopf bifurcation parameters that result in pure imaginary eigenvalues. Substituting $\lambda = i\omega$, for some positive $\omega \in \mathbb{R}$, into (3.58) yields the following system of equations:

$$\begin{aligned}
i\omega &= F_{x_0} + F_{x_1} + \left(F_{x_{0T}} + F_{x_{1T}}\right)\left[\cos\left(\omega T\right) - i\sin\left(\omega T\right)\right] \ , \\
i\omega &= M_{x_0} + M_{x_1} + \left(M_{x_{0T}} + M_{x_{1T}}\right)\left[\cos\left(\omega T\right) - i\sin\left(\omega T\right)\right] \ .
\end{aligned} \tag{3.59}$$

Upon comparing the real and imaginary terms on both sides of each equation in (3.59), we get

$$\begin{aligned}
F_{x_0} + F_{x_1} + \left(F_{x_{0T}} + F_{x_{1T}}\right)\cos\left(\omega T\right) = 0, \quad \left(F_{x_{0T}} + F_{x_{1T}}\right)\sin\left(\omega T\right) = -\omega, \\
M_{x_0} + M_{x_1} + \left(M_{x_{0T}} + M_{x_{1T}}\right)\cos\left(\omega T\right) = 0, \quad \left(M_{x_{0T}} + M_{x_{1T}}\right)\sin\left(\omega T\right) = -\omega.
\end{aligned} \tag{3.60}$$

Numerical evaluation of the equations in (3.60) for two spikes, with $\epsilon = 0.4$ and $L = 0.5/\sqrt{0.2}$, gives that ω and T satisfy (3.60) only if $|\cos(\omega T)| > 1$, which is a contradiction to the cosine function properties. Thus, we conclude that the equilibrium solution in this case is stable for all positive values of delay T. Numerical simulations are shown in Figure 3.5, where we plot various trajectories of $x_j(t)$, $j = 0, 1$, for various values of delay. In this case, no instabilities are triggered and the spikes tend to their equilibrium locations.

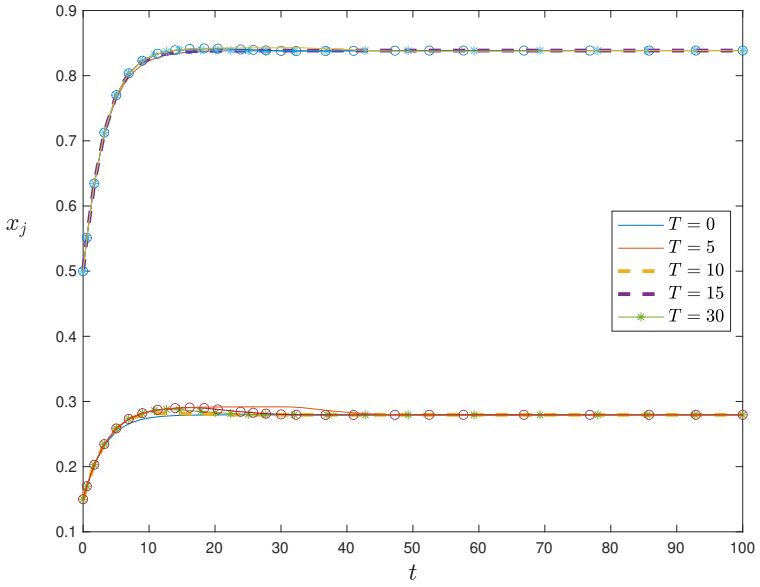

Figure 3.5: Plot of trajectories corresponding to the spike locations versus time, as obtained from the DDAE system in (3.52), for increasing values of delay in the non-linear term of the inhibitor equation. Initial condition as indicated. No oscillations are observed and all trajectories approach the stable equilibrium positions $x_0 = L/4$ and $x_1 = 3L/4$. Parameters used are $k = 2$, $\epsilon = 0.4$, $L = 0.5/\sqrt{0.2}$, $\mu = 1$, and $D = 1$.

Similarly, using $k = 2$, the system in (3.42) can be written as

$$\dot{\mathbf{x}} = -12\ \mathcal{H}_{\mathcal{T}}{}^{-1}\ \mathcal{P}_{\mathcal{T}}\ \boldsymbol{H}_T^2\ , \qquad \boldsymbol{H}_T = 6\ \mathcal{G}_{\mathcal{T}}\ \boldsymbol{H}_T^2\ , \tag{3.61a}$$

where

$$\dot{\mathbf{x}} \equiv \begin{bmatrix} \dot{x}_0(\tau) \\ \dot{x}_1(\tau) \end{bmatrix}\ , \quad \boldsymbol{H}_T \equiv \begin{bmatrix} H_{0T} \\ H_{1T} \end{bmatrix}\ , \quad \boldsymbol{H}_T^2 \equiv \begin{bmatrix} H_{0T}^2 \\ H_{1T}^2 \end{bmatrix}\ , \quad \mathcal{H}_{\mathcal{T}} \equiv \begin{bmatrix} H_{0T} & 0 \\ 0 & H_{1T} \end{bmatrix}\ ,$$

$$\mathcal{P}_{\mathcal{T}} \equiv \begin{bmatrix} \langle G_x(x_{0T}; x_{0T}) \rangle & G_x(x_{0T}; x_{1T}) \\ G_x(x_{1T}; x_{0T}) & \langle G_x(x_{1T}; x_{1T}) \rangle \end{bmatrix}\ , \quad \mathcal{G}_{\mathcal{T}} \equiv \begin{bmatrix} G(x_{0T}; x_{0T}) & G(x_{0T}; x_{1T}) \\ G(x_{1T}; x_{0T}) & G(x_{1T}; x_{1T}) \end{bmatrix}\ . \tag{3.61b}$$

Using the original time-scale we get

$$\begin{bmatrix} \dfrac{dx_0}{dt} \\ \dfrac{dx_1}{dt} \end{bmatrix} = -\epsilon^2 \frac{12}{H_{0T} H_{1T}} \begin{bmatrix} H_{0T}^2\ H_{1T}\ \langle G_x(x_{0T}; x_{0T}) \rangle + H_{1T}^3\ G_x(x_{0T}; x_{1T}) \\ H_{0T}^3\ G_x(x_{1T}; x_{0T}) + H_{0T} H_{1T}^2\ \langle G_x(x_{1T}; x_{1T}) \rangle \end{bmatrix}\ ,$$

$$\begin{bmatrix} H_{0T} \\ H_{1T} \end{bmatrix} = 6 \begin{bmatrix} H_{0T}^2\ G(x_{0T}; x_{0T}) + H_{1T}^2\ G(x_{0T}; x_{1T}) \\ H_{0T}^2\ G(x_{1T}; x_{0T}) + H_{1T}^2\ G(x_{1T}; x_{1T}) \end{bmatrix}\ . \tag{3.62}$$

Substituting the expressions given in (3.42c) into (3.62) gives

$$\begin{aligned}
\frac{dx_0}{dt} &= -\epsilon^2 \frac{6H_{0T}}{\sinh(L)} \left[\sinh(2x_{0T} - L) + 2\left(\frac{H_{1T}}{H_{0T}}\right)^2 \cosh(x_{1T}) \sinh(x_{0T} - L) \right] ; \\
\frac{dx_1}{dt} &= -\epsilon^2 \frac{6H_{1T}}{\sinh(L)} \left[2\left(\frac{H_{0T}}{H_{1T}}\right)^2 \cosh(x_{0T}) \sinh(x_{1T} - L) + \sinh(2x_{1T} - L) \right] ,
\end{aligned} \tag{3.63a}$$

coupled to the algebraic system of equations given by

$$\begin{aligned}
H_{0T} &= \frac{6}{\sinh(L)} \left[H_{0T}^2 \ \cosh(x_{0T}) \cosh(x_{0T} - L) + H_{1T}^2 \ \cosh(x_{1T}) \cosh(x_{0T} - L) \right] , \\
H_{1T} &= \frac{6}{\sinh(L)} \left[H_{0T}^2 \ \cosh(x_{0T}) \cosh(x_{1T} - L) + H_{1T}^2 \ \cosh(x_{1T}) \cosh(x_{1T} - L) \right] .
\end{aligned} \tag{3.63b}$$

As before, we let

$$\frac{dx_0}{dt} = F(x_0, x_{0T}, x_1, x_{1T}) \ , \quad \text{and} \quad \frac{dx_1}{dt} = M(x_0, x_{0T}, x_1, x_{1T}) \ . \tag{3.64}$$

Here we have that $F_{x_0} = F_{x_1} = 0$ and $M_{x_0} = M_{x_1} = 0$. Substituting the small perturbations in (3.55) into (3.64) gives the equations in (3.56), which in turn reduce to (3.58). We seek critical Hopf bifurcation parameter values that result in pure imaginary eigenvalues of the form $\lambda = i\omega$, for some $\omega > 0$, which gives that

$$\begin{aligned}
i\omega &= (F_{x_{0T}} + F_{x_{1T}}) \left[\cos(\omega T) - i \sin(\omega T) \right] \ , \\
i\omega &= (M_{x_{0T}} + M_{x_{1T}}) \left[\cos(\omega T) - i \sin(\omega T) \right] \ .
\end{aligned} \tag{3.65}$$

Comparing the real and imaginary terms in (3.65) gives

$$\begin{aligned}
(F_{x_{0T}} + F_{x_{1T}}) \cos(\omega T) &= 0 \ , \qquad (F_{x_{0T}} + F_{x_{1T}}) \sin(\omega T) = -\omega \ , \\
(M_{x_{0T}} + M_{x_{1T}}) \cos(\omega T) &= 0 \ , \qquad (M_{x_{0T}} + M_{x_{1T}}) \sin(\omega T) = -\omega \ .
\end{aligned} \tag{3.66}$$

Numerical computations of the solution to (3.66), using $\epsilon = 1$ to account for the slow time-scale of the spike motion, with $k = 2$ and $L = 0.5/\sqrt{0.2}$, yields the critical Hopf bifurcation parameter values

$$(\omega_H, T_H) \approx (1.97, 0.80) \ . \tag{3.67}$$

The results are illustrated in Figure 3.6.

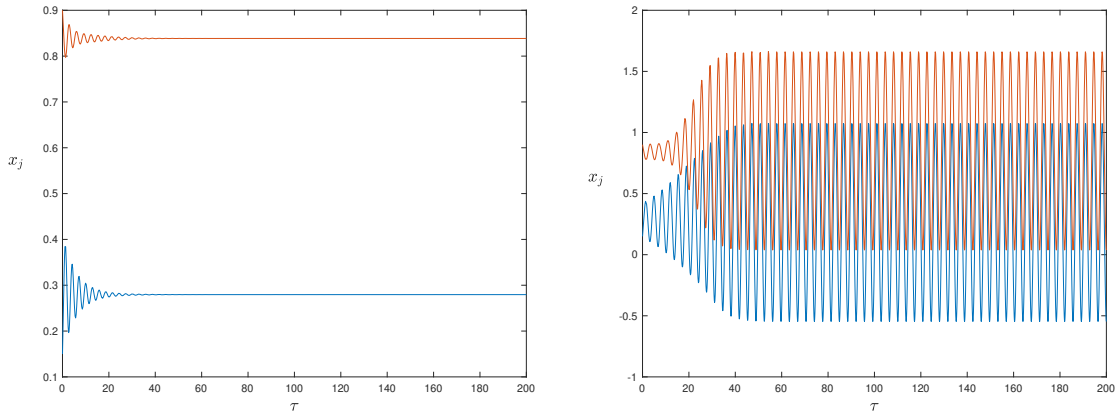

(a) $T = 0.7 < T_H$ (b) $T = 0.9 > T_H$

Figure 3.6: Plot of trajectories x_j corresponding to spike locations versus τ, as obtained from the DDAE system (3.62), with delay in the nonlinear term of the activator equation. Numerical simulations show decaying oscillations when $T = 0.7 < T_H$ (left figure), and sustained oscillations when $T = 0.9 > T_H$ (right figure). Parameters used are $\epsilon = 1$ (slow time-scale of motion), $k = 2$, $L = 0.5/\sqrt{0.2}$, $\mu = 1$, and $D = 1$.

Finally, we consider the system in (3.50). For $k = 2$, we get

$$\dot{\mathbf{x}} = -12\ \mathcal{H}_T^{-1}\ \mathcal{P}_T\ \boldsymbol{H}_T^2\ , \qquad \boldsymbol{H}_T = 6\ \mathcal{G}_T\ \boldsymbol{H}_T^2\ , \tag{3.68a}$$

where

$$\dot{\mathbf{x}} \equiv \begin{bmatrix} \dot{x}_0(\tau) \\ \dot{x}_1(\tau) \end{bmatrix}\ , \quad \boldsymbol{H}_T \equiv \begin{bmatrix} H_{0T} \\ H_{1T} \end{bmatrix}\ , \quad \boldsymbol{H}_T^2 \equiv \begin{bmatrix} H_{0T}^2 \\ H_{1T}^2 \end{bmatrix}\ , \quad \mathcal{H}_T \equiv \begin{bmatrix} H_{0T} & 0 \\ 0 & H_{1T} \end{bmatrix}\ ,$$

$$\mathcal{P}_T \equiv \begin{bmatrix} \langle G_x(x_{0T_1}; x_{0T_2})\rangle & G_x(x_{0T_1}; x_{1T_2}) \\ G_x(x_{1T_1}; x_{0T_2}) & \langle G_x(x_{1T_1}; x_{1T_2})\rangle \end{bmatrix}\ , \quad \mathcal{G}_T \equiv \begin{bmatrix} G(x_{0T_1}; x_{0T_2}) & G(x_{0T_1}; x_{1T_2}) \\ G(x_{1T_1}; x_{0T_2}) & G(x_{1T_1}; x_{1T_2}) \end{bmatrix}\ . \tag{3.68b}$$

In terms of the original times scale, we have that

$$\begin{bmatrix} \dfrac{dx_0}{dt} \\ \dfrac{dx_1}{dt} \end{bmatrix} = -\epsilon^2 \frac{12}{H_{0T} H_{1T}} \begin{bmatrix} H_{0T}^2\ H_{1T}\ \langle G_x(x_{0T_1}; x_{0T_2})\rangle + H_{1T}^3\ G_x(x_{0T_1}; x_{1T_2}) \\ H_{0T}^3\ G_x(x_{1T_1}; x_{0T_2}) + H_{0T} H_{1T}^2\ \langle G_x(x_{1T_1}; x_{1T_2})\rangle \end{bmatrix}\ , \tag{3.69}$$

$$\begin{bmatrix} H_{0T} \\ H_{1T} \end{bmatrix} = 6\ \begin{bmatrix} H_{0T}^2\ G(x_{0T_1}; x_{0T_2}) + H_{1T}^2\ G(x_{0T_1}; x_{1T_2}) \\ H_{0T}^2\ G(x_{1T_1}; x_{0T_2}) + H_{1T}^2\ G(x_{1T_1}; x_{1T_2}) \end{bmatrix}\ .$$

Substituting the expressions given in (3.50c) into (3.69) gives

$$\begin{aligned}\frac{dx_0}{dt} &= -\epsilon^2 \frac{6\ H_{0T}}{\sinh(L)}\Bigg[\cosh(x_{0T_2})\sinh(x_{0T_1}-L)+\sinh(x_{0T_1})\cosh(x_{0T_2}-L)\\ &\qquad +\ 2\ \left(\frac{H_{1T}}{H_{0T}}\right)^2\cosh(x_{1T_2})\sinh(x_{0T_1}-L)\Bigg]\ ,\\ \frac{dx_1}{dt} &= -\epsilon^2 \frac{6\ H_{1T}}{\sinh(L)}\Bigg[\cosh(x_{1T_2})\sinh(x_{1T_1}-L)+\sinh(x_{1T_1})\cosh(x_{1T_2}-L)\\ &\qquad +2\ \left(\frac{H_{0T}}{H_{1T}}\right)^2\cosh(x_{0T_2})\sinh(x_{1T_1}-L)\Bigg]\ ,\end{aligned} \tag{3.70a}$$

coupled to the algebraic system of equations given by

$$\begin{aligned}H_{0T} &= \frac{6}{\sinh(L)}\left[H_{0T}^2\ \cosh(x_{0T_2})\cosh(x_{0T_1}-L)+H_{1T}^2\ \cosh(x_{1T_2})\cosh(x_{0T_1}-L)\right]\ ,\\ H_{1T} &= \frac{6}{\sinh(L)}\left[H_{0T}^2\ \cosh(x_{0T_2})\cosh(x_{1T_1}-L)+H_{1T}^2\ \cosh(x_{1T_2})\cosh(x_{1T_1}-L)\right]\ .\end{aligned} \tag{3.70b}$$

Next, we let

$$\frac{dx_0}{dt} = F(x_{0T_1}, x_{0T_2}, x_{1T_1}, x_{1T_2})\ , \quad \text{and} \quad \frac{dx_1}{dt} = M(x_{0T_1}, x_{0T_2}, x_{1T_1}, x_{1T_2})\ . \tag{3.71}$$

Substituting the small perturbations in (3.55) into (3.71) and simplifying yields the following transcendental eigenvalue equations:

$$\begin{aligned}\lambda &= \left(F_{x_{0T_1}}+F_{x_{1T_1}}\right)e^{-\lambda T_1}+\left(F_{x_{0T_2}}+F_{x_{1T_2}}\right)e^{-\lambda T_2}\ , \quad \text{and}\\ \lambda &= \left(M_{x_{0T_1}}+M_{x_{1T_1}}\right)e^{-\lambda T_1}+\left(M_{x_{0T_2}}+M_{x_{1T_2}}\right)e^{-\lambda T_2}\ ,\end{aligned} \tag{3.72}$$

where $T_2 = 2T_1$. Next, we seek critical Hopf bifurcation parameter values that result in pure imaginary eigenvalues of the form $\lambda = i\omega$, for some $\omega > 0$, which yields

$$\begin{aligned}i\omega &= \left(F_{x_{0T_1}}+F_{x_{1T_1}}\right)\left[\cos(\omega T_1)-i\sin(\omega T_1)\right]+\left(F_{x_{0T_2}}+F_{x_{1T_2}}\right)\left[\cos(\omega T_2)-i\sin(\omega T_2)\right]\ ,\\ i\omega &= \left(M_{x_{0T_1}}+M_{x_{1T_1}}\right)\left[\cos(\omega T_1)-i\sin(\omega T_1)\right]+\left(M_{x_{0T_2}}+M_{x_{1T_2}}\right)\left[\cos(\omega T_2)-i\sin(\omega T_2)\right]\ .\end{aligned} \tag{3.73}$$

Comparing the real and imaginary terms in (3.73) gives

$$\begin{aligned}
\left(F_{x_{0T_1}} + F_{x_{1T_1}}\right)\cos\left(\omega T_1\right) + \left(F_{x_{0T_2}} + F_{x_{1T_2}}\right)\cos\left(\omega T_2\right) &= 0\ , \\
\left(F_{x_{0T_1}} + F_{x_{1T_1}}\right)\sin\left(\omega T_1\right) + \left(F_{x_{0T_2}} + F_{x_{1T_2}}\right)\sin\left(\omega T_2\right) &= -\omega\ , \\
\left(M_{x_{0T_1}} + M_{x_{1T_1}}\right)\cos\left(\omega T_1\right) + \left(M_{x_{0T_2}} + M_{x_{1T_2}}\right)\cos\left(\omega T_2\right) &= 0\ , \\
\left(M_{x_{0T_1}} + M_{x_{1T_1}}\right)\sin\left(\omega T_1\right) + \left(M_{x_{0T_2}} + M_{x_{1T_2}}\right)\sin\left(\omega T_2\right) &= -\omega\ .
\end{aligned} \tag{3.74}$$

Numerical computations of the solution to (3.74), using $\epsilon = 1$ to account for the slow time-scale of the spike motion, with $k = 2$ and $L = 0.5/\sqrt{0.2}$, yields the critical Hopf bifurcation values

$$(\omega_H, T_H) \approx (2.18, 0.76)\ . \tag{3.75}$$

The results are illustrated in Figure 3.7.

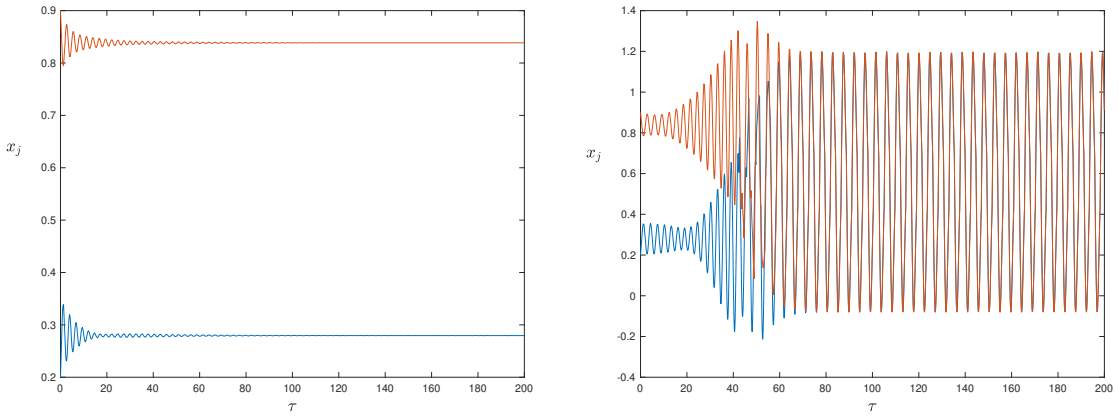

(a) $T_1 = 0.7 < T_H$ (b) $T_1 = 0.8 > T_H$

Figure 3.7: Plot of trajectories x_j corresponding to spike locations versus τ, as obtained from the DDAE system (3.69), with delay in both the activator regulation and inhibitor production. Numerical simulations show decaying oscillations when $T_1 = 0.7 < T_H$ (left figure), and sustained oscillations when $T_1 = 0.8 > T_H$ (right figure). Parameters values are as in the caption of Figure 3.6.

3.4 Hopf Bifurcation in the Large Eigenvalues

We now examine the stability of the k-spike solution constructed in §3.1 to the GM model for two cases of delayed reaction kinetics. We note that a k-spike solution over the interval $[0, L]$ can be constructed from a one-spike solution over the small interval

$[-l, l]$, where $l = L/2k$ is the base length of the spike, using appropriate reflections and translations. In particular, a k-spike solution is constructed over the interval $[-l, (2k-1)l]$ by glueing together k copies of a single spike (see [33, 34, 37, 38, 39, 71]). However, the stability analysis of the k-spike solution is quite different from that of a single spike, as studied in §2.3, since each eigenvalue from a single spike solution now corresponds to k distinct eigenvalues in the k-spike case. To find these eigenvalues, we first consider in §3.4.1 the linearized eigenvalue problem corresponding to the k-spike solution over the interval $[-l, (2k-1)l]$, subject to periodic boundary conditions. We then use a Floquet-type approach (see [37, 38, 58, 71]), where we derive complex boundary conditions and use them to construct a global eigenfunction by piecing together k eigenfunctions, each corresponding to a single spike. Using these Floquet-type boundary conditions, we can then construct the k eigenfunctions. Finally, we show that the stability of the k-spike solution with Neumann boundary conditions can be derived from the stability of $2k$-spike solution with periodic boundary conditions.

For clarity, in §3.4.1 we use the case with no delay to describe the derivation of the corresponding NLEP using a singular perturbation approach. In §3.4.2 and §3.4.3, we analyze the GM model with delayed inhibitor catalyzed production, as well as when delay is in both the activator regulation and inhibitor production. In each case, we find that oscillatory instabilities in the spike amplitudes are triggered as time delay T is increased past a Hopf bifurcation threshold, which we numerically calculate.

3.4.1 Formulation of Eigenvalue Problem: No Delay Case

In this section, we derive the eigenvalue problem associated with linearizing the one-dimensional GM model with no delay given by

$$a_t = \epsilon^2 a_{xx} - a + \frac{a^2}{h} , \qquad 0 < x < L , \ t > 0 , \tag{3.76a}$$

$$0 = h_{xx} - h + \frac{a^2}{\epsilon} , \qquad 0 < x < L , \ t > 0 , \tag{3.76b}$$

$$a_x(0,t) = a_x(L,t) = h_x(0,t) = h_x(L,t) = 0 , \tag{3.76c}$$

around the k-spike equilibrium solution (3.16). In studying the stability of this k-spike equilibrium, we first consider a one-spike solution to (3.76) over the small

interval $[-l, l]$, such that the base length of the spike is given by $2\ l = L/k$. Glueing together k copies of the single spike results in a k-spike solution over the interval $[-l, (2k-1)l]$. This approach has been previously used for various RD systems with k hot-spots and spike-type patterns (see [33, 34, 37, 38, 39, 71]).

Using (a_e, h_e) to denote a 1-spike equilibrium solution to (3.76) over the domain $|x| \leq l$, we introduce the small perturbation

$$a(x,t) = a_e(x) + e^{\lambda t}\phi(x)\ , \qquad h(x,t) = h_e(x) + e^{\lambda t}\psi(x)\ , \tag{3.77}$$

where $\phi \ll a_e$ and $\psi \ll h_e$. Substituting (3.77) into the model equations in (3.76) yields the eigenvalue problem

$$\lambda\phi = \epsilon^2\phi_{xx} - \phi + 2\ \frac{a_e}{h_e}\ \phi - \frac{a_e^2}{h_e^2}\ \psi\ , \tag{3.78a}$$

$$\psi_{xx} - \psi = -2\ \frac{a_e}{\epsilon}\ \phi\ . \tag{3.78b}$$

Following the approach used in [37, 38, 58, 71], we consider the eigenvalue problem in (3.78) on the interval $[-l, l]$, and we impose the Floquet-type boundary conditions

$$\begin{aligned} \phi(l) = z\phi(-l)\ , \quad \phi'(l) = z\phi'(-l)\ , \\ \psi(l) = z\psi(-l)\ , \quad \psi'(l) = z\psi'(-l)\ , \end{aligned} \tag{3.79}$$

where z is a complex parameter to be determined such that (3.78) is an eigenvalue problem corresponding to a k-spike solution on the interval $[-l, (2k-1)l]$ with periodic boundary conditions. This can be achieved by translating the eigenfunctions ϕ and ψ from the interval $[-l, l]$ to the extended interval $[-l, (2k-1)l]$, such that the extended eigenfunctions are continuous and have continuous first derivatives at the points $x = l, 3\ l, 5\ l, \ldots, (2k-3)\ l$. As a result, we get that $\phi((2k-1)l) = z^k\phi(-l)$. Therefore, in order to get periodic boundary conditions on the interval $[-l, (2k-1)l]$, we require that the complex parameter z must also satisfy $z^k = 1$, and we get that

$$z = e^{i\theta}\ , \quad \text{where } \theta = \frac{2\pi j}{k}\ ,\ j = 0, \ldots, k-1\ . \tag{3.80}$$

It follows that the eigenvalue problem in (3.78), using the values of z as defined in (3.80), can be used to analyze the stability of a k-spike equilibrium solution on the domain $[-l, (2k-1)l]$ with periodic boundary conditions.

It remains to show that the stability analysis of a $2k$-spike problem with periodic boundary conditions can be used to derive the stability of a k-spike problem with Neumann boundary conditions. This method has been used in [37] and [38], and we summarize the result in the following Proposition.

Proposition 3.2. *The spectrum of the k-spike eigenvalue problem in* (3.78) *corresponding to the one-dimensional Gierer-Meinhardt model given in* (3.76)*, over the interval $[0, L]$ and subject to Neumann boundary conditions* (3.76c)*, is a subset of the spectrum corresponding to the $2k$-spike problem with periodic boundary conditions, over the interval $[-l, (2k-1)l]$ where $l = L/2k$.*

Proof. Suppose $(\lambda, \phi(x))$ is an eigenpair with Neumann BC on $[0, \zeta]$. Using even reflection, ϕ can be extended to an eigenfunction over the domain $[-\zeta, \zeta]$, which now satisfies periodic boundary conditions over the interval $[-\zeta, \zeta]$. Thus, the eigenvalues of k spikes with Neumann boundary conditions form a subset of ones corresponding to $2k$ spikes with periodic boundary conditions, since every eigenvalue of the Neumann system is also an eigenvalue of the periodic system.

Moreover, If $\phi(x)$ is an eigenfunction with periodic boundary conditions over the interval $[-\zeta, \zeta]$, then $\phi(x)$ satisfies

$$\phi(-\zeta) = \phi(\zeta) \ , \quad \text{and} \quad \phi'(-\zeta) = \phi'(\zeta) \ . \tag{3.81}$$

Next, we define $\hat{\phi}(x)$ such that

$$\hat{\phi}(x) = \phi(x) + \phi(-x) \ . \tag{3.82}$$

Thus, if $\phi(x)$ is odd, we get that $\hat{\phi}(x) \equiv 0$. Using the boundary conditions in (3.81), we get that if $\hat{\phi}(x) \not\equiv 0$, and

$$\hat{\phi}'(0) = 0 \ , \tag{3.83a}$$

$$\hat{\phi}'(\zeta) = \phi'(\zeta) - \phi'(-\zeta) = 0 \ . \tag{3.83b}$$

It follows that the even nonzero eigenfunctions of the periodic system correspond to the eigenfunctions in the Neumann system. Thus, $\hat{\phi}(x) \neq 0$ is an eigenfunction with Neumann boundary conditions on $[0, \zeta]$. In addition, since $\hat{\phi}(x)$ satisfies the linear ODE in (3.82) and the condition in (3.83b), therefore $\hat{\phi}(x) \not\equiv 0$ if and only if $\hat{\phi}(\zeta) \not\equiv 0$, which is true if and only if $\phi(\zeta) \not\equiv 0$. □

We now implement the results of Proposition 3.2 in studying the stability of the k-spike solution (3.16) using the spectrum of the associated eigenvalue problem for different cases of delayed reaction kinetics.

3.4.2 Delay in the Catalyzed Production of Inhibitor

In this section, we extend the notation in §3.4.1 to the case of a k-spike solution to the GM model in (3.17) with delayed inhibitor kinetics, defined over the interval $[0, L]$, with $\mu = 1$ and $D = 1$. Using the k-spike equilibrium in (3.16), the eigenvalue problem (3.78) then becomes

$$\lambda\phi = \epsilon^2\phi_{xx} - \phi + 2\,\frac{a_{e,k}}{h_{e,k}}\,\phi - \frac{a_{e,k}^2}{h_{e,k}^2}\,\psi\ , \qquad 0 < x < L\ , \tag{3.84a}$$

$$0 = \psi_{xx} - \psi + 2\,\frac{a_{e,k}}{\epsilon}\,e^{-\lambda T}\phi\ , \qquad 0 < x < L\ . \tag{3.84b}$$

Using Proposition 3.2, the effect of delay on the stability of the k-spike solution (3.16) can be studied by analyzing the k-large eigenvalues of $O(1)$ admitted by the eigenvalue problem in (3.84).

For boundary conditions, we consider the k-spike configuration over the interval $[-l, (2k-1)l]$. As an example, we consider the case of three spikes. In this case, with $k = 3$, the periodic boundary conditions are given by

$$\begin{aligned} \phi(-l) &= \phi(5l)\ , \qquad \phi'(-l) = \phi'(5l)\ , \\ \psi(-l) &= \psi(5l)\ , \qquad \psi'(-l) = \psi'(5l)\ . \end{aligned} \tag{3.85}$$

The boundary conditions in (3.85) can be written in the form

$$\boldsymbol{P}(-l) = \boldsymbol{P}((2k-1)l)\ , \quad \text{where} \quad \boldsymbol{P} = \begin{bmatrix} \phi \\ \phi' \\ \psi \\ \psi' \end{bmatrix}\ . \tag{3.86}$$

For the general case of k-spikes over the interval $[-l, (2k-1)l]$, (3.86) then becomes

$$\boldsymbol{P}(-l) = z\boldsymbol{P}(l)\ , \tag{3.87a}$$

where

$$z = e^{2\pi i j/k}\ , \qquad \text{for} \quad j = 0, \ldots, k-1\ . \tag{3.87b}$$

Using the Floquet theory approach, we formulate the corresponding NLEP in terms of the Green's function in (3.14) over the interval $[-l, l]$, subject to the Floquet boundary conditions

$$G(l) = zG(-l) \ , \qquad G'(l) = zG'(-l) \ , \tag{3.88}$$

where z is as defined in (3.87b). This yields the solution

$$G(x) = \begin{cases} A \ \cosh(x+l) + B \ \sinh(x+l) \ , & -l < x < 0 \ , \\ z \ A \ \cosh(x-l) + z \ B \ \sinh(x-l) \ , & 0 < x < l \ , \end{cases} \tag{3.89a}$$

such that $G(0^+) = G(0^-)$, and $G'(0^+) - G'(0^-) = -1$. Rewriting the solution in (3.89a) as

$$\begin{bmatrix} (1-z)\cosh l & (1+z)\sinh l \\ (1+z)\sinh l & (1-z)\cosh l \end{bmatrix} \begin{bmatrix} A \\ B \end{bmatrix} = \begin{bmatrix} 0 \\ 1 \end{bmatrix} \ ,$$

and solving for A and B gives

$$A = \frac{(1+z)\sinh(l)}{4 \ z \ \cosh^2(l) - (1+z)^2} \ , \qquad B = \frac{(z-1)\cosh(l)}{4 \ z \ \cosh^2(l) - (1+z)^2} \ . \tag{3.89b}$$

It follows that

$$G(0) = \frac{\sinh(l)\cosh(l)}{\cosh^2(l) + \sinh^2(l) - \cos(\theta)} \ , \quad \text{where } \theta = 2\pi j/k, \ j = 0, \ldots, k-1. \tag{3.90}$$

Therefore, for a k-spike solution, using (3.90), we get the NLEP

$$\lambda\phi = \phi_{yy} - \phi + 2 \ w \ \phi - e^{-\lambda T} \ \chi \ w^2 \left(\frac{\int_{-\infty}^{\infty} w \ \phi \ dy}{\int_{-\infty}^{\infty} w^2 \ dy} \right) \ , \tag{3.91a}$$

where $\phi(y) \to 0$ as $y \to \pm\infty$, and χ is given by

$$\chi = \frac{4 \ \sinh^2(l)}{\cosh^2(l) + \sinh^2(l) - \cos(\theta)} \ , \quad \theta = 2\pi j/k, \ j = 0, \ldots, k-1. \tag{3.91b}$$

Proceeding in the same manner for increasing values of l, we determine the smallest positive value of delay T at which a Hopf bifurcation occurs by seeking pure imaginary eigenvalues satisfying (3.91). Using the notation in §2.3, any unstable eigenvalue of (3.91) must be a root of $g(\lambda) = 0$, as defined in (2.90). Substituting $\lambda = i\lambda_I$ into (2.90) and separating the real and imaginary components gives the coupled

system in (2.91), which satisfies the equations given in (2.92), where χ is as defined in (3.91b).

Numerically, with $k = 2$ and $L = 2/\sqrt{0.2}$, the smallest value of χ is found to be 0.231, and we obtain the critical Hopf bifurcation values given by

$$(\lambda_{IH}, T_H) = (8.68, 0.451) \ . \tag{3.92}$$

To confirm our results, we compute full numerical solutions to (3.17) for delay values below and above the critical Hopf threshold T_H. For $L = 2/\sqrt{0.2}$, delay values greater than T_H trigger an oscillatory instability in the spike amplitudes, as shown in Figure 3.8, where we plot the spike amplitudes $a(x_j)$ versus time t, for delay below and above T_H.

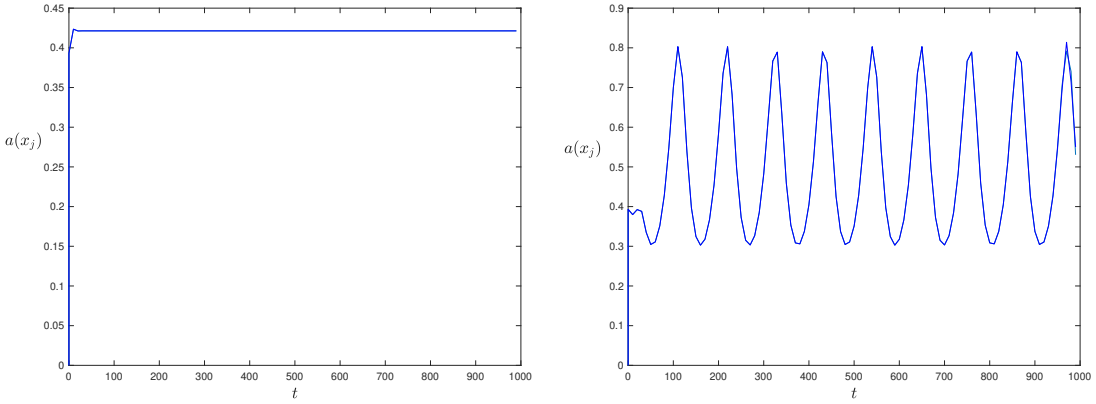

(a) $T = .4 < T_H$ (b) $T = .49 > T_H$

Figure 3.8: Plot of amplitude $a(x_j)$ for a two-spike solution to (3.17) versus time t, for delay below and above the critical value of $T_H \sim 0.451$. Parameters used are $k = 2$, $\epsilon = 0.06$, $L = 2/\sqrt{0.2}$, $\mu = 1$, and $D = 1$.

3.4.3 Delay in Activator Regulation and Inhibitor Production

In this section, we consider the stability of the k-spike equilibrium solution to the GM model (3.43), with delay in both the activator regulation and inhibitor production. The corresponding NLEP for this model is given by

$$\lambda\phi = \phi_{yy} - \phi + 2\ w\ \phi - e^{-2\lambda T}\ \chi\ w^2 \left(\frac{\int_{-\infty}^{\infty} w\ \phi\ dy}{\int_{-\infty}^{\infty} w^2\ dy} \right) \ , \tag{3.93}$$

where $\phi(y) \to 0$ as $y \to \pm\infty$, and χ is as defined in (3.91b). Proceeding in the same manner as in §3.4.2, we get the coupled system

$$g_R(\lambda_I) = g_I(\lambda_I) = 0 \ , \tag{3.94a}$$

where,

$$\begin{aligned}
&g_R(\lambda_I) = C_R(\lambda_I) - f_R(\lambda_I) \ , && g_I(\lambda_I) = C_I(\lambda_I) - f_I(\lambda_I) \ , \\
&C_R(\lambda_I) = Re\left[C(i\lambda_I)\right] \ , && C_I(\lambda_I) = Im\left[C(i\lambda_I)\right] \ , \\
&f_R(\lambda_I) = \frac{\int_{-\infty}^{\infty} wL_0[L_0^2+\lambda_I^2]^{-1}w^2dy}{\int_{-\infty}^{\infty} w^2dy}, && f_I(\lambda_I) = \frac{\lambda_I \int_{-\infty}^{\infty} w[L_0^2+\lambda_I^2]^{-1}w^2dy}{\int_{-\infty}^{\infty} w^2dy}, \\
&C_R(\lambda_I) = \frac{1}{\chi}\cos(2\lambda_I T) \ , && C_I(\lambda_I) = \frac{1}{\chi}\sin(2\lambda_I T) \ .
\end{aligned} \tag{3.94b}$$

Numerical computations, with $k = 2$ and $L = 2/\sqrt{0.2}$, yield that $\chi_{\min} = 0.231$, and predict that a Hopf bifurcation occurs when

$$(\lambda_{IH}, T_H) = (8.68, 0.226) \ . \tag{3.95}$$

To confirm our predictions, we compute full numerical solutions to (3.43) for delay values below and above the critical Hopf threshold T_H. In Figure 3.8, we plot spike amplitudes $a(x_j)$ as a function of time t, for two spikes with $L = 2/\sqrt{0.2}$. From this figure we observe that sustained oscillations occur as delay increases past the critical value T_H.

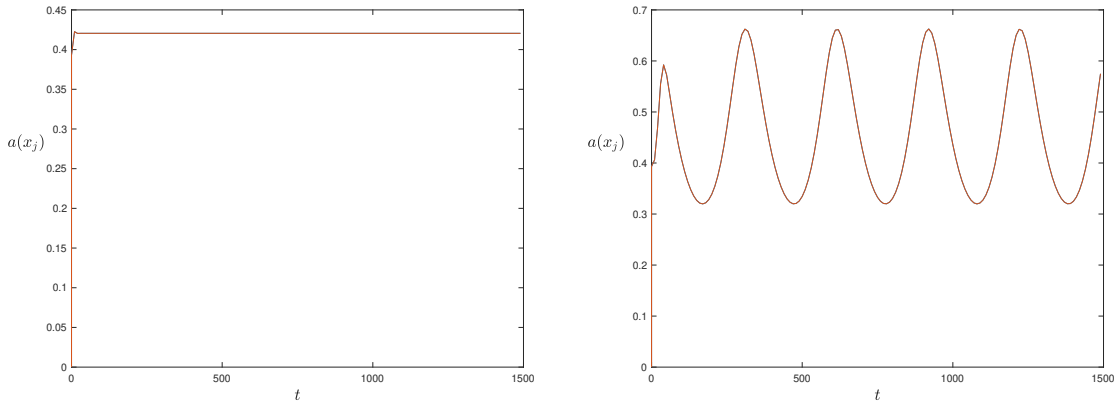

(a) $T = .2 < T_H$ (b) $T = .24 > T_H$

Figure 3.9: Plot of amplitudes $a(x_j)$ for a two-spike solution to (3.43) versus time t, for delay below and above the critical value of $T_H \sim 0.226$. Parameters used are $k = 2$, $\epsilon = 0.05$, $\mu = 1$, $L = 2/\sqrt{0.2}$, and $D = 1$.

We have now formulated a framework for analyzing the stability of spike-type solutions to the one-dimensional GM model with delayed reaction kinetics, using a combination of asymptotic and numerical methods. In the next chapter, we analyze the stability of a coupled cell-bulk model with delayed intracellular dynamics.

Chapter 4

A Coupled Cell-Bulk Model with Delayed Intracellular Dynamics in Two-Dimensional Bounded Domain

In Chapters §2 and §3, we analyzed the stability of spike-type solutions to the GM model in a one-dimensional domain, with delayed reaction kinetics. In this chapter, we consider the coupled cell-bulk PDE model constructed and analyzed in [25] and [26], in a two-dimensional bounded domain. In this model, dynamically active signalling cells, with n-interacting species, release a signalling molecule into an exterior bulk region and the release is regulated by the external bulk concentration at the corresponding cell membrane as well as its density inside the cell. In [25], the authors show that in the case of fast bulk diffusion ($D >> 1$), the bulk region is well-mixed and the PDE-ODE cell-bulk model can be reduced to a nonlinear finite-dimensional ODE system for the bulk concentration field coupled to the intracellular dynamics. In this limiting regime, analysis of the ODE system shows that oscillatory instabilities may arise due to the cell-bulk coupling. In particular, communication between the multiple small spatially segregated signalling cells in the well-mixed system, with multi-component intracellular dynamics, has been shown to lead to quorum sensing behaviour whereby collective oscillations are triggered as the number of cells exceeds a certain threshold, (see for example [3] and the references therein). Other regimes for the diffusion parameter D have also been analyzed (see [25] and [26]), where cell-bulk coupling has been shown to trigger oscillatory instabilities, due to a Hopf bifurcation, which were not present otherwise. In addition, diffusion-sensing behaviour has been observed for the case where $D = O(1)$. In this case, the spatial configuration of the cells in the domain plays an important role in triggering collective synchronous oscillations.

In this chapter, we extend the analysis in [25] to allow for delayed intracellular dynamics and we analyze the effect of this delay on the stability of the steady state solutions in the limit of very large diffusion. The notation and methods used in [25]

carry over with a few changes, and we show that the reduced system of ordinary differential equations becomes a system of delay differential equations.

In §4.1, we consider the coupled cell-bulk model, in a two-dimensional bounded domain, consisting of one signalling cell and n-intracellular interacting species with delayed dynamics. In the limit of very large diffusion, we reduce the dynamics of the coupled cell-bulk model to a system of nonlinear DDEs. In §4.2, for the case of one intracellular component in a small circular cell, we find conditions for the existence of the steady state solutions and we derive the corresponding eigenvalue problem whose spectrum characterizes the stability properties of the steady states. In §4.3, we consider the case where the delayed intracellular dynamics are governed by Hill function-type kinetics and we find the equilibrium solutions to the model. In §4.4, numerical simulations are used to illustrate the destabilizing effect of delay on the steady state solutions to the model, and the corresponding critical Hopf bifurcation delay values are determined. This is in contrast to the results obtained in [25], where it has been shown that in the absence of delay no triggered oscillations can occur for the case with only one cell containing one dynamically active intracellular component.

4.1 Model Formulation: One Signalling Cell with Multiple Interacting Species

We begin by formulating the coupled cell-bulk model in a two-dimensional bounded domain Ω, consisting of a single small circular signalling cell of radius ϵ, denoted by $\Omega_\epsilon \in \Omega$, centered at some point $\boldsymbol{X} \in \Omega$. We assume that there are n interacting species, denoted by $\boldsymbol{\mu} = (\mu^1, \ldots, \mu^n)$, inside the cell such that only one of these intracellular species, μ^1, is capable of leaving the cell into the bulk. The partial differential equations for the model are given by

$$\mathcal{U}_\mathcal{T} = D_B \, \Delta_{\boldsymbol{X}} \mathcal{U} - k_B \, \mathcal{U} \, , \qquad \boldsymbol{X} \in \Omega \setminus \Omega_\epsilon \, , \tag{4.1a}$$

$$\partial_{n_{\boldsymbol{X}}} \mathcal{U} = 0 \, , \qquad \boldsymbol{X} \in \partial\Omega \, , \tag{4.1b}$$

$$D_B \, \partial_{n_{\boldsymbol{X}}} \mathcal{U} = \beta_1 \, \mathcal{U} - \beta_2 \, \mu^1 \, , \qquad \boldsymbol{X} \in \partial\Omega_\epsilon \, , \tag{4.1c}$$

coupled to delayed intracellular dynamics of n interacting species given by the ODE system

$$\frac{d\boldsymbol{\mu}}{d\mathcal{T}} = k_R\ \mu_c\ \boldsymbol{F}(\boldsymbol{\mu}_T/\mu_c) + \boldsymbol{e}_1\ \int_{\partial\Omega_\epsilon} (\beta_1 \mathcal{U} - \beta_2 \mu^1) dS_{\boldsymbol{X}}\ , \tag{4.1d}$$

where $\boldsymbol{e}_1 = (1, 0, \ldots, 0)^T$. Here, $\mathcal{U}(\boldsymbol{X}, \mathcal{T})$ denotes the external concentration of the signalling molecule in the bulk region, $\Omega \setminus \Omega_\epsilon$, at time $\mathcal{T}$; $D_B > 0$ is the diffusion coefficient for the bulk process, and $\partial_{n_{\boldsymbol{X}}}$ represents the outer normal derivative of the domain Ω or the outer normal to Ω_ϵ. The permeability of the cell wall is represented by the positive dimensionless constants β_1 and β_2.

In (4.1d), $k_R > 0$ is the intracellular dynamics reaction rate, and $\boldsymbol{F}(\boldsymbol{\mu}_T/\mu_c)$ is a dimensionless function used to model the delayed intracellular reaction dynamics, for some fixed time delay T. The constant $\mu_c > 0$ is a nondimensional scaling constant used to measure a typical value of μ inside the signalling compartment (see [25]). The flux term $\beta_1\ \mathcal{U} - \beta_2\ \mu^1$, integrated over the cell boundary $dS_{\boldsymbol{X}}$, represents the influx of the signalling molecule into the bulk region, which depends on $\mathcal{U}(\boldsymbol{X}, \mathcal{T})$ at the cell membrane $\partial\Omega_\epsilon$ and the concentration of μ^1 inside the cell.

Next, we introduce the dimensionless variables and parameters given by

$$\begin{gathered} U = \frac{L^2}{\mu_c}\,\mathcal{U}\ , \qquad \boldsymbol{u} = \frac{\mu}{\mu_c}\ , \qquad t = \frac{\mathcal{T}}{t_R}\ , \qquad \boldsymbol{x} = \frac{\boldsymbol{X}}{L}\ , \\ \tau = \frac{k_R}{k_B}\ , \qquad \beta_1 = (k_B L)\frac{d_1}{\epsilon}\ , \qquad \beta_2 = \left(\frac{k_B}{L}\right)\frac{d_2}{\epsilon}\ , \end{gathered} \tag{4.2}$$

where L represents the radius of Ω. With respect to the slow time variable, in the limit $\tau \ll 1$, the intracellular dynamics are much slower than the rate of degradation of the signalling molecule in the bulk region. In addition, we choose t_R depending on the time-scale of the reaction dynamics, and we define a new dimensionless diffusivity parameter D given by

$$t_R = \frac{1}{k_R}\ , \qquad D = \frac{D_B}{k_B\ L^2}\ . \tag{4.3}$$

Using the nondimensionalization process in [25], we get the following nondimensional system for the model in (4.1):

$$\tau U_t = D\Delta U - U\ , \qquad \boldsymbol{x} \in \Omega \setminus \Omega_\epsilon\ , \tag{4.4a}$$

$$\partial_n U = 0\ , \qquad \boldsymbol{x} \in \partial\Omega\ , \tag{4.4b}$$

$$\epsilon D \partial_n U = d_1 U - d_2 u_1\ , \qquad \boldsymbol{x} \in \partial\Omega_\epsilon\ , \tag{4.4c}$$

coupled to the delayed intracellular dynamics given by

$$\frac{d\boldsymbol{u}}{dt} = \boldsymbol{F}(\boldsymbol{u}_T) + \frac{1}{\epsilon\tau}\int_{\partial\Omega_\epsilon}(d_1U - d_2u_1)ds\ \boldsymbol{e}_1\ . \tag{4.4d}$$

We assume fast diffusion of the signalling molecule into a well-mixed bulk region, such that the diffusion coefficient D satisfies $D \gg \mathcal{O}(\nu^{-1})$, for $\nu = -1/\log\epsilon$. As shown in [25], in this case the coupled PDE model in (4.4) can be reduced to the $(n+1)$-dimensional system of delay differential equations given by

$$U_0' = -\frac{1}{\tau}\left(1 + \frac{2\pi d_1}{|\Omega|}\right)U_0 + \frac{2\pi d_2}{\tau|\Omega|}u_1\ , \tag{4.5a}$$

$$\boldsymbol{u}' = \boldsymbol{F}(\boldsymbol{u}_T) + \frac{2\pi}{\tau}\ (d_1U_0 - d_2u_1)\,\boldsymbol{e}_1\ , \tag{4.5b}$$

where $U_0(t)$ and $\boldsymbol{u}$ denote the leading-order average bulk concentration and the cell dynamics, respectively.

4.2 Stability Analysis: One Cell and One Local Component

In this section, we analyze the coupled cell-bulk model in (4.5), with one small circular cell μ centered at the point $x_0 \in \Omega$, and containing one intracellular species $(n = 1)$. We again assume a small disk radius, such that $\epsilon << 1$. Thus, for some delay $T > 0$, the corresponding ODE system is given by

$$U_0' = -\frac{1}{\tau}\left(1 + \frac{2\pi d_1}{|\Omega|}\right)U_0 + \frac{2\pi d_2}{\tau|\Omega|}u\ , \tag{4.6a}$$

$$u' = F(u_T) + \frac{2\pi}{\tau}\ (d_1U_0 - d_2u)\ . \tag{4.6b}$$

Thus the equilibrium solutions U_{0e} and u_e must satisfy

$$0 = F(u_e) + \frac{2\pi}{\tau}\ (d_1\ U_{0e} - d_2\ u_e)\ , \qquad U_{0e} = \left(\frac{2\pi d_2}{|\Omega|}\right)\left(1 + \frac{2\pi d_1}{|\Omega|}\right)^{-1} u_e\ . \tag{4.7}$$

We introduce the small perturbation to the equilibrium solution

$$u = u_e + e^{\lambda t}\phi\ , \qquad U_0 = U_{0e} + e^{\lambda t}\eta\ , \tag{4.8}$$

where $|\phi| \ll |u_e|$ and $|\eta| \ll |U_{0e}|$. Substituting (4.8) into (4.6) and linearizing gives

$$\lambda\phi = e^{-\lambda T}\phi\ F_u^e + \frac{2\pi}{\tau}(d_1\eta - d_2\phi)\ , \tag{4.9a}$$

$$\eta = \frac{s}{\tau\lambda + r}\ \phi\ , \tag{4.9b}$$

where $r = 1 + \dfrac{2\pi d_1}{|\Omega|}$, and $s = \dfrac{2\pi d_2}{|\Omega|}$.

Thus, λ must be a root of the equation $\mathcal{Q}(\lambda) = 0$, where $\mathcal{Q}(\lambda)$ is the quasi-polynomial given by

$$\mathcal{Q}(\lambda) \equiv -\frac{\tau(r + \tau\lambda)}{2\pi d_2(1 + \tau\lambda)} - \frac{1}{det(\lambda I - Je^{-\lambda T})} \ . \tag{4.10}$$

Here J is the Jacobian of F evaluated at the steady state $u = u_e$. It follows that

$$det(\lambda I - Je^{-\lambda T}) = \lambda - F_u^e \ e^{-\lambda T} \ , \qquad \text{where} \quad F_u^e = \left.\frac{dF}{du}\right|_{u=u_e} . \tag{4.11}$$

Stability is then determined by the roots of the quasi-polynomial

$$\lambda^2 + \lambda \ p_1(\lambda) + p_2(\lambda) = 0 \tag{4.12a}$$

where

$$\begin{aligned} p_1(\lambda) &= \frac{1}{\tau}\left(1 + \frac{2\pi d_1}{|\Omega|}\right) - e^{-\lambda T} \ F_u^e + \frac{2\pi d_2}{\tau} \ , \\ p_2(\lambda) &= -\frac{e^{-\lambda T} F_u^e}{\tau}\left(1 + \frac{2\pi d_1}{|\Omega|}\right) + \frac{2\pi d_2}{\tau^2} \ . \end{aligned} \tag{4.12b}$$

For the case with no delay, we get the following result (from [25]) for (4.12).

Principal Result 4.1. *(From [25]): Let $T = 0$ and $n = 1$. Then, no Hopf bifurcation can occur for the steady state solution to* (4.5)*. Moreover, if*

$$F_u^e < F_{th} \equiv \frac{2\pi d_2}{\tau} \ \left[1 + \frac{2\pi d_1}{|\Omega|}\right]^{-1} \tag{4.13}$$

then $Re(\lambda) < 0$, and the steady state is linearly stable. On the other hand, if $F_u^e > F_{th}$, the linearization has exactly one positive eigenvalue.

The result above shows that, for the case with no delay, cell-bulk coupling can result in a linearly stable steady state solution to (4.5), even for $F_u^e > 0$ when the reaction kinetics are self-activating. In addition, from (4.13) we have that the stability threshold F_{th} decreases as τ increases. Thus, in the absence of delay, fast cell dynamics result in a decreased threshold for the self-activating reaction kinetics, while the stability of the steady state solution to the coupled system is maintained.

To analyze the effect of delay, we solve (4.12) for the smallest positive critical value of T which gives rise to pure imaginary eigenvalues. Substituting $\lambda = i\omega$, for some positive $\omega \in \mathbb{R}$, into (4.12) and rearranging gives

$$-\omega^2 + i\omega\ p_1(\omega) + p_2(\omega) = 0\ , \tag{4.14a}$$

where

$$\begin{aligned} p_1(\omega) &= \frac{1}{\tau}\left(1 + \frac{2\pi d_1}{|\Omega|}\right) - e^{-i\omega T}\ F_u^e + \frac{2\pi d_2}{\tau}\ , \\ p_2(\omega) &= -\frac{e^{-i\omega T} F_u^e}{\tau}\left(1 + \frac{2\pi d_1}{|\Omega|}\right) + \frac{2\pi d_2}{\tau^2}\ . \end{aligned} \tag{4.14b}$$

To simplify the analysis, we introduce the parameters a and b defined by

$$a = \frac{r}{\tau} = \frac{1}{\tau}\left(1 + \frac{2\pi d_1}{|\Omega|}\right)\ , \qquad b = \frac{2\pi d_2}{\tau^2}\ . \tag{4.15}$$

Using (4.15) as well as the Euler formula expansion $e^{-i\omega T} = \cos(\omega T) - i\sin(\omega T)$, equation (4.14) simplifies to

$$\cos(\omega T) - i\sin(\omega T) = P(\omega) - iQ(\omega)\ , \tag{4.16a}$$

where $P(\omega)$ and $Q(\omega)$ are given by

$$P(\omega) = \frac{\omega^2\ \tau b + ab}{F_u^e\left(a^2 + \omega^2\right)}\ , \qquad Q(\omega) = \frac{\omega\ \left(b - \ a^2 - \tau ab\right) - \omega^3}{F_u^e\left(a^2 + \omega^2\right)}\ , \tag{4.16b}$$

whenever $F_u^e \neq 0$. From (4.16), we get that $P(\omega)$ and $Q(\omega)$ must satisfy the equations

$$P^2(\omega) + Q^2(\omega) = 1\ , \tag{4.17a}$$

$$\tan(\omega T) = \frac{Q(\omega)}{P(\omega)}\ . \tag{4.17b}$$

Equation (4.17a) gives that

$$\left(\omega^2\ \tau b + ab\right)^2 + \omega^2\ \left(-\omega^2 + b - \ a^2 - \tau ab\right)^2 = \left(F_u^e\right)^2\left(a^2 + \omega^2\right)^2\ . \tag{4.18}$$

Using the scaling $Z = \omega^2$, we obtain from (4.18) that $Z > 0$ must be a root of the cubic equation

$$Z^3 + a_1\ Z^2 + a_2\ Z + a_3 = 0\ , \tag{4.19a}$$

where

$$
\begin{aligned}
a_1 &= \tau^2 b^2 - 2b + 2\ a^2 + 2\tau ab - (F_u^e)^2\ , \\
a_2 &= 2\tau ab^2 + \ (b - \ a^2 - \tau ab)^2 - 2\ a^2\ \ (F_u^e)^2\ , \\
a_3 &= a^2 b^2 - a^4\,(F_u^e)^2 = a^2(b^2 - a^2\,(F_u^e)^2) = a^2(b + aF_u^e)(b - aF_u^e)\ .
\end{aligned}
\tag{4.19b}
$$

Moreover, since $\tau a > 1$, therefore we get from (4.17b) that

$$
\tan(\omega T) = \frac{-\omega\ \ (b(\tau a - 1) + \ a^2 + \omega^2)}{\omega^2\ \tau b + ab}\ < 0\ . \tag{4.20}
$$

Next, we consider a specific form for the local kinetics and we determine conditions for which oscillatory instabilities occur.

4.3 Stability Analysis: Hill Function Dynamics

In this section, we analyze (4.6), with intracellular reaction dynamics governed by a delayed Hill function of the form

$$
F(u_T) := \frac{u_T^2}{1 + u_T^2} - \gamma\ u_T\ , \tag{4.21}
$$

for some positive real parameter γ. At the steady state solution, the partial derivative of F is given by

$$
F_u^e = \frac{2u_e}{(1 + u_e^2)^2} - \gamma\ . \tag{4.22}
$$

Substituting (4.21) and (4.22) into (4.7) yields

$$
U_{0e} = \left(\frac{2\pi d_2}{|\Omega| + 2\pi d_1}\right)\ u_e\ , \quad 0 = -\frac{u_e^2}{1 + u_e^2} + \left(\gamma + \frac{2\pi d_2}{\tau}\right)\ u_e - \frac{2\pi d_1}{\tau} U_{0e}\ . \tag{4.23}
$$

We are interested in the equilibrium solution u_e at the intersection point of the two nullclines in (4.23). Thus, we seek a solution u_e which satisfies

$$
\frac{u_e^2}{1 + u_e^2} = \kappa\ u_e\ , \qquad \text{where} \quad \kappa = \gamma + \frac{b}{a}\ , \tag{4.24}
$$

and the parameters a and b are as defined in (4.15). Solving (4.24) for u_e yields the solutions

$$
u_e = 0\ , \qquad u_e^* = \frac{1 \pm \sqrt{1 - 4\kappa^2}}{2\kappa}\ . \tag{4.25}
$$

We note that for the nontrivial steady state solutions u_e^* to exist, we require that $1 - 4\kappa^2 \geq 0$, or $0 \leq \kappa \leq \frac{1}{2}$. It follows that γ, a, and b must satisfy

$$0 \leq \gamma + \frac{b}{a} \ \leq \ \frac{1}{2} \ . \tag{4.26}$$

In terms of the original parameters of the model, we fix $\gamma < 0.5$ and we get the condition

$$\tau > \frac{4\pi|\Omega|d_2}{(1-2\gamma)\left(|\Omega| + 2\pi d_1\right)} \ , \qquad \text{for some fixed } \ \gamma < \frac{1}{2} \ . \tag{4.27}$$

The two nontrivial solutions u_e^* in (4.25) coalesce when $\gamma + \dfrac{b}{a} = 0.5$, or when

$$\tau = \frac{4\pi|\Omega|d_2}{(1-2\gamma)\left(|\Omega| + 2\pi d_1\right)} \ , \qquad \text{for some fixed } \ \gamma < \frac{1}{2} \ . \tag{4.28}$$

The condition in (4.28) is satisfied exactly when the line $\kappa\ u_e$ in (4.24) intersects the sigmoidal curve $\dfrac{u_e^2}{1+u_e^2}$ tangentially at the bifurcation point $u_e^* = 1$.

The Jacobian matrix J for (4.6) evaluated at the nontrivial steady state solution (U_{0e}^*, u_e^*) is given by

$$J = \begin{bmatrix} -\dfrac{1}{\tau}\left(1 + \dfrac{2\pi d_1}{|\Omega|}\right) & \dfrac{2\pi d_2}{\tau|\Omega|} \\ \\ \dfrac{2\pi d_1}{\tau} & \dfrac{2u_e}{\left(1+u_e^2\right)^2} - \gamma - \dfrac{2\pi d_2}{\tau} \end{bmatrix} \ , \tag{4.29}$$

where the trace and determinant of J are given by

$$\mathrm{Tr}(J) = F_u^e - (a + \tau b) \ , \qquad \det(J) = b - aF_u^e \ . \tag{4.30}$$

At the trivial steady state $(0,0)$, (4.30) yields

$$\mathrm{Tr}(J) = -(\gamma + a + \tau\ b) < 0 \ , \qquad \det(J) = b + a\gamma > 0 \ , \tag{4.31}$$

which implies that the origin is a stable spiral. We note that in the absence of delay the trivial steady state is a stable node, since $(\mathrm{Tr}(J))^2 - 4\det(J) > 0$.

For the nontrivial steady state solutions in (4.25), we get that

$$\det(J) = (b + a\gamma)\left(\frac{u_e^2 - 1}{1 + u_e^2}\right) \ , \tag{4.32}$$

which is negative when $0 < u_e^* < 1$, and positive when $u_e^* > 1$.

4.4 Numerical Simulations

We now consider how increasing delay can bring about oscillations, thereby destabilizing the steady state solutions to (4.6). We again assume Hill function-type dynamics for $F(u_T)$, as defined in (4.21), and we choose parameter values such that the condition in (4.27) is satisfied.

Using the MatLab package `dde23`, we analyze numerically the effect of delay using the following set of parameter values:

$$\tau = 8\ , \quad d_1 = 1.5\ , \quad d_2 = 0.2\ , \quad |\Omega| = 10\ , \quad \gamma = 0.3\ . \tag{4.33}$$

With (4.33), we plot equilibrium curves for the steady state solution u_e as a function of the parameters τ, d_1, and γ, as shown in Figures 4.1(a), 4.1(b), and 4.2, respectively.

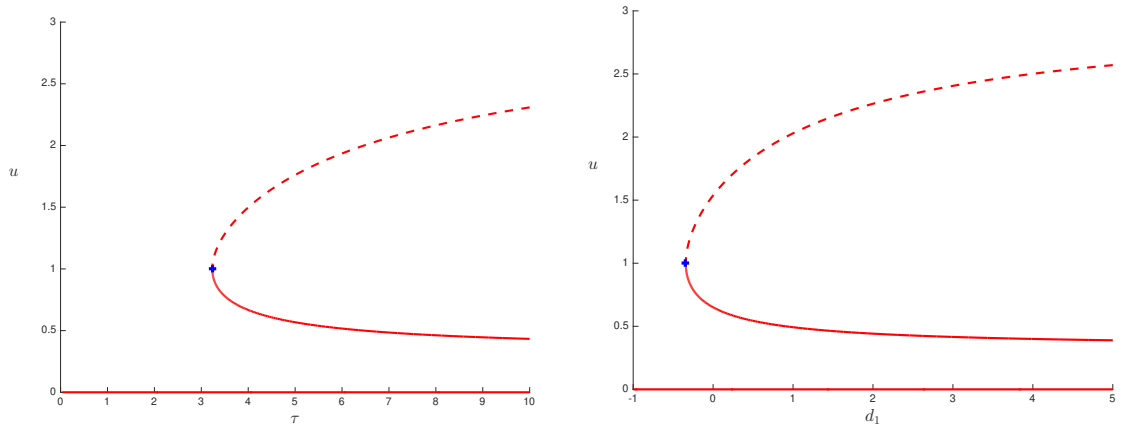

(a) (b)

Figure 4.1: Bifurcation diagram of u versus τ for $d_1 = 1.5$ (left), and u versus d_1 for $\tau = 8$ (right). Parameter used are $d_2 = 0.2$, $|\Omega| = 10$, and $\gamma = 0.3$.

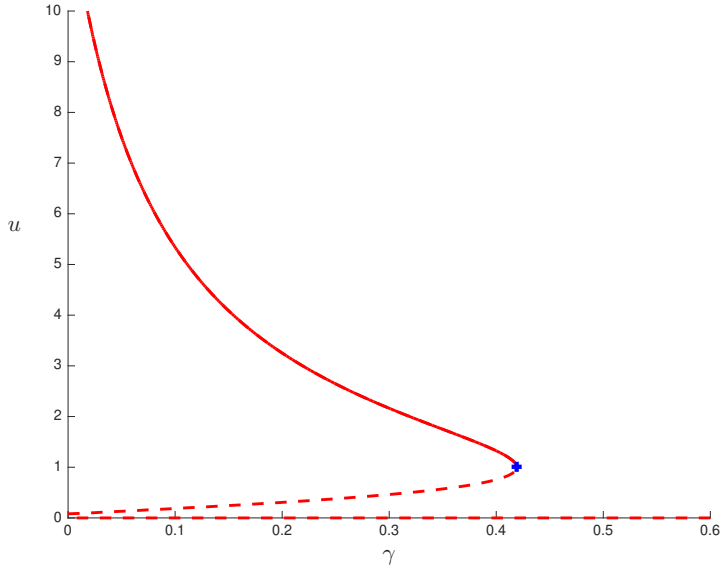

Figure 4.2: Bifurcation diagram of u versus γ. Parameter values are $\tau = 8$, $d_1 = 1.5$, $d_2 = 0.2$, $|\Omega| = 10$.

A plot of the intersection of the sigmoidal curve and the line κu_e in (4.24) is shown in Figure 4.3. As seen, there are three steady state solutions for the set of parameter values used: a trivial solution located at the origin, as well as two positive solutions given by

$$(\tilde{U}^*_{0e}, \tilde{u}^*_e) = (0.03, 0.46) \ , \qquad \text{and} \qquad (U^*_{0e}, u^*_e) = (0.14, 2.16) \ . \tag{4.34}$$

In this case, we find that the trivial steady state and the nontrivial solution $(U^*_{0e}, u^*_e) = (0.14, 2.16)$ are both stable.

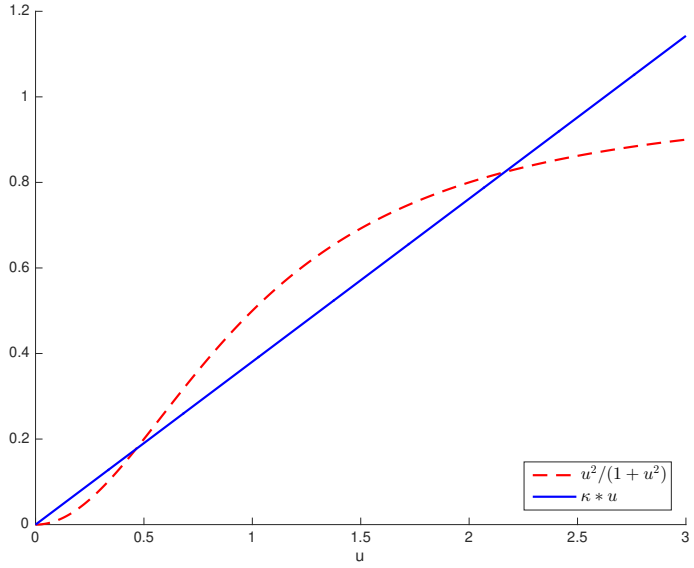

Figure 4.3: Plot of the sigmoidal curve $\dfrac{u^2}{1+u^2}$ and $\kappa\, u$, with parameter values $\tau = 8$, $d_1 = 1.5$, $d_2 = 0.2$, $|\Omega| = 10$, and $\gamma = 0.3$.

Numerical computations give that $F_u^e = -0.3$ for the trivial solution. For the steady states in (4.34), we get $F_u^e = 0.32763$ and -0.16589, respectively. The corresponding critical Hopf bifurcation values are calculated to be

$$(\omega_H, T_H) = \{\ (0.24, 8.31),\ (0.27, 7.35),\ (0.11, 19.98)\ \}\ . \tag{4.35}$$

Numerical simulations are used to validate these results, and we find that as delay T is increased past the critical Hopf bifurcation values, the trivial and the highest positive steady states become unstable giving rise to sustained oscillations. These results are illustrated in Figures 4.4-4.7.

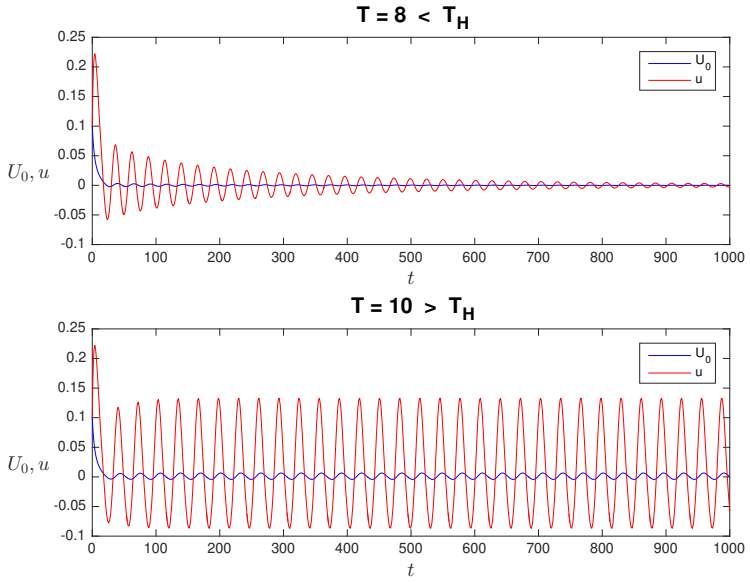

Figure 4.4: Plot of U_0 and u versus time t, illustrating the stability of the trivial steady state to the model in (4.6) with delayed Hill function dynamics. Initial condition used is $(U_0, u) = (0.1, 0.1)$. Top: Decaying oscillations are observed for delay below the Hopf bifurcation value. Bottom: Sustained oscillations for delay above the critical Hopf bifurcation value. Parameter values are $\tau = 8$, $d_1 = 1.5$, $d_2 = 0.2$, $|\Omega| = 10$, and $\gamma = 0.3$.

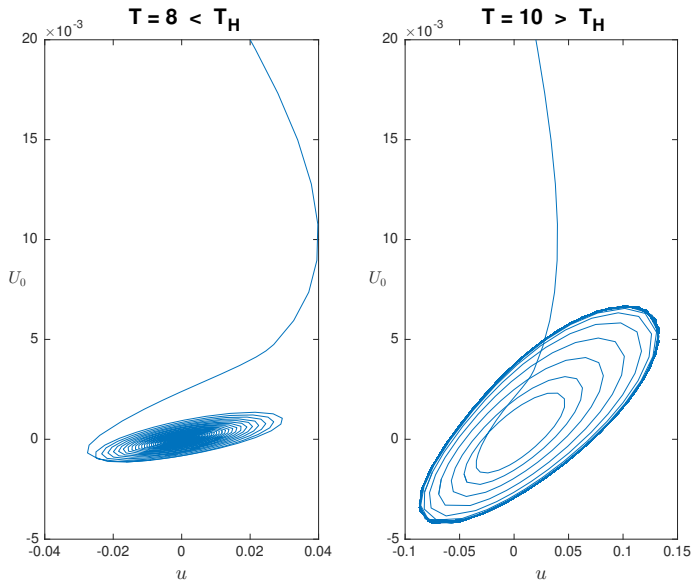

Figure 4.5: Plots of U_0 versus u showing sustained oscillations as delay increases past the critical Hopf bifurcation value for the trivial steady state. Initial condition used is $(u, U_0) = (0.02, 0.02)$. Parameter values are as in the caption of Figure 4.4.

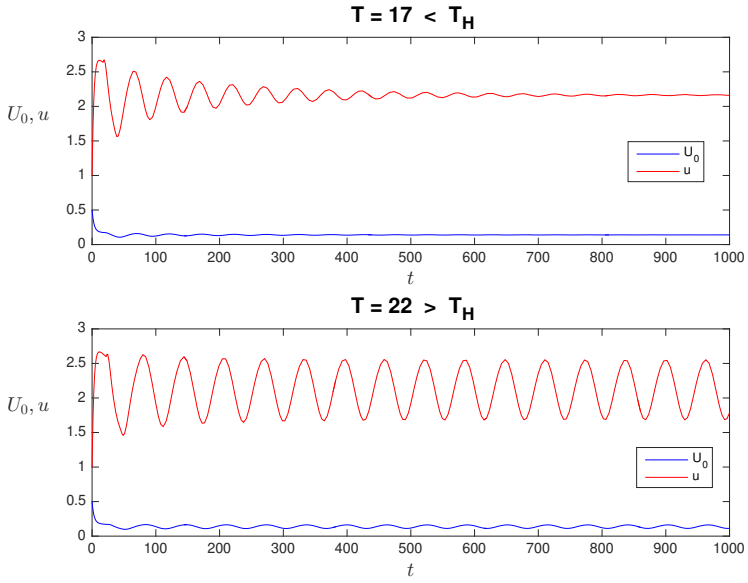

Figure 4.6: Plot of U_0 and u versus time t illustrating the stability of the highest positive steady state solution $(U_{0e}^*, u_e^*) = (0.14, 2.16)$ to the model in (4.6) with delayed Hill function dynamics. Initial condition used is $(U_0, u) = (0.5, 1)$. Top: Decaying oscillations towards the stable steady state are observed for delay below the Hopf bifurcation value. Bottom: Sustained oscillations for delay above the critical Hopf bifurcation value. Parameter values are as in the caption of Figure 4.4.

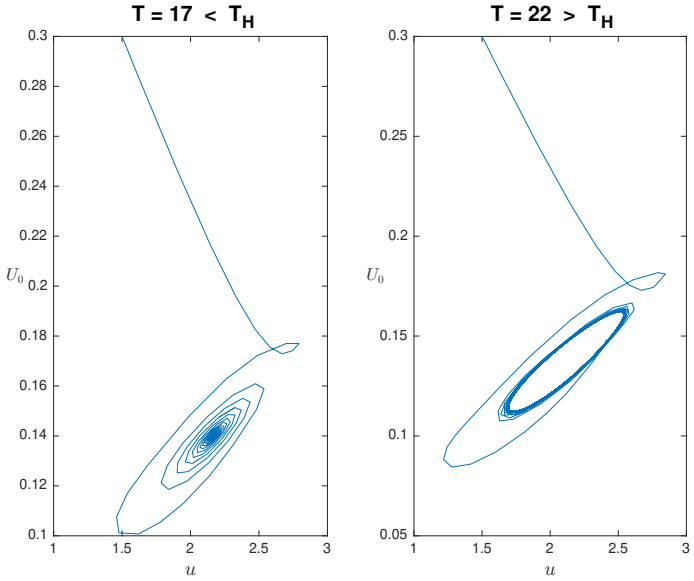

Figure 4.7: Plots of U_0 versus u, for the highest positive steady state $(U_{0e}^*, u_e^*) = (0.14, 2.16)$, showing sustained oscillations as delay increases past the critical Hopf bifurcation value. Initial condition used is $(u, U_0) = (1.5, 0.3)$. Parameter values are as in the caption of Figure 4.4

Chapter 5

Discussion

In this thesis, we have analyzed two types of reaction-diffusion models with delayed kinetics. Steady state solutions have been obtained using asymptotic analysis methods, and the effect of delay on the dynamics and stability has been analyzed both analytically and numerically.

In Chapters 2 and 3, we have analyzed the stability of slow evolving spike-type equilibrium solutions to the one-dimensional GM model with delayed reaction kinetics, subject to Neumann boundary conditions. Delay is a natural extension of the GM model and is well motivated biologically due to the fact that time delays are needed for protein synthesis and gene expression. As a result, we have delayed various nonlinear terms in the model in order to mimic all the possible ways delay could show up in the reaction, with the assumption that $0 < \epsilon << 1$ and $D = O(1)$. The analysis and results given have been derived using asymptotic methods which have been numerically verified.

In §2.1, we show that the system of delay partial differential equations can be reduced to a system of DDEs representing the motion for the corresponding spike solution. In §2.1.1, the model with delay in the inhibitor equation is analyzed. In this case, the slow moving spike tends towards a stable equilibrium. In §2.1.2, delay in the activator equation results in sustained oscillations due to a Hopf bifurcation. In §2.1.3, although the original PDE system has only one delay, the resulting reduced asymptotic ODE has two different delays. In §2.1.4 and §2.1.5, the presence of delay in the activator catalysis term introduces some complications to the analysis. In all cases, we have shown that simulations of the reduced system agree with simulations of the full PDE system.

In §2.2, we Hopf bifurcation in the reduced system. Such a bifurcation would cause oscillation in the spike positions. In all cases where such a bifurcation is possible, the critical value of the delay is $O(\epsilon^{-2})$, and a Hopf bifurcation causing a

profile instability will have already occurred. Thus, as delay increases beyond the critical Hopf bifurcation value, sustained oscillations due to a Hopf bifurcation are observed first in the spike amplitude.

In §2.3, we analyze instabilities due to a Hopf bifurcation of the large eigenvalues. Such a bifurcation results in oscillations of the spike amplitude. In this case the critical delay value is of $O(1)$. We find that increasing delay causes a Hopf bifurcation in all cases except for the systems in (2.39) and (2.54). In these cases increasing delay does not cause a Hopf bifurcation in neither the small nor the large eigenvalues. Simulations of the system of partial differential equations with large delay values verify the absence of a Hopf bifurcation. Simulations of the full system suggest that the Hopf bifurcation of the large eigenvalue are all sub-critical and the resulting oscillations are unstable.

Finally in §2.4, we have analyzed the GM model with delay in the activator degradation. Such a system is not biologically relevant. However, this is the only example of a Hopf bifurcation of the small eigenvalues for the GM system, contrary to the previously considered cases where oscillations in the spike amplitude are observed well before those in the spike position. Simulations of the system suggest that this bifurcation is super-critical and the oscillations are sustained.

The GM models in this thesis are for the exponent set $(p, q, m, s) = (2, 1, 2, 0)$. An interesting special case is analyzed in [56], where the exponents of the general GM model equations satisfy $p = 2m - 3$ and $m > 2$. Extending the analysis in [56] to the case where the activator kinetics are delayed, and upon analyzing the corresponding transcendental equation for the large eigenvalue parameter, we get that a Hopf bifurcation in the spike profile occurs as delay increases beyond a critical value, thereby destabilizing the steady state solution.

In Chapter 3, we have studied the stability and dynamics of a k-spike equilibrium solution to the GM model with various cases of delayed reaction kinetics, similar to the analysis in Chapter 2. In §3.1, a k-spike equilibrium solution is constructed using the method of matched asymptotics, in the limit $\epsilon \to 0$. In §3.2, we have reduced the delay PDE system to a system of delay differential-algebraic equations representing the location of the spikes. In §3.2.2 and §3.2.3, the reduced DDAE systems are derived for the case where delay is in the activator production, as well as the case

where delay is in both the activator regulation and the inhibitor production, respectively. In §3.3, numerical simulations of the reduced DDAE systems in §3.2 show the possibility of oscillatory dynamics due to a Hopf bifurcation as delay increases past a threshold value, T_H. In §3.4, instabilities in the large eigenvalues of order $O(1)$ for the GM model with delayed reaction kinetics are analyzed. In §3.4.1, we have formulated the NLEP for the GM with no delay. In §3.4.2, we have analyzed the stability of the large eigenvalues for the model with delayed inhibitor kinetics. Numerical computations show that a Hopf bifurcation occurs as delay is increased past the critical bifurcation threshold, which in turn results in sustained oscillations in the spike amplitudes. Similarly, for the case where the activator regulation and inhibitor production are both delayed, the stability of the large eigenvalues has been analyzed in §3.4.3, and the corresponding Hopf bifurcation threshold has been determined. Similar results are obtained in [17], where it is shown that the one-spike equilibrium solution can become highly unstable when inhibitor delay effects are included.

The results obtained in §3.4 are in direct contrast to the results found in [18], where the authors show that delay in only the nonlinear autocatalytic activator kinetics enhances the stability of the localized spike solution to the GM model. Thus delay in only the activator kinetics is stabilizing in the sense that there exists a wider region in parameter space where the one-spike solution is linearly stable than when there is no delay in the reaction kinetics.

In Chapter 4, we have studied a two-dimensional coupled cell-bulk model and we have shown that delaying the intracellular dynamics leads to oscillatory instabilities thereby destabilizing the steady state solutions to the model. In §4.1, we formulate a model with one small circular signalling cell, in a two-dimensional bounded domain, coupled to delayed intracellular dynamics of n-interacting intracellular species. Using the assumption that the signalling molecule has fast diffusion, such that the diffusion coefficient D satisfies $D \gg \mathcal{O}(\nu^{-1})$, for $\nu = -1/\log\epsilon$ and $\epsilon << 1$, we get a well-mixed bulk region, and we reduce the cell-bulk PDE system to a finite $(n+1)$-dimensional system of DDEs for the spatially constant bulk concentration field coupled to delayed intracellular dynamics. In §4.2 and §4.3, we use a singular perturbation approach to formulate the eigenvalue problem associated with linearizing around the steady state solution for the case where there is one circular cell with one intracellular species

governed by a delayed Hill function-type dynamics. Numerical simulations in §4.4 confirm that as the delay parameter T is increased past the critical Hopf bifurcation thresholds, the trivial and the highest positive steady state solutions become unstable giving rise to sustained oscillations.

5.1 Future Work

The study of delay partial differential equations is a relatively new field and there are very few analytical results. The behaviour of systems with highly localized solutions can be analyzed by considering a much simpler system of ODEs. This reduction allows us to study the effect of delay on a system of partial differential equations. The methods considered in this thesis can be applied to any RD system which supports highly localized solutions. We have only considered models with spike-type solutions. Investigation into systems which support front type solutions could yield more interesting results. In addition, there is a great deal of work to be done in the area of numerical simulations of partial differential equations with delay.

A possible extension to our analysis in Chapters 2 and 3 is to study the dynamics of spike solutions to the GM model with delayed reaction kinetics in the limiting case of exponentially large diffusivity coefficient D. It would also be interesting to analyze the GM model with delayed kinetics for different exponent sets (p, q, m, s). Moreover, it is still an open problem to derive and analyze the reduced asymptotic ODE representing the slow dynamics of a spike solution to the GM model with delayed kinetics on multi-dimensional domains, or on an unbounded domain. Another possible extension to our analysis of the GM model with delayed reaction kinetics is to determine stability properties for spikes at arbitrary positions.

A possible extension to the work done in Chapter 4 is the study of quorum sensing behaviour through analyzing the effect of delayed intracellular dynamics on the stability of steady state solutions to models with multiple signalling cells. It would also be interesting to consider other forms of delayed intracellular kinetics, as well as other diffusion rate regimes such as $D = \mathcal{O}(1)$ and $D = \mathcal{O}(\nu^{-1})$. Another interesting direction is to study the effect of delayed intracellular kinetics for the class of models in [57], where there is more than one bulk diffusing species.

Bibliography

[1] N. Azer, P. van den Driessche, *Competition and dispersal delays in patchy environments*, Math. Biosci. Eng., **3**(2), (2006), pp. 283-296.

[2] C. Baker and C. Paul, *Discontinuous solutions of neutral delay differential equations*, Appl. Numer. Math., **56**, (2006), pp. 284-304.

[3] M. V. Barbarossa, C. Kuttler, *Mathematical modeling of bacteria communication in continuous cultures*, Appl. Sci., **6**(5), (2016), 149.

[4] S. Chen, J. Shi, *Global attractivity of equilibrium in Gierer-Meinhardt system with activator production saturation and gene expression time delays*, Nonlinear Analysis: Real World Applic., **14**(4), (2013), pp. 1871-1886.

[5] S. Chen, J. Shi, J. Wei, *Time delay-induced instabilities and Hopf bifurcations in general reaction-diffusion systems*, J. Nonl. Sci., **23**(1), (2013), pp. 1-38.

[6] X. Chen, M. Kowalcyzk, *Dynamics of an interior spike in the Gierer-Meinhardt system*, SIAM J. Math. Anal., **33**, (2001), pp. 172-193.

[7] X. Chen, M. Kowalcyzk, *Slow dynamics of interior spikes in the shadow Gierer-Meinhardt system*, Adv. in Diff. Equat., **6**(7), (2001), pp. 847-872.

[8] T. Chou, M. R. D'Orsogna, *Multistage absorption of diffusing macromolecules and viruses*, J. Chem. Phys., **127**(1), (2007), 105101.

[9] F. Crauste, M. L. Hbid, A. Kacha, *A delay reaction-diffusion model of the dynamics of botulinum in fish*, Math. Biosci., **216**(1), (2008), pp. 17-29.

[10] R. V. Culshaw, S. Ruan, *A delay-differential equation model of HIV infection of CD4(+) T-cells*, Math. Biosci., **165**(1), (2000), pp. 27-39.

[11] S. De Monte, F. d'Ovidio, S. Danø, P. G. Sørensen, *Dynamical quorum sensing: population density encoded in cellular dynamics*, Proc. Nat. Acad. Sci., **104**(47), (2007), pp. 18377-18381.

[12] M. Del Pino, P. Felmer, M. Kowalczyk, *Boundary Spikes in the Gierer-Meinhardt System*, Commun. Pure Appl. Anal., **1**(1), (2002), pp. 137-156.

[13] O. Diekmann, S. A. van Gils, S. M. Verduyn Lunel, H.-O. Walther, *Delay equations: Functional-, Complex-, and Nonlinear Analysis. Applied mathematical sciences*, Vol. 110, Springer, New York, (1995).

[14] A. Doelman, R. A. Gardner, T. Kaper, *Large stable pulse solutions in reaction-diffusion equations*, Indiana Univ. Math. J., **50**(1), (2001), pp. 443-507.

[15] S. Dutta, D. S. Ray, *Effects of delay in a reaction-diffusion system under the influence of an electric field*, Phys. Rev. E, **77**(3), (2008), 036202.

[16] T. Erneux, *Applied delay differential equations*, Springer-Verlag, New York, (2009).

[17] N. Fadai, M. J. Ward, J. Wei, *Delayed reaction-kinetics and the stability of spikes in the Gierer-Meinhardt model*, SIAM J. Appl. Math., **77**(2), (2017), pp. 664-696.

[18] N. Fadai, M. J. Ward, J. Wei *A Time-Delay in the Activator Kinetics Enhances the Stability of a Spike Solution to the Gierer-Meinhardt Model*, DCDS-B, **23**(4), (2018), pp. 1431-1458.

[19] T. Faria, *Stability and bifurcation for a delayed predator-prey model and the effect of diffusion*, J. Math. Anal. Appl., **254**(2), (2001), pp. 433-463.

[20] E. A. Gaffney, N. A. M. Monk, *Gene expression time delays and Turing pattern formation systems*, Bull. Math. Bio., **68**, (2006), pp. 99-130.

[21] P. Ghosh, *Control of the Hopf-Turing transition by time-delayed global feedback in a reaction-diffusion system*, Phys. Rev. E, **84**, (2011), 016222.

[22] P. Ghosh, S. Sen, D. S. Ray, *Reaction-Cattaneo systems with fluctuating relaxation time*, Phys. Rev. E, **81**, (2010), 026205.

[23] A. Gierer, H. Meinhardt, *A theory of biological pattern formation*, Kybernetik, **12**, (1972), pp. 30-39.

[24] A. Gomez-Marin, J. Garcia-Ojalvo, J. M. Sancho, *Self-sustained spatiotemporal oscillations induced by membrane-bulk coupling*, Phys. Rev. Lett., **98**(16), (2007), 168303.

[25] J. Gou, M. J. Ward, *Asymptotic analysis of a 2-D model of dynamically active compartments coupled by bulk diffusion*, J. Nonl. Sci., **26**(4), (2016), pp. 979-1029.

[26] J. Gou, M. J. Ward, *Oscillatory dynamics for a coupled membrane-bulk model with Fitzhugh-Nagumo membrane kinetics*, SIAM J. Appl. Math., **76**(4), (2016), pp. 776-804.

[27] K. P. Hadeler, S. Ruan, *Interaction of diffusion and delay*, Discrete Contin. Dyn. Syst., Ser. B **8**(1), (2007), pp. 95-105.

[28] L. Harrison, D. Holloway, *Order and localization in reaction-diffusion pattern*, Phys. A, **222**, (1995), pp. 210-233.

[29] A. V. M. Herz, S. Bonhoeffer, R. M. Anderson, R. M. May, M. A. Nowak, *Viral dynamics in vivo: limitations on estimates of intracellular delay and virus decay*, Proc. Natl. Acad. Sci. USA, **93**(14), (1996), pp. 7247-7251.

[30] G.-P. Hu, W.-T. Li, *Hopf bifurcation analysis for a delayed predator-prey system with diffusion effects*, Nonlinear Anal., Real World Appl., **11**(2), (2010), pp. 819-826.

[31] D. Iron, *Metastability of the Gierer-Meinhardt equations*, M.Sc. Thesis, Department of Mathematics, Institute for Applied Mathematics, University of British Columbia, (1997).

[32] D. Iron, M. J. Ward, *A metastable spike solution for a non-local reaction-diffusion model*, SIAM J. Appl. Math., **60**(3), (2000), pp.778-802.

[33] D. Iron, M. J. Ward, *The dynamics of multispike solutions to the one-dimensional Gierer-Meinhardt model*, SIAM J. Appl. Math., **62**(6), (2002), pp. 1924-1951.

[34] D. Iron, M. J. Ward, J. Wei, *The stability of spike solutions to the one-dimensional Gierer-Meinhardt model*, Physica D, **150**(1-2), (2001), pp. 25-62.

[35] N. Khalil, D. Iron, T. Kolokolnikov, *Stability and dynamics of spike-type solutions to delayed Gierer-Meinhardt equations*, submitted, (2018).

[36] T. Kolokolnikov, *Pattern formation in reaction-diffusion models far from the Turing regime*, Ph.D. Thesis, Department of Mathematics, Institute for Applied Mathematics, University of British Columbia, (2004).

[37] T. Kolokolnikov, J. Wei, *Stability of spike solutions in a competition model with cross-diffusion*, SIAM J. Appl. Math., **71**(4), (2011), pp. 1428-1457.

[38] T. Kolokolnikov, M. J. Ward, J. Wei, *The stability of steady-state hot-spot patterns for a reaction-diffusion model of urban crime*, DCDS-B, **19**(5), (2014), pp. 1373-1410.

[39] T. Kolokolnikov, J. Wei, M. Winter, *Existence and stability analysis of spiky solutions for the Gierer-Meinhardt system with large reaction rates*, Physica D: Nonlinear Phenomena, **238**(16), (2009), pp. 1695-1710.

[40] Y. Kuang, *Delay differential equations with applications in population dynamics. Mathematics in Science and Engineering*, Vol. 191, third edition, Academic Press, Boston, (1993).

[41] D. Kulginov, V. P. Zhdanov, B. Kasemo, *Oscillatory surface reaction kinetics due to coupling of bistability and diffusion limitations*, J. Chem. Phys., **106**(8), (1997), pp. 3117-3128.

[42] S. Lee, E. A. Gaffney, N. A. M. Monk, *The influence of gene expression time delays on Gierer-Meinhardt pattern formation systems*, Bull. Math. Bio., **72**(8), (2010), pp. 2139-2160.

[43] S. Lee, E. A. Gaffney, *Aberrant behaviors of reaction-diffusion self-organization models on growing domains in the presence of gene expression time delays*, Bull. Math. Bio., **72**(8), (2010), pp. 2161-2179.

[44] S. Lee, E. A. Gaffney, R. E. Baker, *The dynamics of Turing patterns for morphogen-regulated growing domains with cellular response delays*, Bull. Math. Bio., **73**, (2011), pp. 2527-2551.

[45] H. Levine, W. J. Rappel, *Membrane bound Turing patterns*, Phys. Rev. E., **72**, (2005), 061912.

[46] C. Levy, D. Iron, *Dynamics and stability of a three-dimensional model of cell signal transduction*, J. Math. Bio., **67**(6-7), (2013), pp. 1691-1728.

[47] C. Levy, D. Iron, *Dynamics and stability of a three-dimensional model of cell signal transduction with delay*, Nonlinearity, **28**(7), (2015), pp. 2515-2554.

[48] A. Love, *Developmental Biology*, The Stanford Encyclopedia of Philosophy, Edward N. Zalta (ed.), (2015).

[49] Maple (2019). *Maplesoft, a division of Waterloo Maple Inc.*, Waterloo, Ontario.

[50] H. Meinhardt, *Models of biological pattern formation*, Academic Press, London, (1982).

[51] I. Moyles, M. J. Ward, *Existence, stability, and dynamics of ring and near-ring solutions to the Gierer-Meinhardt model with saturation in the semi-strong regime* , SIAM J. Appl. Dyn. Sys., **16**(1), (2017), pp. 597-639.

[52] J. Müller, C. Kuttler, B. A. Hense, *Cell-cell communication by quorum sensing and dimension-reduction*, J. Math. Biol., **53**(4), (2006), pp. 672-702.

[53] J. Müller, H. Uecker, *Approximating the dynamics of communicating cells in a diffusive medium by ODEs - homogenization with localization*, J. Math. Biol., **67**(5), (2013), pp. 1023-1065.

[54] J. D. Murray, *Mathematical biology*, second edition, Berlin, Springer (1993).

[55] J. D. Murray, *Mathematical biology. I: An introduction*, third edition, Springer-Verlag, New York, (2002).

[56] Y. Nec, M. J. Ward, *An explicitly solvable nonlocal eigenvalue problem and the stability of a spike for a sub-diffusive reaction-diffusion system*, Math. Model. of Nat. Phenom., **8**(2), (2013), pp. 55-87.

[57] E. M. Raucha, M. M. Millonas, *The role of trans-membrane signal transduction in turing-type cellular pattern formation*, J. Theor. Biol., **226**(4), (2004), pp. 401-407.

[58] V. Rottschäfer, J. Tzou, M. J. Ward, *Transition to blow-up in a reaction-diffusion model with localized spike solutions*, Europ. J. Appl. Math., **28**(6), (2017), pp. 1015-1055.

[59] D. J. Schwab, A. Baetica, P. Mehta, *Dynamical quorum-sensing in oscillators coupled through an external medium*, Physica D, **241**(21), (2012), pp. 1782-1788.

[60] S. Sen, P. Ghosh, S. S. Riaz, D. S. Ray, *Time-delay-induced instabilities in reaction-diffusion systems*, Phys. Rev. E, **80**(4), (2008), 046212.

[61] L. Shampine, I. Gladwell, S. Thompson, *Solving ODEs with MATLAB*, Cambridge University Press, (2003).

[62] L. Shampine, S. Thompson, *Solving DDEs in MATLAB*, Appl. Numer. Math., **37**, (2001), pp. 441-458.

[63] H. Smith, *An Introduction to delay differential equations with applications to the life sciences*, Springer-Verlag, New York, (2011).

[64] I. Takagi, *Point-condensation for a reaction-diffusion system*, J. Diff. Eqns., **61**, (1986), pp. 208-249.

[65] L. Tanet, C. Tamburini, C. Baumas, M. Garel, G. Simon, L. Casalot, *Bacterial bioluminescence: Light emission in photobacterium phosphoreum is not under quorum-sensing control*, Front. Microbiol., **10**, (2019), pp. 365.

[66] M. R. Tinsley, A. F. Taylor, Z. Huang, F. Wang, K. Showalter, *Dynamical quorum sensing and synchronization in collections of excitable and oscillatory catalytic particles*, Physica D, **239**(11), (2010), pp. 785-790.

[67] D. J. Schwab, A. Baetica, P. Mehta, *Dynamical quorum-sensing in oscillators coupled through an external medium*, Physica D, **241**(21), (2012), pp. 1782-1788.

[68] A. Turing, *The chemical basis of morphogenesis*, Phil. Trans. Roy. Soc. B, **327**, (1952), pp. 37-72.

[69] J. J. Tyson, H. G. Othmer, *The dynamics of feedback control circuits in biochemical pathways*, Prog. Theor. Biol., **5**, (1978), pp. 1-62.

[70] J. C. Tzou, M. J. Ward, T. Kolokolnikov, *Slowly varying control parameters, delayed bifurcations, and the stability of spikes in reaction-diffusion systems*, Phys. D, **290**, (2015), pp. 24-43.

[71] H. Van der Ploeg, A. Doelman, *Stability of spatially periodic pulse patterns in a class of singularly perturbed reaction-diffusion equations*, Indiana Univ. Math. J., **54**(5), (2005), pp. 1219-1301.

[72] M. Van Dyke, *Perturbation methods in fluid mechanics*. Applied Mathematics and Mechanics, **8**, (1964).

[73] M. J. Ward, W. D. Henshaw, J. B. Keller, *Summing logarithmic expansions for singularly perturbed eigenvalue problems*, SIAM J. Appl. Math., **53**(3), (1993), pp. 799-828.

[74] M. J. Ward, D. McInerney, P. Houston, D. Gavaghan, P. Maini, *The dynamics and pinning of a spike for a reaction-diffusion model*, SIAM J. Appl. Math., **62**(4), (2002), pp. 1297-1328.

[75] M. J. Ward, J. Wei, *Asymmetric spike patterns for the one-dimensional Gierer-Meinhardt model: Equilibria and Stability*, Europ. J. Appl. Math., **13**(3), (2002), pp. 283-320.

[76] M. J. Ward, J. Wei, *Hopf bifurcation of spike solutions for the shadow Gierer-Meinhardt model*, Europ. J. Appl. Math., **14**(6), (2003), pp. 667-711.

[77] M. J. Ward, J. Wei, *Hopf bifurcation and oscillatory instabilities of spike solutions for the one-dimensional Gierer-Meinhardt model*, J. Nonlinear Science, **13**(2), (2003), pp. 209-264.

[78] J. Wei, *On single interior spike solutions for the Gierer-Meinhardt system: uniqueness and stability estimates*, Europ. J. Appl. Math., **10**(4), (1999), pp. 353-378.

[79] J. Wei, *Existence and stability of spikes for the Gierer-Meinhardt system*, book chapter in *Handbook of Differential Equations, Stationary Partial Differential Equations*, Vol. 5 (M. Chipot ed.), Elsevier, (2008), pp. 489-581.

[80] J. Wei, M. Winter, *Spikes for the two-dimensional Gierer-Meinhardt system: the weak coupling case*, J. Nonlinear Sci., **11**(6), (2001), pp. 415-458.

[81] W. Zuo, J. Wei, *Stability and Hopf bifurcation in a diffusive predatory-prey system with delay effect*, Real World Appl., **12**(4), (2011), pp. 1998-2011.

Appendix A

Numerical Source Code

A.1 MatLab Code for Solving Asymptotic DDEs in Chapter 2 for the Motion of a Spike

```
function sol=gmdde
sol = ddesd(@x0dderhs,[1.9],@x0hist,[0, 200]);
figure;
plot(sol.x,sol.y)
xlabel({'$\tau$'}, 'FontSize', 16, 'Interpreter', 'latex');
ylabel({'$x_0$'}, 'FontSize', 16, 'Interpreter', 'latex',...
'Rotation', -360, 'Position', [-20 1.2]);
function s = x0hist(t)
s=0.3694;
function dydt = x0dderhs(t,y,Z)
ylag = Z(:,1);
L=2;
dydt = -sinh(2*ylag(1)-L)/(cosh(ylag(1)-L)*cosh(ylag(1)));
```

A.2 MatLab Code for Solving GM PDE Model in (2.100) with Delayed Activator Degradation

```
clf; hold off;
tlag=1.04;
L=2;
eps=0.06;
dt=0.025; Tmax=1500;
N=100;
```

```
maxht=zeros(1,2);

maxloc=zeros(1,2);
x=linspace(0,L, N)';
a_init=sech((x-.9)/2/eps).^2;
h_init=1+x*0;
I=eye(N);
dx=x(2)-x(1);
Lap=-2*diag(ones(1,N))+diag(ones(1,N-1),1)+diag(ones(1,N-1),-1);
Lap(1,2)=2;Lap(N,N-1)=2;
Lap=Lap/dx.^2;
tout=0;
storelen=max(3,ceil(tlag/dt+2));
th=zeros(1,storelen);
hh=zeros(N,storelen);
ah=zeros(N,storelen);
h=h_init; a=a_init;
idx=0;
for t=0:dt:Tmax
    idx=idx+1;
    th=circshift(th, -1);
    hh=circshift(hh', -1)';
    ah=circshift(ah', -1)';
    th(end)=t;
    hh(:,end)=h;
    ah(:,end)=a;
    tprev=t-tlag;
    if idx<storelen
        hT=h;
        aT=a;
```

```
    else
        hT=interp1(th, hh', tprev)';
        aT=interp1(th, ah', tprev)';
    end;
    hp = (I-Lap)\(a.^2/eps);
    oo=a.^2./h-aT;
    ap=(I/dt-eps^2*Lap)\(oo+a/dt);
    h=hp;
    a=ap;
    if isnan(max(a))
        stop;
    end;
    if t>tout
        tout=tout+10;
        [t1,t2]=max(a);
        x1=a(t2-1);
        x2=a(t2);
        x3=a(t2+1);
        tt1=dx*(t2-2);
        tt2=dx*(t2-1);
        tt3=dx*(t2);
        a1=(4*x2-x3-3*x1)/(2*dx);
        a2=-(2*x2-x3-x1)/(2*(dx)^2);
        tmax=-a1/(2*a2)+tt1;
        maxht(end+1,:)=[t,t1];
        maxloc(end+1,:)=[t,tmax];
        subplot(3,1,1); plot(x,a, 'b'); hold on;plot(x,h, 'r');hold off;
        subplot(3,1,2); plot(maxloc(:,1),maxloc(:,2));
        subplot(3,1,3); plot(maxht(:,1),maxht(:,2));
        title(sprintf('t=%g',t));
xlabel({'$t$'}, 'FontSize', 16, 'Interpreter', 'latex');
ylabel({'$x_0$'}, 'FontSize', 16, 'Interpreter', 'latex',...
```

```
'Rotation', -360, 'Position', [-120 1.05]);
ylim([0.4 1.5]);
drawnow;
    end;
end;
```

A.3 Maple Code for Large Eigenvalues of GM Model (2.39) with Delay in Activator Regulation and Catalyzation

```
restart; with(LinearAlgebra): with(plots):
Mat:=proc(lam,n,T,delta)
   local w,chi,A,i,j,w1,f,eps,h,xi,xj;
   h:=1/(n-1):
   eps:=0.1;
   with(LinearAlgebra):
   w:=3/2*sech((x-.5)/2/eps)^2:
   w1:=unapply(w, x):
   chi:=2:
   f:= Matrix(n):      #, datatype=complex):
   for i from 1 to n do
    for j from 1 to n do
      f(i,j):=0.0:
    end do:
   end do:
   f(1,1):=-2.0*eps^2/h^2-1+2*w1(0)*exp(-lam*T):
   f(1,2):=2.0*eps^2/h^2:
   f(n,n):=-2.0*eps^2/h^2-1+2*w1(1)*exp(-lam*T):
   f(n,n-1):=2.0*eps^2/h^2:
   for i from 2 to n-1 do
     xi:=(i-1)*h;
     f(i,i):=-2.0*eps^2/h^2:
```

```
      f(i,i-1):=eps^2/h^2:
      f(i,i+1):=eps^2/h^2:
      f(i,i):=evalf(f(i,i)-1+2*w1(xi)*exp(-lam*T)):
    end do:
    for i from 1 to n do
    for j from 1 to n do
       xi:=(i-1)*h:
       xj:=(j-1)*h:
       f(i,j):=evalf(f(i,j)-delta/eps*(1/n*chi*exp(-lam*T)*w1(xi)^2/6*w1(xj))):
    end do:
    end do:
f;
end proc:
counter:=1:
N:=100:
T:=0:
lam[1]:=2:
with(ListTools):
M:=Mat(lam[1],N,T,0):
E:=Eigenvalues(evalf(M)):
(v,e):=Eigenvectors(M):
convert(E,list):
pos:=FindMaximalElement((convert(Re(E),list)),position)[2];
pos2:=FindMaximalElement((convert(Re(v),list)),position)[2];
E[pos];
listplot([seq(Re(e[i][pos]),i=1..N)]);
ll[1]:=E[pos];
for i from 1 to 25 do
  delta:=i/50:
  M1:=Mat(lam[1],N,T,delta):
  (v1,e1):=Eigenvectors(M1):
  v2:=[seq(norm(convert(v1,list)[i]-v[pos],2),i=1..N)]:
```

```
  pos:=FindMinimalElement(v2,position)[2]:
  v:=v1:
  print(delta,v[pos]):
  counter:=counter+1:
  ll[counter]:=v[pos]:
  TT[counter]:=T;
end do:
convert(v,list):
pos;
v(pos);
delta:=26/50:
M1:=Mat(lam[1],N,T,delta):
(v1,e1):=Eigenvectors(M1):
v2:=[seq(norm(convert(v1,list)[i]-v(pos),2),i=1..N)]:
v:=v1:
counter:=counter+1;
pos:=FindMinimalElement(v2,position)[2];
convert(v,list):
pos;
v(97);
ll[counter]:=v[97];TT[counter]:=T;
delta:=27/50:
M1:=Mat(lam[1],N,T,delta):
(v1,e1):=Eigenvectors(M1):
v2:=[seq(norm(convert(v1,list)[i]-v(97),2),i=1..N)]:
v:=v1:
pos:=FindMinimalElement(v2,position)[2];
convert(v,list):
v(91);
counter:=counter+1;
ll[counter]:=v(91);TT[counter]:=T;
delta:=28/50:
```

```
M1:=Mat(lam[1],N,T,delta):
(v1,e1):=Eigenvectors(M1):
v2:=[seq(norm(convert(v1,list)[i]-v(91),2),i=1..N)]:
v:=v1:
pos:=FindMinimalElement(v2,position)[2];
for i from 29 to 50 do
  delta:=i/50:
  M1:=Mat(lam[1],N,T,delta):
  (v1,e1):=Eigenvectors(M1):
  v2:=[seq(norm(convert(v1,list)[i]-v[pos],2),i=1..N)]:
  pos:=FindMinimalElement(v2,position)[2]:
  v:=v1:
  print(delta,v[pos]):
  counter:=counter+1:
  ll[counter]:=v[pos]:
  TT[counter]:=T:
end do:
listplot({seq([Re(ll[i]),Im(ll[i])],i=1..counter)});
T:=0.01:
M1:=Mat(v[pos],N,T,delta):
(v1,e1):=Eigenvectors(M1):
v2:=[seq(norm(convert(v1,list)[i]-v[pos],2),i=1..N)]:
pos1:=FindMinimalElement(v2,position)[2]:
pos;
pos1;
while (norm(v1[pos1]-v[pos],2))>0.00000000001 do
    v:=v1:
    pos:=pos1:
    M1:=Mat(v[pos],N,T,delta):
    (v1,e1):=Eigenvectors(M1):
    v2:=[seq(norm(convert(v1,list)[i]-v[pos],2),i=1..N)]:
    pos1:=FindMinimalElement(v2,position)[2]:
```

```
    print(v[pos]):
end do:
counter;
ll[50];
counter:=counter+1:
ll[counter]:=v[pos];TT[counter]:=T;
for i from 1 to 79 do
  T:=0.001*i:
  M1:=Mat(v[pos],N,T,delta):
 (v1,e1):=Eigenvectors(M1):
 v2:=[seq(norm(convert(v1,list)[i]-v[pos],2),i=1..N)]:
 pos1:=FindMinimalElement(v2,position)[2]:
 while (norm(v1[pos1]-v[pos],2))>0.000000001 do
    v:=v1:
    pos:=pos1:
    M1:=Mat(v[pos],N,T,delta):
    (v1,e1):=Eigenvectors(M1):
    v2:=[seq(norm(convert(v1,list)[i]-v[pos],2),i=1..N)]:
    pos1:=FindMinimalElement(v2,position)[2]:
    print(T,v[pos]):
  end do:
  counter:=counter+1:
  ll[counter]:=v[pos]:
  TT[counter]:=T;
end do:
p1:=listplot({seq([Re(ll[i]),Im(ll[i])],i=50..130)},color=red);
for i from 1 to 100 do
  T:=0.001*79+.0001*i:
  M1:=Mat(v[pos],N,T,delta):
 (v1,e1):=Eigenvectors(M1):
 v2:=[seq(norm(convert(v1,list)[i]-v[pos],2),i=1..N)]:
 pos1:=FindMinimalElement(v2,position)[2]:
```

```
 while (norm(v1[pos1]-v[pos],2))>0.000000001 do
    v:=v1:
    pos:=pos1:
    M1:=Mat(v[pos],N,T,delta):
    (v1,e1):=Eigenvectors(M1):
    v2:=[seq(norm(convert(v1,list)[i]-v[pos],2),i=1..N)]:
    pos1:=FindMinimalElement(v2,position)[2]:
    #print(T,v[pos]):
  end do:
  print(T,v[pos]):
  counter:=counter+1:
  ll[counter]:=v[pos]:
  TT[counter]:=T:
end do:
p1:=listplot({seq([Re(ll[i]),Im(ll[i])],i=50..138)},color=red);
pc1:=listplot({seq([Re(ll[i]),-Im(ll[i])],i=50..138)},color=red);
p2:=listplot({seq([Re(ll[i]),Im(ll[i])],i=139..counter)},color=red);
display({p1,p2});
T;
counter;
for i from 1 to 150 do
  T:=0.089+.01*i:
  M1:=Mat(v[pos],N,T,delta):
 (v1,e1):=Eigenvectors(M1):
 v2:=[seq(norm(convert(v1,list)[i]-v[pos],2),i=1..N)]:
 pos1:=FindMinimalElement(v2,position)[2]:
 while (norm(v1[pos1]-v[pos],2))>0.000000001 do
    v:=v1:
    pos:=pos1:
    M1:=Mat(v[pos],N,T,delta):
    (v1,e1):=Eigenvectors(M1):
    v2:=[seq(norm(convert(v1,list)[i]-v[pos],2),i=1..N)]:
```

```
    pos1:=FindMinimalElement(v2,position)[2]:
    print(T,v[pos]):
  end do:
  counter:=counter+1:
  ll[counter]:=v[pos]:
  TT[counter]:=T:
end do:
counter;
p3:=listplot({seq([Re(ll[i]),Im(ll[i])],i=232..250)},color=red);
display({p1,p2,p3});
p4:=listplot({seq([Re(ll[i]),Im(ll[i])],i=251..275)},color=red);
p5:=listplot({seq([Re(ll[i]),Im(ll[i])],i=275..283)},color=red);
p6:=listplot({seq([Re(ll[i]),Im(ll[i])],i=283..305)},color=red);
pc6:=listplot({seq([Re(ll[i]),-Im(ll[i])],i=283..305)},color=red);
p7:=listplot({seq([Re(ll[i]),abs(Im(ll[i]))],i=306..350)},color=red);
p8:=listplot({seq([Re(ll[i]),abs(Im(ll[i]))],i=351..368)},color=red);
p9:=listplot({seq([Re(ll[i]),abs(Im(ll[i]))],i=369..380)},color=red);
pc9:=listplot({seq([Re(ll[i]),-abs(Im(ll[i]))],i=369..380)},color=red);
display({p1,pc1,p2,p3,p4,p6,pc6,p7,p8,p9,pc9});
counter;
T;
for i from 1 to 150 do
  T:=1.589+0.005*i:
  M1:=Mat(v[pos],N,T,delta):
 (v1,e1):=Eigenvectors(M1):
 v2:=[seq(norm(convert(v1,list)[i]-v[pos],2),i=1..N)]:
 pos1:=FindMinimalElement(v2,position)[2]:
 while (norm(v1[pos1]-v[pos],2))>0.000000001 do
    v:=v1:
    pos:=pos1:
    M1:=Mat(v[pos],N,T,delta):
    (v1,e1):=Eigenvectors(M1):
```

```
    v2:=[seq(norm(convert(v1,list)[i]-v[pos],2),i=1..N)]:
    pos1:=FindMinimalElement(v2,position)[2]:
    print(T,v[pos]):
  end do:
  counter:=counter+1:
  ll[counter]:=v[pos]:
  TT[counter]:=T:
end do:
counter;
p10:=listplot({seq([Re(ll[i]),abs(Im(ll[i]))],i=381..394)},color=red);
pc10:=listplot({seq([Re(ll[i]),-abs(Im(ll[i]))],i=381..394)},color=red);
p11:=listplot({seq([Re(ll[i]),abs(Im(ll[i]))],i=395..counter)},color=red);
display({p1,pc1,p2,p3,p4,p6,pc6,p7,p8,p9,pc9,p10,pc10,p11});
listplot({seq([TT[i],abs(Im(ll[i]))],i=50..counter)},color=red);
listplot({seq([TT[i],Re(ll[i])],i=50..counter)},color=red);
```

A.4 MatLab Code for Solving GM PDE Model in Chapter 3, for Two Spikes, with Delayed Reaction Kinetics

```
clf;
hold off;
tlag=0.1;
L=2/sqrt(.2);
eps=0.1;
Dh=1;
dt=0.0125; Tmax=500;
N=201;
maxht1=zeros(1,2);
maxloc1=zeros(1,2);
maxht2=zeros(1,2);
maxloc2=zeros(1,2);
```

```
x=linspace(0,L,N)';
dx=x(2)-x(1);
x00=.3/sqrt(.2);
x01=1.7/sqrt(.2);
x00i=floor(x00/dx)+1;
x01i=floor(x01/dx)+1;
h=nonlin([x00 x01],[x00,x01]);
a_init=1.5*(h(1)*sech((x-x00)/2/eps).^2+h(2)*sech((x-x01)/2/eps).^2);
h_init=1+x*0;
I=eye(N);
dx=x(2)-x(1);
Lap=-2*diag(ones(1,N))+diag(ones(1,N-1),1)+diag(ones(1,N-1),-1);
Lap(1,2)=2;Lap(N,N-1)=2;
Lap=Lap/dx.^2;
tout=0;
storelen=max(3,ceil(tlag/dt+2));
th=zeros(1,storelen);
hh=zeros(N,storelen);
ah=zeros(N,storelen);
h=h_init; a=a_init;
idx=0;
for t=0:dt:Tmax
    idx=idx+1;
    th=circshift(th, -1);
    hh=circshift(hh', -1)';
    ah=circshift(ah', -1)';
    th(end)=t;
    hh(:,end)=h;
    ah(:,end)=a;
    tprev=t-tlag;
    if idx<storelen
        hT=h;
```

```
    aT=a;
else
    hT=interp1(th, hh', tprev)';
    aT=interp1(th, ah', tprev)';
end;
hp = (I-Dh*Lap)\(a.^2/eps);
oo=a.^2./hT-a;
ap=(I/dt-eps^2*Lap)\(oo+a/dt);
h=hp;
a=ap;
if isnan(max(a))
    stop;
end;
if t>tout
    tout=tout+1;
    [t11,t211]=max(a(x00i-10:x00i+10));
    t211=t211+x00i-11;
    x11=a(t211-1);
    x21=a(t211);
    x31=a(t211+1);
    tt1=dx*(t211-2);
    tt2=dx*(t211-1);
    tt3=dx*(t211);
    a1=(4*x21-x31-3*x11)/(2*dx);
    a2=-(2*x21-x31-x11)/(2*(dx)^2);
    tmax=-a1/(2*a2)+tt1;
   maxht1(end+1,:)=[t,t11];
   maxloc1(end+1,:)=[t,tmax];
   x00i=floor(tmax/dx)+1;
  [t12,t22]=max(a(x01i-10:x01i+10));
   t22=t22+x01i-11;
    x12=a(t22-1);
```

```
         x22=a(t22);
         x32=a(t22+1);
         tt1=dx*(t22-2);
         tt2=dx*(t22-1);
         tt3=dx*(t22);
         a1=(4*x22-x32-3*x12)/(2*dx);
         a2=-(2*x22-x32-x12)/(2*(dx)^2);
         tmax=-a1/(2*a2)+tt1;
        maxht2(end+1,:)=[t,t12];
        maxloc2(end+1,:)=[t,tmax];
        x01i=floor(tmax/dx)+1;
subplot(3,1,1); plot(x,a, 'b'); hold on;plot(x,h, 'r--');hold off;
subplot(3,1,2); plot(maxloc1(:,1),maxloc1(:,2),'r');hold on;
plot(maxloc2(:,1),maxloc2(:,2),'g');hold off;
subplot(3,1,3); plot(maxht1(:,1),maxht1(:,2),'r');hold on;
plot(maxht2(:,1),maxht2(:,2),'g');hold off;
drawnow;
   end;
end;
```